An Energy Balance Based Analysis of Solar Domestic Hot Water Systems

An Energy Balance Based Analysis of Solar Domestic Hot Water Systems

BY
YING YU, B. Eng.

A THESIS

SUBMITTED TO THE DEPARTMENT OF MECHANICAL ENGINEERING

AND THE SCHOOL OF GRADUATE STUDIES

OF MCMASTER UNIVERSITY

IN PARTIAL FULFILMENT OF THE REQUIREMENTS

FOR THE DEGREE OF

MASTER OF APPLIED SCIENCE

Master of Applied Science (2020) McMaster University

(Mechanical Engineering) Hamilton, Ontario, Canada

TITLE: An Energy Balance Based Analysis of Solar Domestic Hot Water Systems

AUTHOR: Ying Yu

B.Eng., (Mechanical Engineering)

McMaster University, Hamilton, Canada

SUPERVISOR: Dr. Marilyn Lightstone

NUMBER OF PAGES: xx, 153

Abstract

Solar Domestic Hot Water (SDHW) systems collect energy from the sun to heat the household water. In the context of a system energy balance, numerical simulations were conducted using the commercial software "TRNSYS-17" to study the SDHW system performance (solar fraction) influenced by the critical parameters in various sizes of the thermal storage tank (TES) tank. The key parameters were the magnitude of the collector mass flow rate, degree of thermal stratification within the TES tank, and the duration of the mass flows through the collector.

An empirical correlation was obtained to determine the operating collector mass flow rate and TES volume to deliver the peak system performance. The correlation was preliminarily verified with different weather data. The studies showed that the optimal collector mass flow rate occurred when the same amount of total daily household demand passed through the collector. Furthermore, when the twofold amount of the household demand passed through the collector, the optimal dimensionless tank volume became insensitive to the change of collector flow rate and remained constant at 0.84.

Researchers discovered that promoting thermal stratification within the TES tank would enhance system performance. Thermal stratification within a TES improves the system performance by sending colder water to the solar collector and hotter water to the household. This research challenges the research community's focus on thermal stratification by showing that solar fraction is directly related to the solar collector heat losses. As such, the role of the TES tank is to supply cold fluid to the collector to minimize collector losses. Thermal stratification in the top portion of the tank is thus unimportant in influencing solar fraction.

In this research, the pump is turned on/off by monitoring the temperature difference between the collector inlet and outlet. Different pump control strategies at different collector mass flow rates were implemented to adjust the pump-on time. The studies showed the system performance was negligibly affected (~0.5%) by employing different pump control strategies while the collector mass flow rate was held constant.

Acknowledgments

It was not my initial intention to commit to a graduate degree in the field of thermofluid due to my skepticism in the competence of heat transfer. However, the respect and admiration I have towards my supervisor, Dr. Marilyn F. Lightstone, gave me a reason to reconsider, and I would like to express my utmost gratitude and appreciation to Dr. Lightstone for her influence and motivation. It has been a sincere blessing to learn from such an esteemed and talented mentor who has always been modest, amiable, patient, and supportive of me throughout my studies and research.

I would also like to extend my heartfelt appreciation to the dear friends I have made during my journey, particularly Mohamed Salim and Brianna Harris, who always gave me their endless support, guidance, inspiration, and always had faith in me. I also wish to thank my dear alumni colleagues – Cody Unrau, Hebattallah Teamah, Raf Hirmiz, and many others.

Finally, I have been immensely blessed with unconditional love and support from my beloved family overseas. There are no words to describe the depths of the love and gratitude I have for them. The selfless sacrifices they have made provided me with the priceless learning opportunities I have had and will continue to experience in the future.

Notation and abbreviations

Symbol	Description	Unit
ρ	Fluid density	kg/m^3
β	Thermal expansion coefficient	1/K
$\eta_{collector}$	Collector efficiency	-
$\kappa_{\tau\alpha}$	Incidence Angle Modifier	-
τ_p	Pump-on time	hr
Δt	Size of time step	s
Δx	Grid spacing	m
A	Tank surface area	m^2
A_c	Collector aperture area (North America)	m^2
C_p	Heat capacity	J/kg-°C
f_{max}	Solar fraction at the optimal operation	-
F'	Collector efficiency factor	-
F_R	Collector heat removal factor	-

$F_R(\tau\alpha)$	The intercept of the collector efficiency versus $(T_i-T_a)/G$ curve	-
F_RU_L	The negative slope of the collector efficiency versus $(T_i-T_a)/G$ curve	$W/m^{2-}K$
G	Solar irradiance	kJ/m^2
H	Height of the tank between the inlet and outlet	m
IAM	Incidence Angle Modifier	-
k	Thermal conductivity	W/m-K
$\dot{m}_{coll}$	Collector mass flow rate	kg/hr
M_{coll}	Daily mass of fluid through the collector	kg
M_{load}	Daily mass of the household demand	kg
n	Number of data	-
Q_{aux}	Auxiliary energy consumed by the SDHW system	kJ
Q_{load}	Total energy required to fulfill the load demands	kJ
$Q_{TankLosses}$	Total thermal losses of the thermal energy storage (TES) tank and the auxiliary tank	kJ
Q_u	Useful energy harnessed by the collector	kJ
T_a	Ambient temperature	°C
T_{charge}	Temperature of the charging fluid	°C

T_i	Collector inlet temperature	°C
$T_{initial}$	Tank initial temperature	°C
T_o	Collector outlet temperature	°C
T_{set}	Predetermined temperature of service water to household (60 °C)	°C
TES	Thermal energy storage	-
u_{in}	Fluid velocity at the tank inlet	m/s
U	Heat loss coefficient	W/m^2-K
U_L	Collector overall heat loss coefficient	W/m^2-K
V_{daily}	Daily household demand volume	m^3
V_{TES}	TES tank volume	m^3

Table of Contents

List of Figures

Chapter 1
Introduction

1.1 Background

Fossil fuels have been and continue to be a dominant primary energy source worldwide since the Industrial Revolution. In 2017, fossil fuels represented 81% and 76% of the total global and Canadian primary energy supply, respectively [1]. The concern regarding the consumption of fossil fuel has risen in the past decades due to its detrimental effects on the global environment. The increasing levels of greenhouse gas emission and the political tensions associated with fossil fuels are contrary to sustainable development. They are the main driving forces to seek alternative renewable energy to offset dependence on fossil fuels. As a member of the G7, Canada pledged to phase out on fossil fuels and reformed fiscal support for oil and gas production to seek a low carbon economy [2]. Renewable resources like solar, wind, tidal, and biomass show high potentials to meet the requirements of sustainable development with a low carbon economy, and solar energy is the most abundant among those above.

In Canada, 17% of the total energy produced is consumed by households, and 82% of this amount is utilized for space and water heating [3]. Solar thermal systems are promising applications to mitigate the dependence of fossil fuels for domestic heating needs. The solar collector captures and converts solar energy into thermal energy to fulfill household demands. A successful precedent near Calgary, Alberta,

is the Drake Landing Solar Community (DLSC), where more than 90% of the residential space heating demand was fulfilled by solar energy over the 2012- 2016 period [4]. During the summer season, solar energy was harnessed and converted into thermal energy. The energy that was not immediately needed was stored underground using the borehole thermal energy storage, where it could be accessed during the wintertime when solar irradiance was less intense. It showed a reduction of approximately five tonnes of annual greenhouse gas emissions per home. This demonstrated the great advantage of solar thermal systems for sustainable development and low carbon economy.

Although Ontario does not receive as much solar irradiance as Alberta (Fig 1.1), solar water heating systems have the potential for a significant reduction in non-renewable energy consumption in single house applications. For instance, an SDHW system can meet 50% of hot water demands for a four-person household and reduce up to two tonnes of CO_2 emissions annually [5]. Given that a better understanding of the SDHW system is beneficial for a low-carbon economy and their exploitation, this thesis is motivated to study the performance of an SDHW in a single household.

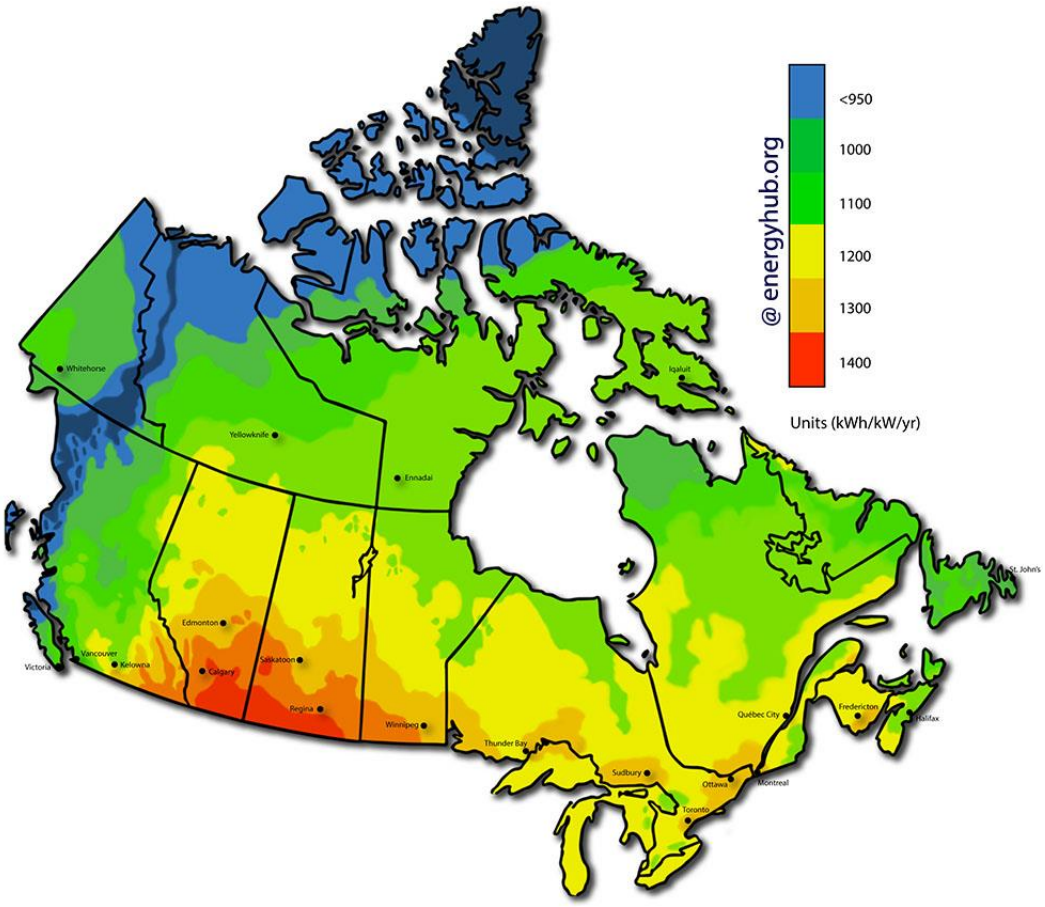

Figure 1.1 Solar irradiance map for Canada [6].

Numerical simulations are cost-effective, time-efficient, and allow for quick adjustment of system parameters. In this thesis, the commercial system simulation computer code TRNSYS-17 [7] is used to study system performance under a range of operating conditions.

1.2 Research Motivation

A typical SDHW system for a single household consists of a solar collector, thermal energy storage (TES) tank, auxiliary tank, etc. as Fig 1.2. The collector harnesses the energy from the sun and heats the fluid passing through the collector. The heated fluid enters the top of the TES tank for storage. Concurrently, the fluid from the bottom of the TES will be drawn at the same flow rate to the collector. When household demand occurs, hot water from the top of the auxiliary tank is extracted and sent to the user. The same amount of cold water from the mains simultaneously enters the bottom of the TES.

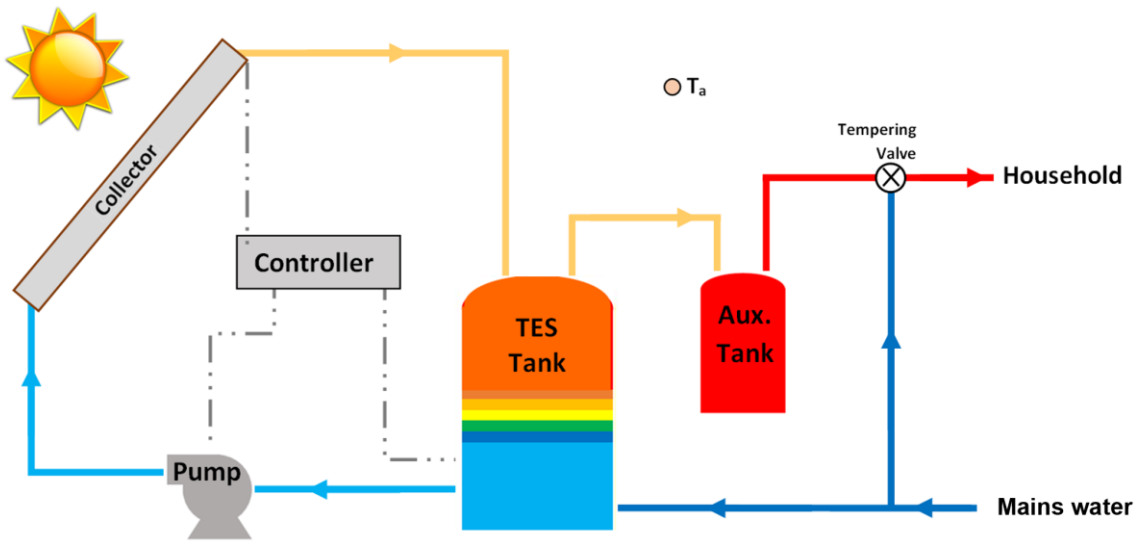

Figure 1.2 Schematic diagram for a forced SDHW system. T_a represents the ambient temperature.

Due to the sporadic nature of solar irradiance and the stochastic characteristic of household demand, a TES is required to preserve the thermal energy from the collector to meet the household demand when the solar radiation is insufficient. Researchers have discovered that by promoting thermal stratification within a TES will substantially enhance system performance in comparison to a well-mixed TES [8]–[10]. System performance is demonstrated in Fig 1.3 for a perfectly stratified tank and a well-mixed tank over a year, and the perfectly stratified tank yields a higher solar fraction. In a perfectly stratified tank system, the cold fluid at the bottom of the tank is sent to the collector inlet, and the collector performance is enhanced. Consequently, system performance is also promoted. In the case of the fully mixed tank system, the temperature distribution is uniform across the tank; thus, the warmer fluid is sent to the collector. The system incurs more collector losses, which leads to poor system performance. Therefore, significant attention has been paid in the research community to enhance thermal stratification in the TES tank ever since.

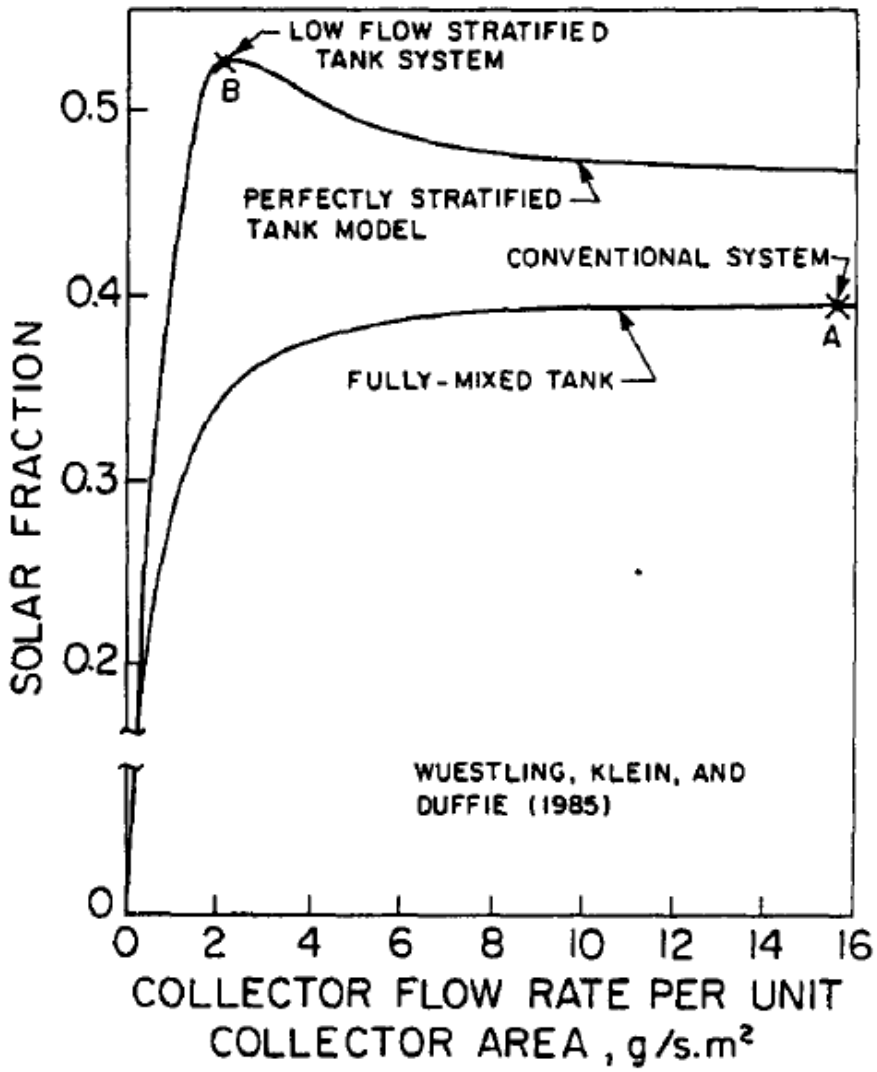

Figure 1.3 Annual fraction solar vs. collector flow rate [8].

Thermal Stratification within the TES

Thermal stratification in a TES can be achieved through the careful introduction of fluid into the tank at the inlet and outlet ports to avoid mixing with the adjacent fluid. Buoyancy can enhance stratification if the incoming fluid is hotter than the fluid at the top of the tank and if inlet jet mixing is minimized. If the incoming fluid is cooler than the adjacent fluid, however, buoyancy will act to enhance mixing through plume entrainment. This has motivated the development of special diffusers that act to reduce the vertical component of momentum [11]–[13], or to release the incoming fluid at the appropriate height in the tank to maintain the stratification [14], [15]. A well stratified, moderately stratified, and a well-mixed tank is demonstrated in Fig 1.4 (a) (b) (c).

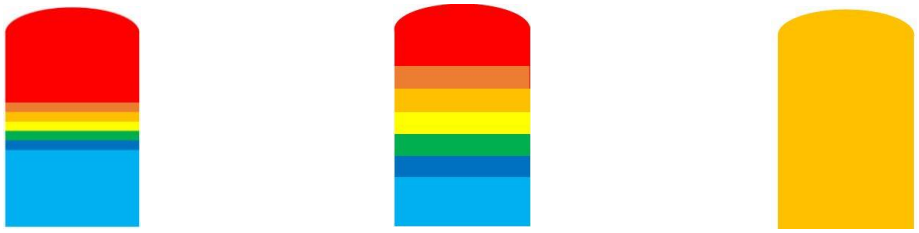

(a) (b) (c)

Figure 1.4 Different degrees of thermal stratification within a TES tank subject to the same amount of energy stored. (a) Highly stratified, (b) moderately stratified, and (c) unstratified or well-mixed tank.

The accepted explanation for the system performance benefits of thermal stratification within the solar thermal research community is that mixing within the tank will result in sending warmer fluid to the solar collector, thus reducing collector performance due to increased heat losses. Moreover, mixing acts to reduce the temperature at the top of the tank results in the household receiving cooler fluid and thus increasing auxiliary power requirements.

An energy balance on a solar thermal system (Chapter 2) reveals, however, that the annual performance is actually dictated by the heat losses from the collector. As such, the role of thermal stratification is in maintaining cool water at the bottom of the tank. This suggests that the research focus should be on reducing inlet jet mixing during tank discharging to maintain cool mains water at the tank bottom, rather than on reducing mixing at the top of the tank. Moreover, the emphasis on stratification within the community has resulted in a promotion of low flow rates through the solar collector. As will be discussed in Chapter 2, the use of a low collector flow rate acts to reduce collector efficiency, thus increasing collector heat losses. This thesis will use numerical modeling to explore solar thermal system performance to assess the relative importance of these effects.

1.3 Objective and Strategy

This thesis aims to numerically study the role of the TES in determining the SDHW system performance. In the context of a system energy balance, the system performance, measured using solar fraction, will be evaluated from the perspective of the bottom temperature in the TES.

The commercial software, TRNSYS-17, will be used to simulate the system behaviors. TRNSYS uses the finite difference method (FDM) to solve a series of differential equations that describe the entire system. The results will be supported by the completion of the components and system verifications. Subsequently, the TES thermal behaviors and system performance will be investigated at various mass flow rates in the collector and load side and also in different TES volumes.

1.4 Thesis Outline

This thesis is divided into chapters for a review of literature, verification of the TRNSYS models, and discussion of the results.

Chapter 2 is a literature review for SDHW systems, including the operation, classification and assessment of the system, classification and performance of solar collectors, thermal stratification and mechanisms that destroy stratification within the TES, classification of the load profiles and system modeling will be discussed as well.

Chapter 3 includes the verification of components such as the solar collector, TES tank, auxiliary tank, and system model. The TRNSYS simulation results for the collector and the tanks will be compared to the analytical solutions. The system model will be verified with published results.

Chapter 4 explores the system performance influenced by the key parameters, including the magnitude of the collector mass flow rate, degree of thermal stratification, and duration of fluid passing through the collector.

Chapter 2
Literature Review

Introduction

The thermal energy storage (TES) tank plays a significant role in determining the solar domestic hot water (SDHW) system performance and will be extensively discussed in this literature review chapter. This chapter will also emphasize the following:

2.1 The operation, classification, and assessment of the SDHW system

2.2 Collector classification and performance

2.3 TES tank

- Thermal stratification
  - mechanisms that destroy thermal stratification
  - techniques that enhance thermal stratification
- Effect of tank volume on system performance

2.4 The classification of the load profiles

2.5 System modeling

2.1 The SDHW system

An SDHW system can be divided into the solar collector side and load side, as demonstrated in Fig 2.1. The solar collector side consists of solar irradiance, solar collector, controller, pump, and TES tank. The load side contains the TES tank, auxiliary tank, tempering valve, household demands, and the mains water. In this subsection, the operation and classifications of SDHW systems will be summarized, and the assessment of system performance will be discussed as well.

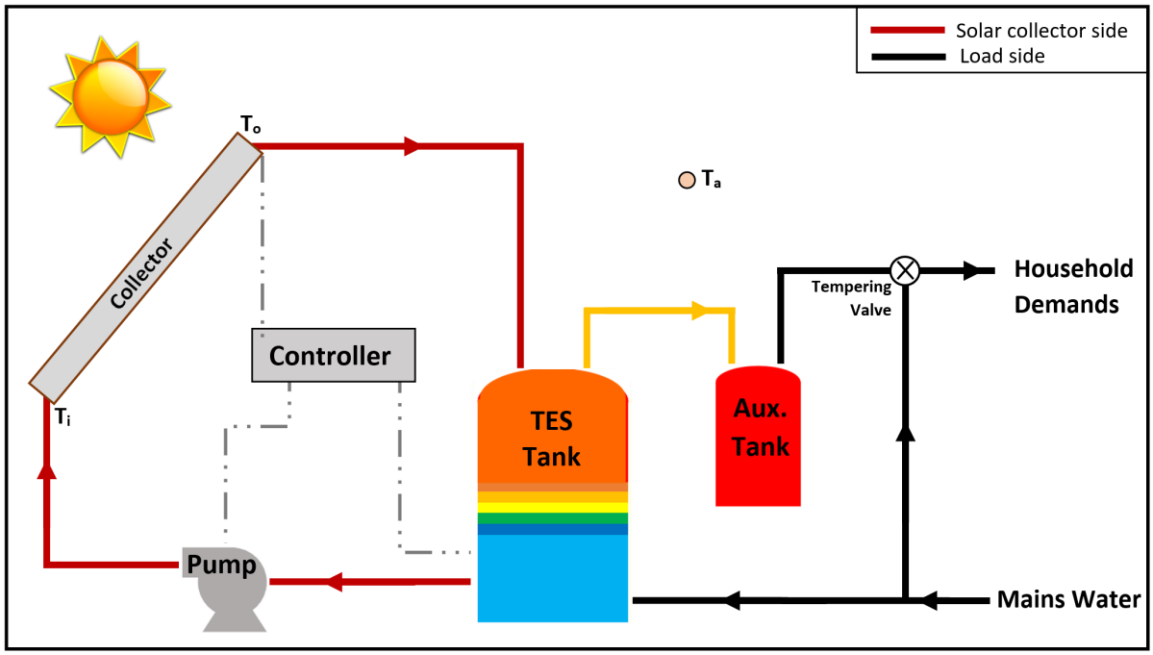

Figure 2.1 Schematic diagram for a forced SDHW system. T_i, T_o, and T_a represent the collector inlet, outlet, and ambient temperature, respectively.

Operation of SDHW Systems

On the solar collector side, two thermal sensors are installed at the bottom of the TES and the outlet of the solar collector, respectively. They will continuously provide feedback to the controller to determine the activation of the pump. The most common pump control strategy used is to monitor the temperature difference between the collector inlet and outlet (ΔT). The pump will be activated when ΔT exceeds an upper temperature deadband (ΔT_{on}) and remain active until ΔT drops below a lower temperature deadbnd (ΔT_{off}).

On the solar collector side, heated fluid exits the collector and enters the top of the TES. If the entering fluid is hotter than the fluid near the inlet, then the buoyancy force opposes the inlet momentum. As a result, a negative buoyant plume is created, whereas a positive buoyant plume occurs when cooler fluid enters the TES. Both cases introduce turbulence and plume entrainment, which will de-stratify the TES tank, and these mechanisms will be discussed in detail in Section 2.3. While the heated water enters the top of the TES, the same amount of water at the bottom of the TES enters the collector concurrently.

On the load side, when the household demand occurs, the water on the top of the TES will be sent to the auxiliary tank, and the top portion of the auxiliary tank will

be extracted to the user. Simultaneously, the same amount of mains water will be introduced to the bottom of the TES. If the service water is cooler than the preset household temperature, T_{set} (60°C), the electric heater in the auxiliary tank will supplement such temperature difference. In contrast, when the service water is hotter than T_{set}, a tempering valve will introduce cold water from the mains to dilute the “overheated” fluid to preclude scalding.

Classification of SDHW Systems

Depending on the method used to transfer the fluid, SDHW systems are classified as either active (forced) or passive. The fluid is circulated by a pump in an active system, whereas the fluid is transferred passively due to the thermosyphon effects in a passive system. Similarly, depending on the methods of energy transfer, SDHW systems can be characterized as direct or indirect systems. A direct system transfers thermal energy by heating the service water through the solar collector. The service water subsequently enters the thermal energy storage tank directly. An indirect system employs a heat exchanger between the solar collector and the thermal storage tank. This arrangement is required in cold climates since an anti-freeze glycol solution is used in the collector to complete the energy transfer. Since thermal energy can be stored as either sensible or latent heat, SDHW systems can

be categorized by their respective thermal energy storage methods. In a sensible heat storage system, thermal energy is stored by raising the temperature of the fluid. In a latent heat storage system, thermal energy is preserved with the occurrence of a phase change process. A comprehensive outline of SDHW systems is illustrated in Fig 2.2 [16]. This thesis involves studying an active direct SDHW system with a sensible energy storage method.

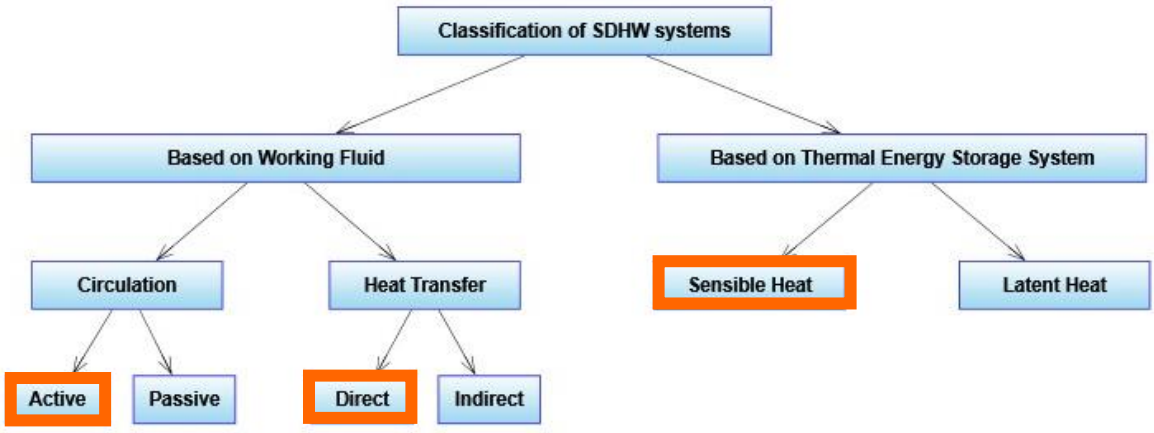

Figure 2.2 Classification of SDHW systems [16]. This study will focus on an active direct system with sensible heat storage.

Assessment of the SDHW System

The thermal performance of a SDHW system is usually evaluated over a period, and the two figures of merit commonly used are the solar fraction and the solar saving fraction. The solar fraction (Equation 2.1) is the ratio of useful energy harnessed by the solar system to the total energy required to meet the load demand.

$$f = \frac{Q_{from\ SDHW\ system\ to\ load}}{Q_{load}} \tag{2.1}$$

The solar fraction neglects the parasitic electrical energy consumed by the pump, controller, or other electric components within the system; whereas, the solar saving fraction counts the effects of these parasitic electrical costs. It was found that increasing the pump work by 35% lead to a 2% drop in system performance. For the scope of this thesis, the pump work is neglected, and the solar fraction will be used to evaluate the performance of a SDHW system.

2.2 Collector Classification and Performance

The solar collector harvests and converts solar energy into thermal energy, which is transferred by a passing fluid. A collector can be classified by its concentration ratio as either non-concentrating (stationary) or concentrating [17]. A stationary collector directly harnesses the beam radiation to its receiving area; whereas a sun-tracking concentrating collector is usually equipped with a concaved surfaces to harness solar energy. A comprehensive summary of various collectors is listed in Table 2.1 [17].

A most commonly used stationary solar collector is the flat plate collector (FPC), which is suitable for low-temperature applications under 100°C and will be used in this study. A typical FPC is shown in Fig 2.3 [18], [19]. Solar radiation passes through the transparent outer shield (usually glass) and impinges onto the energy-absorbing surface (usually coated with chromium). Insulation materials are installed on the bottom of the FPC to reduce the heat losses to the surroundings. A large portion (~50%) of radiation is captured and goes toward heating the fluid for immediate use or storage. In addition, the FPC is often permanently oriented towards the equator, and the optimum tilt angle is equivalent to the latitude of the location with a tolerance of 10-15° [18].

Table 2.1 Solar Energy Collectors Summary [18].

Motion	Collector type	Concentration ratio	Indicative temperature range (°C)
Stationary	Flat plate collector (FPC)	1	30-80
	Evacuated tube collector (ETC)	1	50-200
	Compound parabolic collector (CPC)	1-5	60-240
Single-axis tracking	Linear Fresnel reflector (LFR)	10-40	60-250
	Parabolic trough collector (PTC)	15-45	60-300
	Cylindrical trough collector (CTC)	10-50	60-300
Two-axes tracking	Parabolic dish reflector (PDR)	100-1000	100-500
	Heliostat field collector (HFC)	100-1500	150-2000

***note: the concentration ratio is defined as the ratio of the aperture area to the receiver area.**

(a)

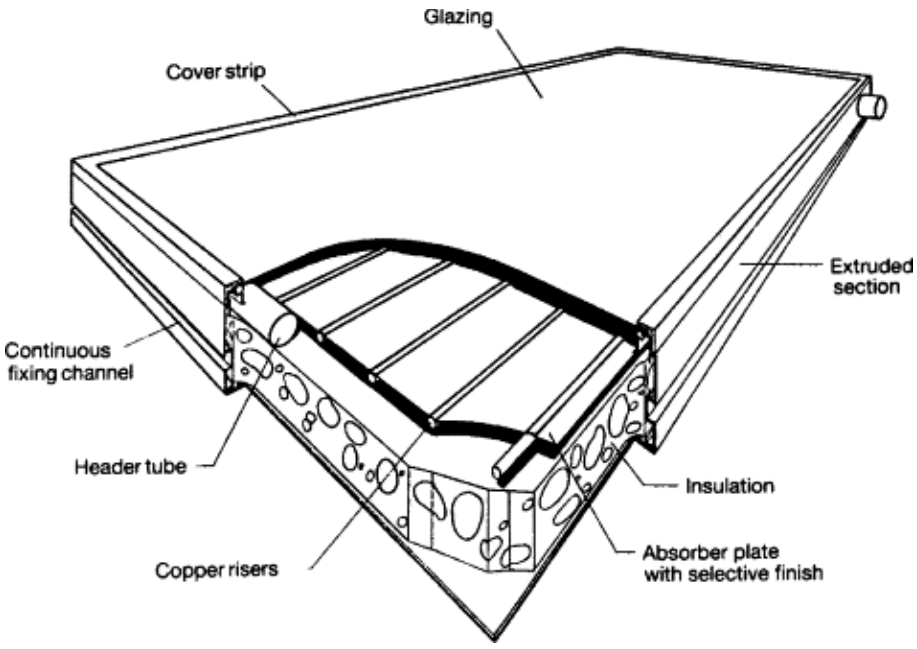

(b)

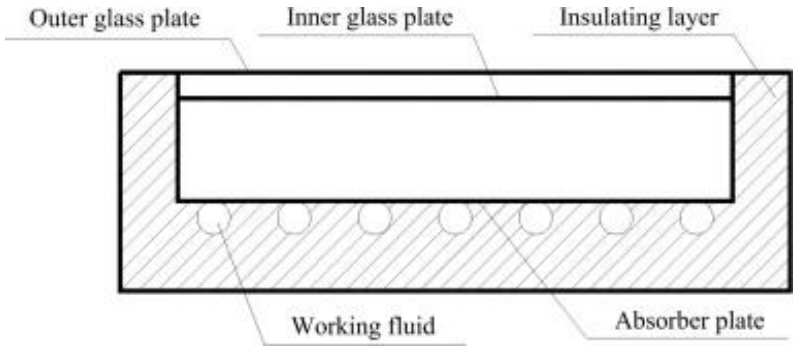

Figure 2.3 Schematic of a Flat-Plate Collector. (a) Pictorial view of an FPC [18]. (b) Cross-section view of an FPC [19].

Flat-plate collector (FPC) performance is characterized by the Hottel-Whillier-Bliss relationship (Equation 2.2). The heat removal factor, F_R, is defined in Equation 2.3. While the collector mass flow rate, $\dot{m}_{coll}$, is reduced, F_R is consequently reduced; hence, the solar collector performance is downgraded. However, reducing $\dot{m}_{coll}$ enhances the thermal stratification within a TES tank and results in the working fluid entering the solar collector at the coldest possible temperature, thus improving the collector performance. Reducing $\dot{m}_{coll}$ causes two contrary effects, the benefit of sending cold fluid to the collector inlet outweighs the collector losses due to the reduction in F_R [8], [9], [20]. When $\dot{m}_{coll}$ is maintained high and T_i is kept low, the collector performance will be at an optimum. More analysis of the collector performance influenced by $\dot{m}_{coll}$ and the collector area (A_c) is available in Appendix A.

$$\eta_{collector} = \frac{Q_u}{A_c * G} = F_R(\tau\alpha) - F_R U_L \frac{T_i - T_a}{G} \quad (2.2)$$

$$F_R = \frac{\dot{m}_{coll} * C_p}{A_c U_L}\left[1 - exp\left(-\frac{A_c U_L F'}{\dot{m}_{coll} * C_p}\right)\right] \quad (2.3)$$

Where Q_u = useful energy collected by the flat plate solar collector

A_c = collector area

G = solar radiation per unit area incident on collector plane (solar irradiance)

$F_R(\tau\alpha)$ = intercept of the collector efficiency versus $(T_i-T_a)/G$ curve

$F_R U_L$ = negative slope of the collector efficiency versus $(T_i-T_a)/G$ curve

T_i = collector inlet temperature

T_a = ambient temperature

F' = collector efficiency factor

2.3 Thermal Energy Storage Tank

The availability of solar radiation does not always temporally coincide with household demands. This mismatch leads to the need for a TES tank to reserve thermal energy in order to fulfill the household demands until it is needed, particularly when solar radiation is less intense. Extensive studies have proven that enhancing thermal stratification will improve SDHW system performance [8], [9], [21]. An understanding of thermal stratification is thus critical to analyze and study SDHW system performance.

Thermal Stratification

A layering of the fluid based on temperature (thermal stratification) tends to occur in a TES tank due to the buoyancy effect. The degree of thermal stratification within the tank is dependent on numerous factors such as the amount of mixing due to the inlet jets, the inlet temperature of the fluid in comparison to the fluid temperature in the vicinity of the port, and thermal losses through the tank walls. The degree of thermal stratification is often indicated by the thickness of the thermocline, which is the region between the hot and cold fluid. Fluid mixing in the tank acts to increase the thickness of the thermocline region, thus influencing the stratification, as shown in Fig 2.4.

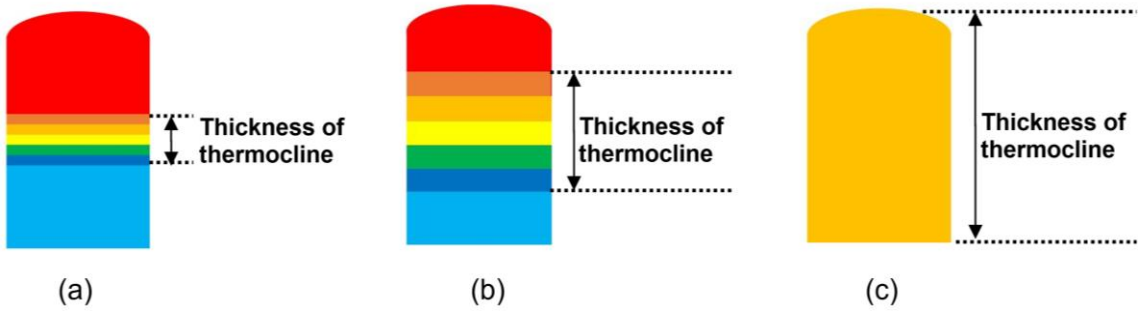

Figure 2.4 Demonstration for the different degrees of thermal stratification within a TES tank when subjected to the same energy content. (a) a highly stratified tank, (b) a moderately stratified tank, and (c) an unstratified or well-mixed tank.

Mechanisms that Destroy Stratification

Several mechanisms that destroy a thermal stratification, including inlet jet mixing, plume entrainment, conduction within the fluid, and heat losses to the environment, will be discussed in this subsection.

Inlet Jet Mixing and Plume Entrainment

When the heated fluid from the collector enters the top of the TES, the momentum of the entering fluid causes shear stress against the fluid on top and promotes mixing in the vicinity of inlet. In addition to generating recirculation zones in the vicinity of the inlet, the tank fluid is entrained into the inlet jet region. Plume entrainment is thus detrimental to thermal stratification.

In terms of the alignment between the directions of momentum and the buoyant force, plume entrainment is classified as negative or positive. When the entering fluid temperature is higher than the fluid temperature in the vicinity of the inlet, a “negative buoyant plume” develops. Under this condition, the buoyancy force acts to reduce the momentum of the inlet jet and tends to drive the hot fluid towards the top of the tank, thus acting to enhance stratification. This is illustrated in Fig 2.5 by Nizami et al. [22]. Their study established mathematical models that capture the effects of inlet jet mixing caused by negative buoyant plume entrainment in a vertical TES tank. In contrast, if the fluid entering the top of the tank is cooler than the fluid in the vicinity of the inlet, a positive buoyant plume is formed since both buoyancy forces and momentum act in the same downward direction. This is prone to happen in the late afternoon when solar radiation is less intense. A cooler fluid enters the tank, and as the fluid penetrates further, it entrains the surrounding fluids until the elevation with appropriate density is reached. Consequently, significant turbulent mixing is introduced. The degree of mixing that occurs for both negative and positive buoyant plumes is influenced by the ratio of the buoyancy force to the inlet jet momentum. This ratio is given by the Richardson number, which is defined in equation 2.3:

$$Richardson\ number, Ri = \frac{g\ \beta\ (T_{in} - T_{initial})H}{{u_{in}}^2} \quad (2.3)$$

Where, g = gravitational acceleration

β = thermal expansion coefficient

T_{in} = fluid temperature at the tank inlet

$T_{initial}$ = initial temperature within the tank

H = height between the tank inlet and outlet

u_{in} = fluid velocity at the tank inlet

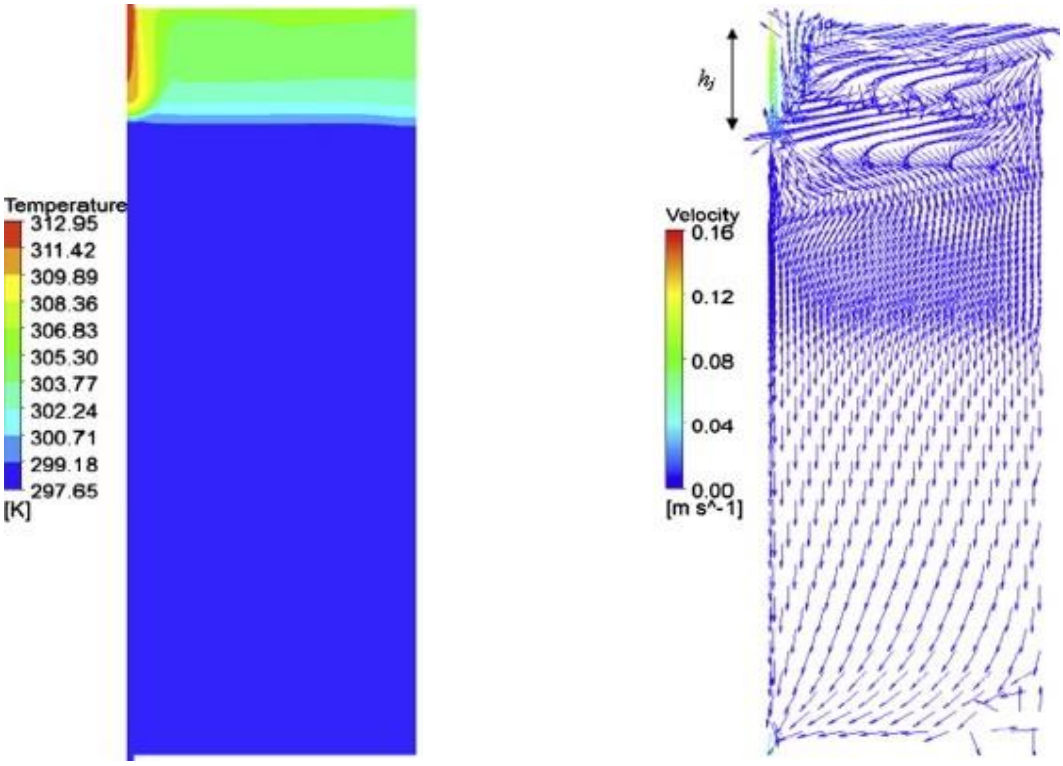

Figure 2.5 CFD predictions of the transient temperature with the occurrence of a negative plume within a TES [22].

Heat Losses within a TES tank and to the Environment

Thermal de-stratification due to conduction heat transfer within the fluid is not significant since charging and discharging occur frequently. Even under idling conditions, which occur when charging and discharging are absent, the tank is isothermal in the radial direction, and its temperature degrades slowly along the vertical direction [23]. Jaluria and Gupta [8] experimentally investigate the decay of thermal stratification within an enclosed tank, where no fluid entered or exited the tank. They found that the temperature initially dropped in the top surface, accompanied by a temperature rise in the bottom of the tank. Later, the temperature dropped throughout the tank. They also revealed that the stratification decay could be modeled as a one-dimensional conduction problem.

Techniques to Enhance Stratification

Enhancing thermal stratification within a TES tank improves the SDHW system performance. Inlet and outlet configuration plays a significant role in thermal stratification enhancement, including port location, employment of baffles, diffusers, and stratifiers. Research has been conducted to verify various effects on thermal stratification, including the tank geometry and inlet/outlet configuration.

Researchers [10], [24], [25] found that a higher aspect ratio (L/D) TES tank during charging simulations is more efficient. Lavan and Thompson [10] found that the aspect ratio of 3-4 appears the most optimal, given the tradeoff between the cost and performance. Furthermore, they concluded that the location and geometry of the inlet port are more crucial than the outlet port.

Zuirigat et al. [26] numerically investigated the inlet geometry effects on the thermocline in a cylindrical thermal storage tank. They also validated the numerical solutions with experimental data. They discovered that the inlet geometry no longer influences the thermal stratification when the Richardson number limit, 3.6, is reached.

The eddy vorticities introduced at the inlet and outlet of the tank will destroy thermal stratification. Numerous studies have demonstrated the enhancement in thermal stratification by employing baffles, diffusers, and plates [11]–[13], [27]. Adams and Davidson[14], [15] experimentally investigated the degree of thermal stratification within a storage tank using rigid and flexible, porous manifolds subject to both charging and discharging conditions. They proved that the thermal stratification was maintained by engaging such a device.

Thermal Energy Storage Volume

As discussed in section 2.2, solar collector efficiency is enhanced by increasing the collector flow rate and by reducing the collector inlet temperature, which is strongly influenced by the volume of the storage tank and the degree of stratification. The tank volume is thus a key variable in the assessment of solar system performance.

Shariah and Lof [28] numerically studied the thermosyphon SDHW system performance influenced by the TES geometry, such as the tank height, and the storage tank volume to collector area ratio (V_{TES}/A_c). The simulations were conducted in TRNSYS with the weather data of Los Angeles, California for a full year, and a load profile where the high-load-demands scattered in the morning and evening (RAND profile) was imposed. It had a negligible influence on solar fraction when the tank height exceeded 1m. Furthermore, the solar fraction increased substantially before V_{TES} reached 150 L and remained nearly constant until 200L, then decreased slightly after 200L for a $4m^2$ collector. Later, Hawlader and Ullah [29] also discovered a similar trend for the solar fraction in a solar-assisted-heat-pump water heating system. They concluded that the system performance would not be significantly affected when the TES volume exceeded

100L per unit collector area when operating under meteorological conditions in Singapore.

Comakli et al. [30] simulated the transient SDHW system, which was subjected to the weather in Erzurum, Turkey, using MATLAB. They found that increasing the volume of the TES would benefit collector performance with accompanying a decrease in the temperature of the TES.

2.4 Load Profile

Residential Domestic Hot Water (DHW) load demand is stochastic and time-dependent. It is significantly influenced by factors such as geographic location, time of the year, and the number of occupants. The magnitude and timing of the load are crucial to determine whether a system is capable of meeting the demand. Despite the improvement of accuracy that comes from using a real DHW load profile in predicting system performance, it is common practice to use repeating daily profiles in simulation studies [31]–[33]. Some other researchers relied upon probability methods to calculate load profile [34]–[36]. Edwards et al. [37], however, gathered annual load data from 73 houses in Quebec, Canada, and discovered that both the magnitude and drawn time could significantly influence the simulation predictions in TRNSYS.

Fig 2.6 is the time-dependent RAND profile adopted from Csordas [38], where the high-load-demands scatter in the morning and evening. Duffie and Beckman [39] suggested that minor modifications in the time dependence of loads will not have a significant impact on the annual performance of an SDHW system.

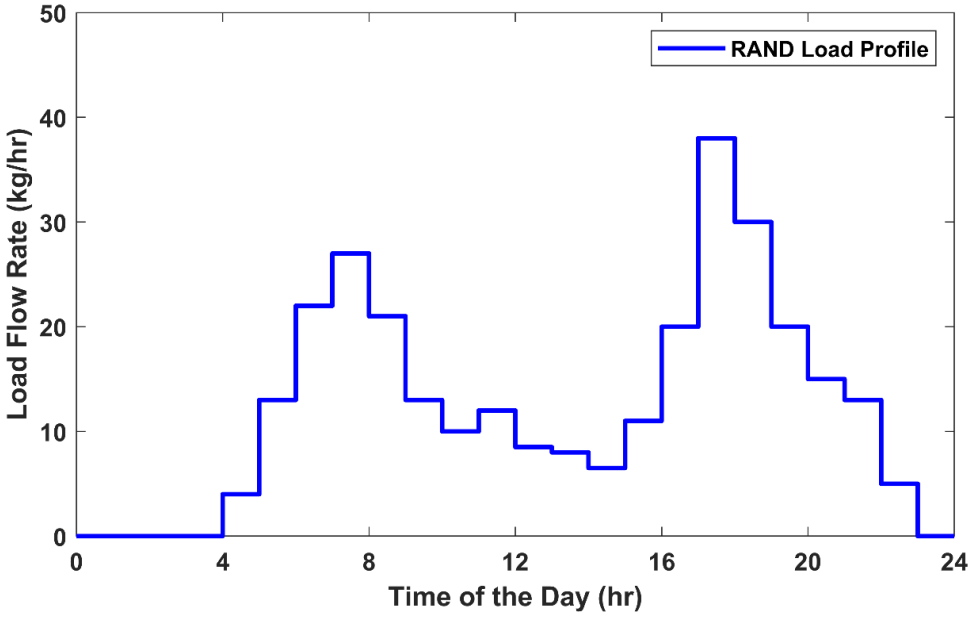

Figure 2.6 RAND Profile adopted from Csordas et al. [38]

Load profile studies conducted in the 1980s by the Canadian Standard Association (CSA) [32] indicate three typical draw profiles of DHW systems for different family sizes, including 150L (1-2 persons), 225L (3-4 persons), and 300L (5 or more persons). These profiles were employed by Dickinson [32] to investigate the effect of discharge configurations on thermal stratification of multi-tank storage. The three load profiles are illustrated in Fig 2.7 (a-c), respectively.

(a)

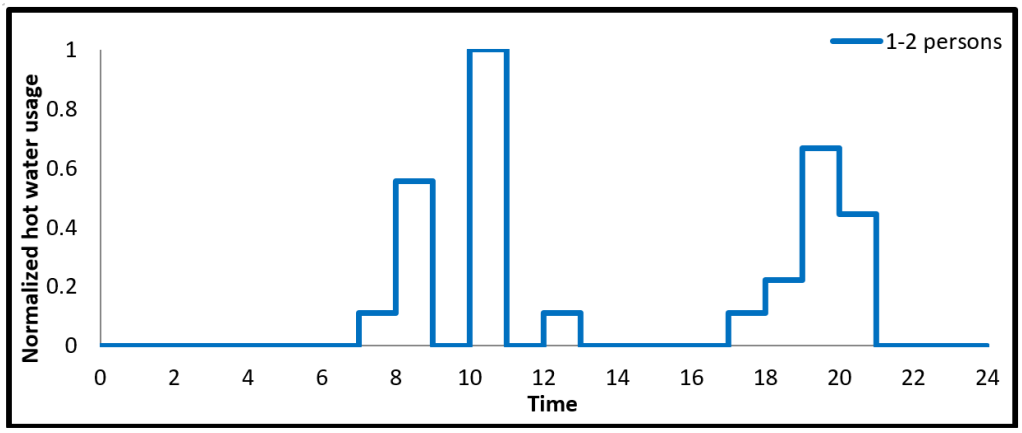

(b)

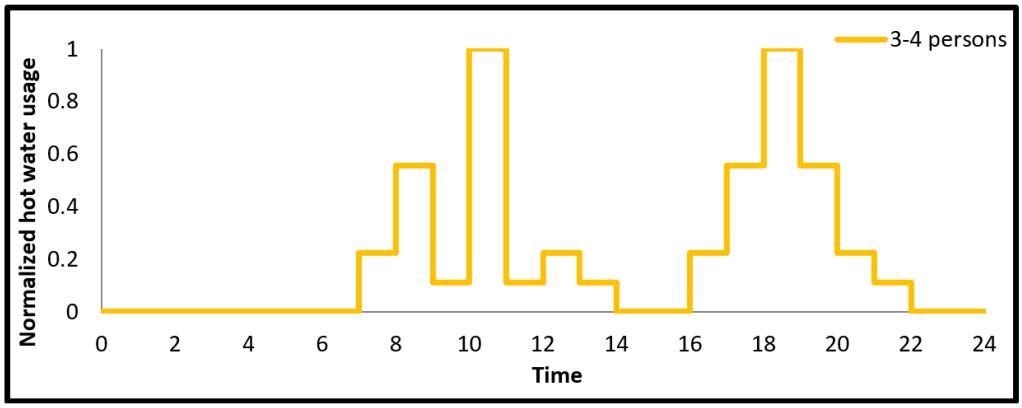

(c)

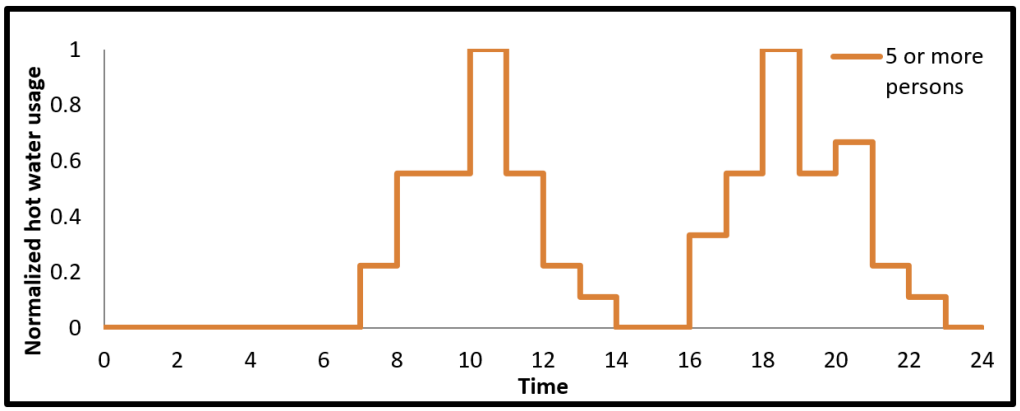

Figure 2.7 Canadian Standards Association load profiles for various family sizes [32]. (a) family of 1-2 persons, (b) family of 3-4 persons, and (c) family of 5 or more persons.

2.5 System Modelling

Proper sizing of an SDHW system is a complex problem that involves interactions between components and unpredictable weather and load data inputs. Numerical studies of SDHW systems allow for quick parameter adjustments, leading to a thorough understanding of the system.

TRNSYS is commercial software developed by the Solar Energy Laboratory, University of Wisconsin-Madison, which will be used as the simulation tool in this thesis. TRNSYS uses a finite difference method (FDM) to solve the series of differential equations, and is capable of simulating and predicting the performance of thermal transient systems. Weather data of more than 1000 locations are available in over 150 countries.

System Energy Balance

In the context of system energy balance, the rate of energy change of the system shown in Fig 2.8 is reflected in Equation 2.4. Assuming the initial and final conditions for the system are identical, Equation 2.5 demonstrates the energy balance for the system over a year. It yields an equation for solar fraction (f), which is calculated in terms of solar radiation ($Q_{sun\ in}$), thermal losses from both TES and auxiliary tanks ($Q_{LossTanks}$), collector losses ($Q_{LossColl}$), useful energy gain from the

collector (Q_u = $Q_{sun\ in}$ - $Q_{LossColl}$) and the household heating demand (Q_{load}) in equation 2.6.

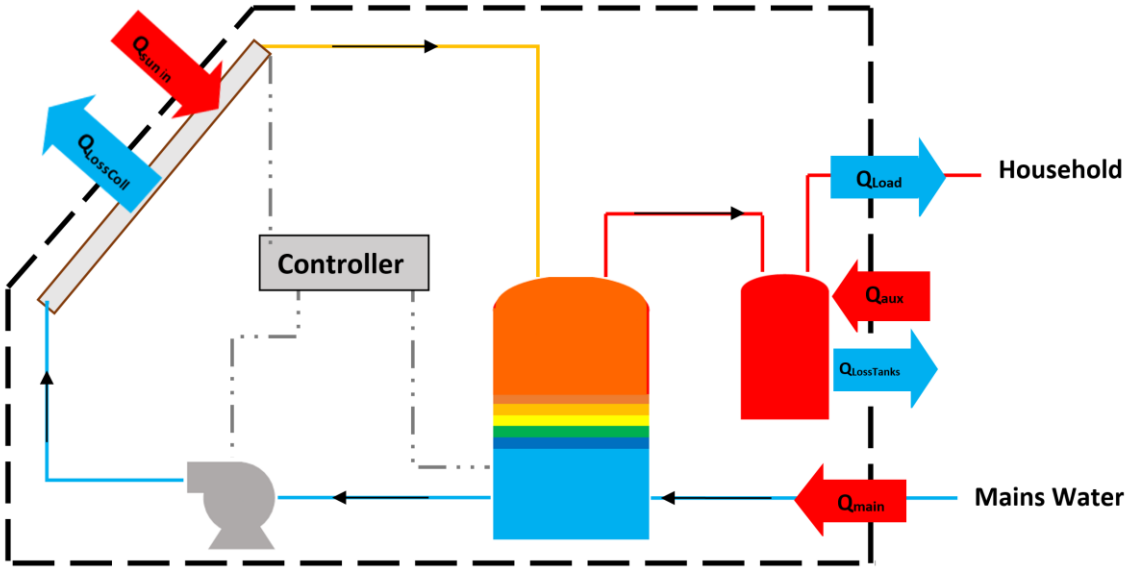

Figure 2.8 Energy balance for the SDHW system.

$$\frac{dE}{dt} = \dot{Q}_{sun\ in} + \dot{Q}_{aux} - \dot{Q}_{loss\ Tank} - \dot{Q}_{lossColl} - \dot{m}C_p(T_{load} - T_{main}) \qquad (2.4)$$

$$Q_{sun\ in} + Q_{aux} - (Q_{lossColl} + Q_{lossTanks}) - Q_{load} = 0 \qquad (2.5)$$

$$f = \frac{Q_{sun\ in} - (Q_{LossTanks} + Q_{LossColl})}{Q_{load}} = \frac{Q_u - Q_{LossTanks}}{Q_{load}} \qquad (2.6)$$

Numerous studies were conducted to better understand SDHW system performance and the effects of individual components on the system performance by adjusting input parameters. However, the previous studies usually focused on a predetermined volume of a TES tank. They rarely considered the effects of various TES tank volumes in the context of system energy balance. This subsection summarizes the literature pertaining to the system performance in the context of a system energy balance perspective.

Buckles and Klein [33] numerically studied the influences on the system performance as a function of the number of tanks, insulation, storage capacity, and daily draw value. Four types of SDHW systems were modeled over a month, and their solar fractions were compared in TRNSYS simulations. The four types systems are Type 1 - single tank, direct system (Fig 2.9-a), Type 2 - dual tank, direct system (Fig 2.9-b), Type 3 - single tank, indirect system (Fig 2.9-c), and Type 4 - dual tank, indirect system (Fig 2.9-d). The system performance was assessed by solar fraction, which was defined by an energy balance for the entire system. The three methods of determining a solar fraction were demonstrated in Equation (2.7-9), and equation 2.8 was used in their study.

$$f_1 = \frac{Q_{load} + Q_{loss} - Q_{aux}}{Q_{load} + Q_{loss}} \tag{2.7}$$

$$f_2 = \frac{Q_{load} - Q_{aux}}{Q_{load}} \tag{2.8}$$

$$f_3 = 1 - \frac{Q_{aux}}{Q_{aux-nonsolar}} \tag{2.9}$$

The study discovered that the system performed nearly identically when the tank(s) was(were) insulated. In systems with the well-insulated tank(s), Type 1 system (least tank surface) performed best among the four, and Type 4 (most tank surface) ranked last mainly due to the thermal loss from the tank. However, the study did not investigate the collector inlet temperature, and the tank was poorly stratified (3 nodes), which lead to skepticism in the accuracy of the predictions.

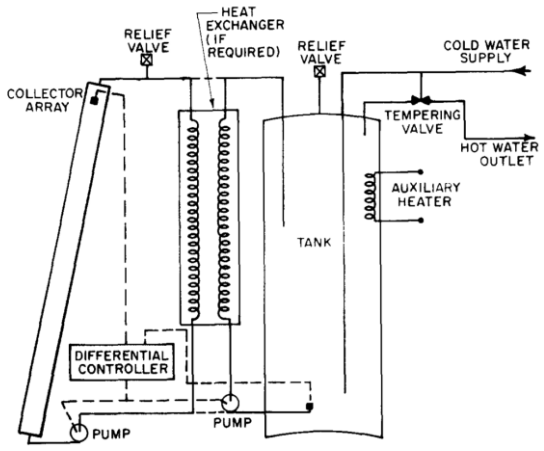

(a) Single tank, direct system

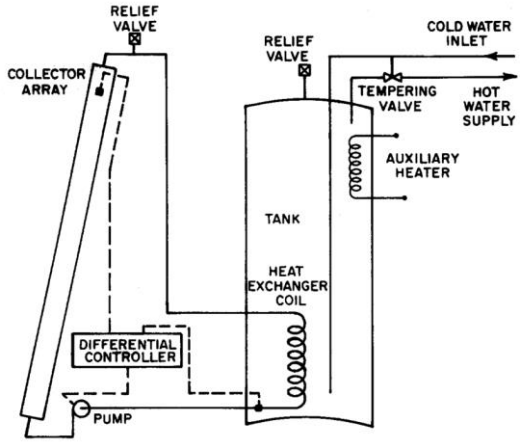

(c) Single tank, indirect system

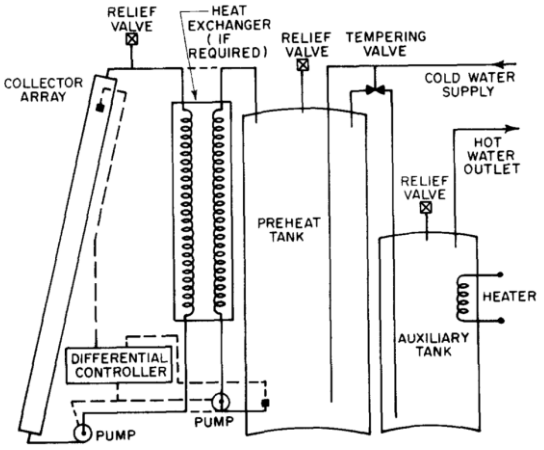

(b) Dual tank, direct system

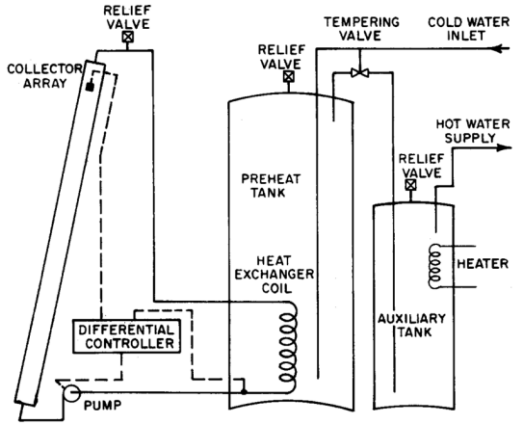

(d) *Dual t*ank, indirect system

Figure 2.9 Four SDHW systems studied by Buckles and Klein: (a) single tank, direct system; (b) dual tank, direct system; (c) single tank, indirect system; (d) dual tank, indirect system [33].

Recently, Teamah et al. [40] also estimated the solar fraction in the context of system energy balance to investigate the benefits of engaging phase change materials (PCMs) in an SDHW system. The enthalpy-porosity method was utilized to model the phase change process, and the study defined a tank to be undersized when the tank volume was less than the total daily household demand. The incorporation of PCMs in an undersized TES tank will lead to better system performance; this is because colder fluid was sent to the collector inlet by engaging the PCMs, thus leading to a reduction in collector losses. However, the system exhibited less sensitivity to such benefits as the tank capacity was enlarged.

Conclusion

This chapter summarized a variety of types of SDHW systems, their operation principles and also introduced the main components of an SDHW system. It was established that the TES tank thermal behavior is a crucial factor in determining SDHW system performance. The mechanisms that destroy thermal stratification, such as inlet jet mixing, plume entrainment, and heat losses within the tank or to the surroundings, were discussed. The effects of the TES volume were summarized as well. The load profile also plays a role in determining whether the household heating demands will be met and directly relates to system performance. The chapter ends with a discussion of the system modeling and energy balance.

Chapter 3
Verification for the SDHW System and Components

Introduction

TRNSYS is a commercial simulation tool that connects a series of components to predict the behaviors of a transient system, such as a solar domestic hot water (SDHW) system. TRNSYS employs a finite difference method to solve differential equations that describe the entire system. The TRNSYS model of the SDHW system studied in this research is illustrated in Fig 3.1. Successful verification of the models and their coupling provides confidence in predictions of system behaviors.

This chapter summarizes the model verifications of the main components, including the flat plate solar collector, thermal energy storage (TES) tank and auxiliary tank. The timestep sensitivity of each component model was studied, and the grid size sensitivity for both tanks was explored. The simulation results of these components were compared to their respective analytical solutions. Finally, the SDHW system model was verified with published results by Wuestling et al. [9].

This chapter will be divided into the following sections:

3.1 Collector model verification

3.2 Tank model verification for the TES and auxiliary tank

3.3 System verification

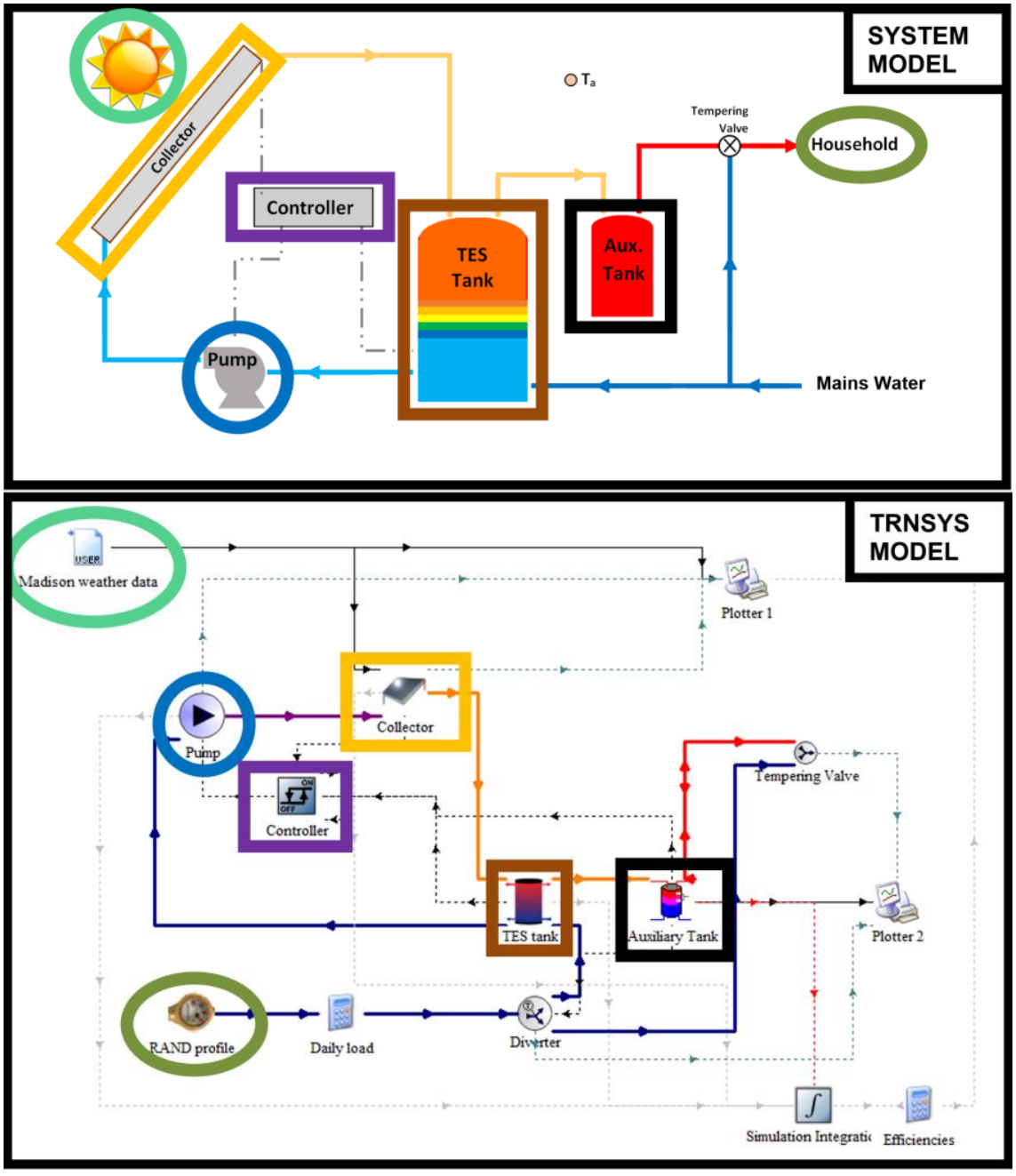

Figure 3.1 The SDHW system layout and its model in TRNSYS. The upper diagram represents the SDHW system layout, and the bottom diagram illustrates the system model in TRNSYS.

3.1 Solar Collector Model Verification

The TRNSYS model of the flat plate collector (Type 1b) was verified in this subsection. Type 1b models the thermal behaviors (collector outlet temperature and the useful energy gain) of a flat plate solar collector by applying an incidence angle modifier to the Hottel-Whillier-Bliss relationship. The Hottel-Whillier-Bliss equation provides an expression for the energy collected as a function of solar collector properties and operating parameters, collector fluid inlet temperature, and weather data. Further information on the modified Hottel-Whillier-Bliss equation is given in Appendix B. TRNSYS predictions for the useful energy gain (Q_u) and collector outlet temperature (T_o) were compared to their respective analytical solutions, which were completed manually. The methods of calculating analytical solutions are also available in Appendix B.

The simulations were conducted on a spring day (May 9) and a winter day (Jan 1), respectively. The typical meteorological year (TMY) weather data used were extracted from the TRNSYS database for Madison, Wisconsin, US [7]. The timestep sensitivity of the model was explored by performing the simulation at two timesteps (30 s and 300 s) over 24 hours, and more collector parameters are shown in Table 3.1.

The simulation results of Q_u and T_o are plotted in Fig 3.2 and Fig 3.3, respectively. It indicates that TRNSYS predictions aligned with the analytical solutions, and model performance is insensitive to the size of the timestep.

Table 3.1 Collector and system parameters for collector verification.

Description	Value (unit)
Collector area, A_c	4.2 (m^2)
$(F_R(\tau\alpha))_{test}$	0.805 (-)
$(F_R U_L)_{test}$	4.73 (W/m^2 °C)
Collector flow rate at testing condition, $(\dot{m}_{coll})_{test}$	72 l/hr- m^2
Collector flow rate used in the simulation, $(\dot{m}_{coll})_{use}$	60 (kg/hr)
Incidence angle modifier coefficient, b_o	0.0989
Incidence angle, θ	45°
Solar irradiance, G	Madison weather on: • May 9 • Jan 1
Ambient temperature, T_a	Madison weather on: • May 9 • Jan 1
Collector inlet temperature, T_i	• May 9: 17.7 (°C) • Jan 1: 8.2 (°C)
Fluid specific heat capacity, C_p	4190 (J/kg K)
Timestep, dt, or Δt	30, or 300 (s)
Simulation time, t	24 (hr)

(a)

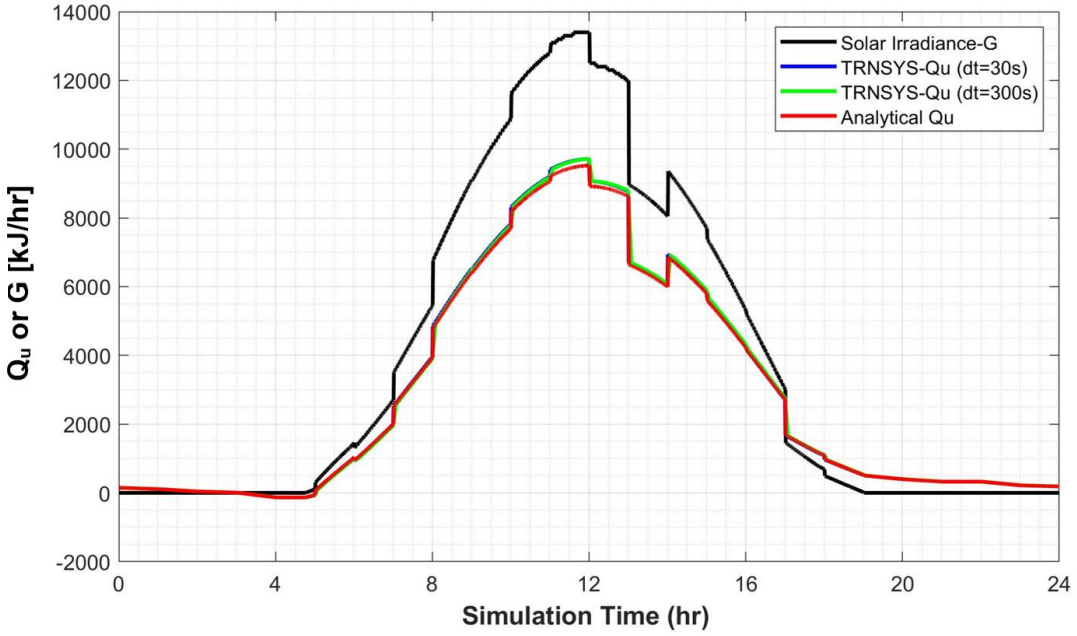

(b)

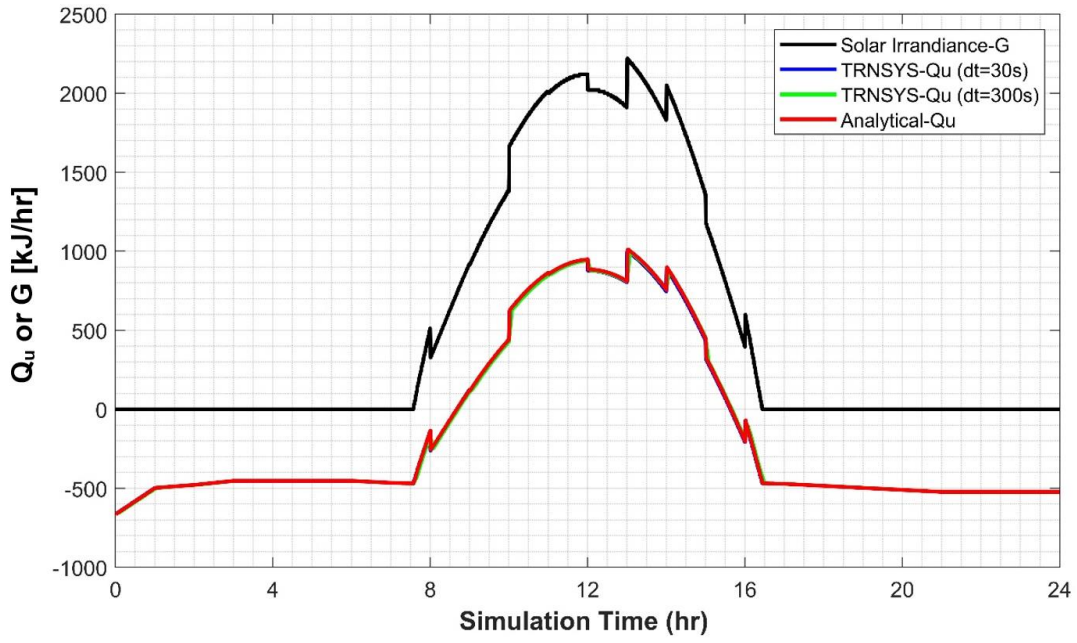

Figure 3.2 TRNSYS prediction of Q_u versus time using (a) spring weather (May 9), and (b) winter weather (Jan 1) in Madison, Wisconsin, US.

(a)

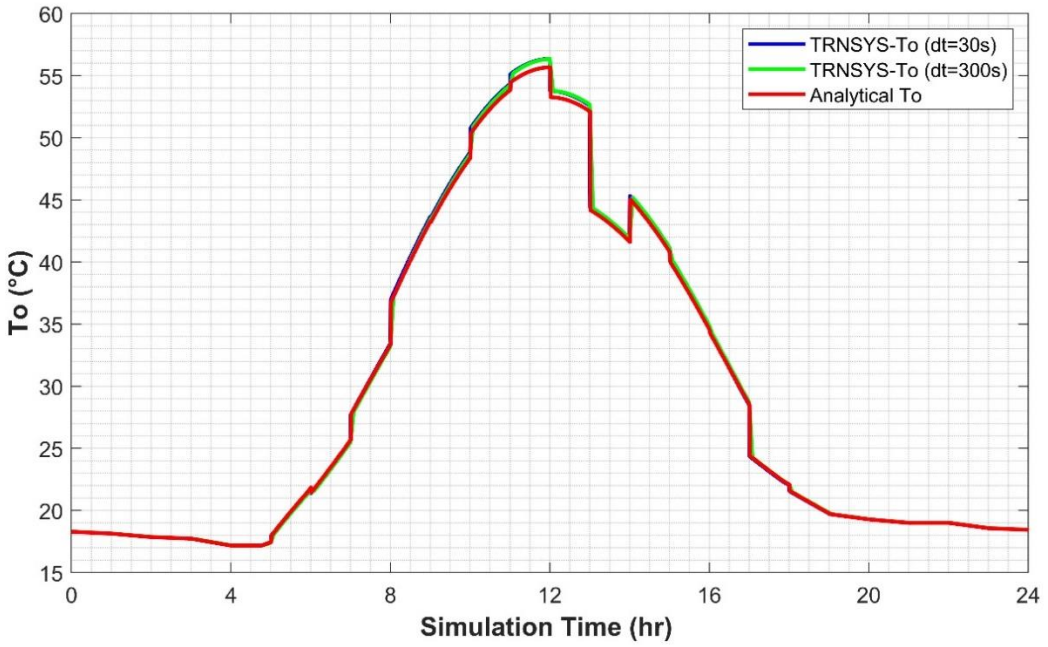

(b)

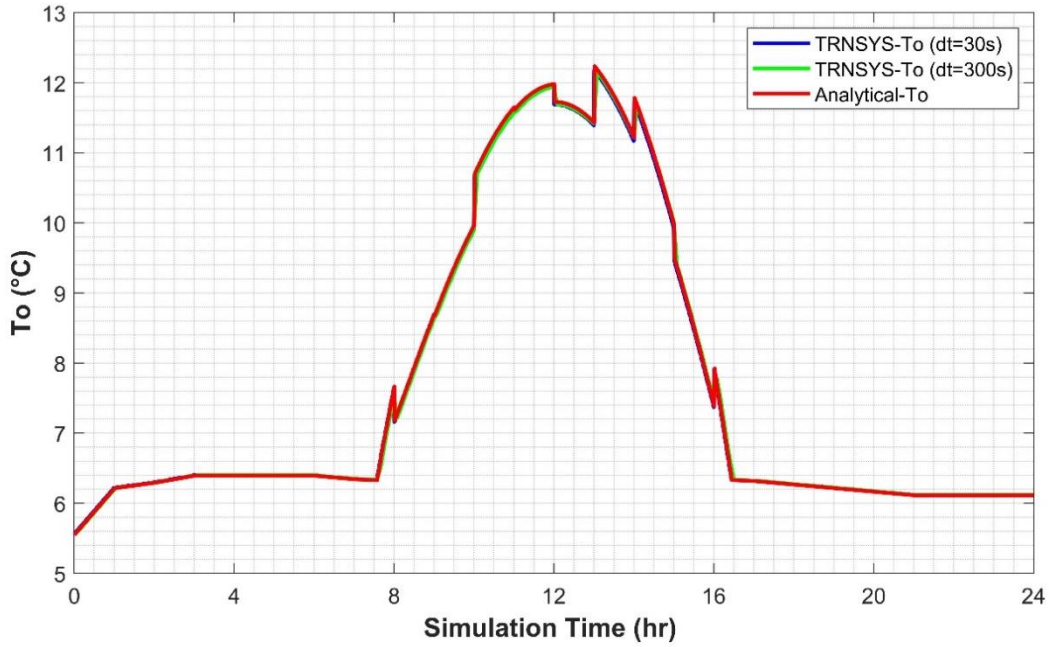

Figure 3.3 TRNSYS prediction of T_o versus time using (a) spring weather (May 9), and (b) winter weather (Jan 1) in Madison, Wisconsin, US.

3.2 Tank Model Verifications

TRNSYS supports numerous one-dimensional tank models. Depending on the method of determining the size of a node (grid spacing), they can be classified as either a predetermined node tank (nodal) or a variable node tank (algebraic). Temperature profiles within the tank model are found from the solution of the one-dimensional transient thermal energy equation where energy transport is via fluid advection, axial heat conduction, and heat losses through the tank wall.

A nodal tank model consists of N isothermal nodes, which are achieved by fully mixing the incoming fluid with the existing fluid in the nodes. The differential equation based on the energy balance of each node is simultaneously solved at the end of each timestep. Type 4, Type 60, and Type 534 are the most frequently used nodal tank models. Type 4 and Type 60 use an implicit scheme to solve the differential equations. Furthermore, the degree of thermal stratification is dependent on the magnitude of N.

The algebraic tank model, Type 38, determines the number of nodes (N) by the magnitude of the timestep, and flow rate of both charging and discharging. A new node is created for the entering fluid unless the temperature difference is within 0.5°C with the existing node, and this is attained by using variable node sizes. This

also implies that the numerical diffusion is kept at a minimum when compare it in a nodal tank model.

A comprehensive summary of numerous TRNSYS tank models was completed by Allard et al. [41] and adopted in Table 3.2.

Table 3.2 TRNSYS tank model characteristics adopted from Allard et al. [41].

	Type 4 (nodal)	**Type 60 (nodal)**	**Type 534 (nodal)**	**Type 38 (algebraic)**
NODES				
Maximum number of nodes	100	100	500	45
Unequal size nodes	Yes	Yes		Yes
INLET MODE				
Load flow enters at the specified node	Yes	Yes	Yes	
HEATING ELEMENTS				
Maximum number of heating elements	2	2	# of nodes	1
Internal temperature control	Yes	Yes		Yes
ENERGY BALANCE				
Fully mixed before entering each node	Yes	Yes	Yes	
Constant overall loss coefficient	Yes	Yes		Yes
Nodes specified loss coefficient	Yes	Yes	Yes	
Accounts for thermal conductivity (fluid + tank wall)		Yes	Yes	Yes
Fully mix appropriate nodes	Yes	Yes	Yes	Yes

Most tank models include the option of an internal heat exchanger, multiple heaters, and rock beds. Some tanks also provide Variable Inlet (VI) and Fixed Inlet (FI) features. The VI model inserts the incoming fluid to the node closest in temperature and allows the maximum degree of thermal stratification. In contrast, the FI model introduces the fluid to a predetermined location and mixes with the adjacent node(s) if a temperature inversion presents. Since the degree of thermal stratification influences TES performance, both VI and FI models are explored. Both **Type 4** and **Type 38** models successfully predicted the thermal behaviors of a tank in both VI and FI modes and were chosen to model the TES tank. Their thermal behaviors were investigated in the **TES Tank Verification** section.

Type 60 model offers the option of one inlet and one outlet mode. Also, Unrau[31] has thoroughly studied the Type 60 model and demonstrated its ability to predict the thermal behaviors of the tank. It will be used to model the auxiliary tank in this research. Its thermal behaviors will be verified in the **Auxiliary Tank Verification** section.

The size of grid spacing and the timestep determine the convergence and the accuracy of a numerical solution. In an implicit solving scheme, which is used by Type 4 and Type 60 models, the convergence of a solution is usually guaranteed, and the accuracy of the solution can be improved by refining the size of the node

and timestep. Therefore, the effects of the grid spacing and timestep were investigated in the two models. The accuracy of TRNSYS prediction was assessed by the Root Mean Square (RMS) error.

This section will be divided into the following subsections:

- TES Tank Verification (Type 4 and Type 38 models)
- Auxiliary Tank Verification (Type 60 model)

TES Tank Model Verification

Since solar irradiance does not always temporally align with the household demand, the TES tank is considered as a buffer between the solar collector side and the load side. On the solar collector side, it stores the heated fluid from the collector and supplies cold fluid in return. On the load side, it sends the heated fluid to the auxiliary tank and receives the same quantity in return form the mains. The Type 4 and Type 38 models were both selected to model the TES tank, and their thermal behaviors were studied through the following cases:

Case 1: Studying the temperature distribution within an insulated tank ($T_{initial}$ = 20°C) by constantly charging the tank with 50°C water at a flow rate

of 54 kg/hr. The problem was considered as a semi-finite wall problem, and the temperatures along the axial direction were compared to the analytical solutions.

Case 2: Investigating the thermal decay within the tank and thermal losses to its surroundings. The tank was initially at a uniform temperature without charging or discharging. The simulation results were verified with the analytical solutions.

TES Model Verification - Type 4 Model Case 1: Thermal Diffusion

This case studied the evolution of the thermocline in a Type 4 model by investigating the temperature distribution along the axial direction in the tank. The thermal behaviors of the tank at various grid sizes and time steps were explored. Since the collector inlet temperature influences the heat losses from the collector and thus the solar fraction, the ability of the model to accurately predict this temperature was assessed. The collector inlet temperature (T_i) is equivalent to the temperature of the fluid that leaves the bottom of the TES (T_{bottom}).

The verification considers an insulated tank was initially at 20°C and charged with 50°C fluid at a constant flow rate of 54 kg/hr entering from the top. More simulation parameters are summarized in Table 3.3.

The simulation results of various grid spacings (Fig 3.4) and time steps (Fig 3.5) were compared to the analytical solution, respectively. The methods to calculate the analytical solution can be found in Appendix C.

The temperature predictions in Fig 3.4 and Fig 3.5 were plotted against the normalized elevation within the TES. Fig 3.4 (a) and (b) show the temperature distribution along the tank elevation at one hour and two hours for three different grid spacings, respectively. The temperature gradients of the thermocline were

steep, and the centers of the thermocline were located at the normalized elevation of 0.18 (t = 1 hr) and 0.37 (t = 2 hr), respectively. The thermocline broadened with increased time.

Table 3.3 Simulation parameters for Type 4 TES tank verification Case 1.

Description	Value (unit)
Tank volume	0.303 (m^3)
Tank height	1.5 (m)
Tank heat loss coefficient	0 (W/m^2 °C)
Tank initial temperature	20 (°C)
Fluid Properties:	
Thermal diffusivity	1.55 E-07 (m^2/s)
Charging condition:	
Uniform charing flow rates	54 (kg/hr)
Temperature of the charging fluid	50 (°C)
Number of nodes	79, 50, 20 (-)
Timestep	0.5, 1, 10 (min)

The accuracy of TRNSYS prediction was assessed by the root mean square error. The method used to evaluate the RMS error for the temperature (T) is demonstrated in equation (3.1), where n represents the quantity of data.

$$RMS\ error = \sqrt{\frac{\sum\left[T_{TRNSYS} - T_{Analytical}\right]^2}{n}} \tag{3.1}$$

In Fig 3.4, it can be observed that a significant amount of numerical diffusion was found in a coarse grid space (N=20), and this numerical diffusion diminished when a finer grid space was used. For instance, increasing N from 20 to 79 resulted in a 2°C drop in the RMS error. Fig 3.5 demonstrates that the tank performance can also be enhanced by refining the size of the timestep. There was a 0.7°C drop in the RMS error when the timestep was reduced from 10 to 0.5 minutes. Therefore, a finer grid spacing and timestep would promote the accuracy of the TRNSYS prediction.

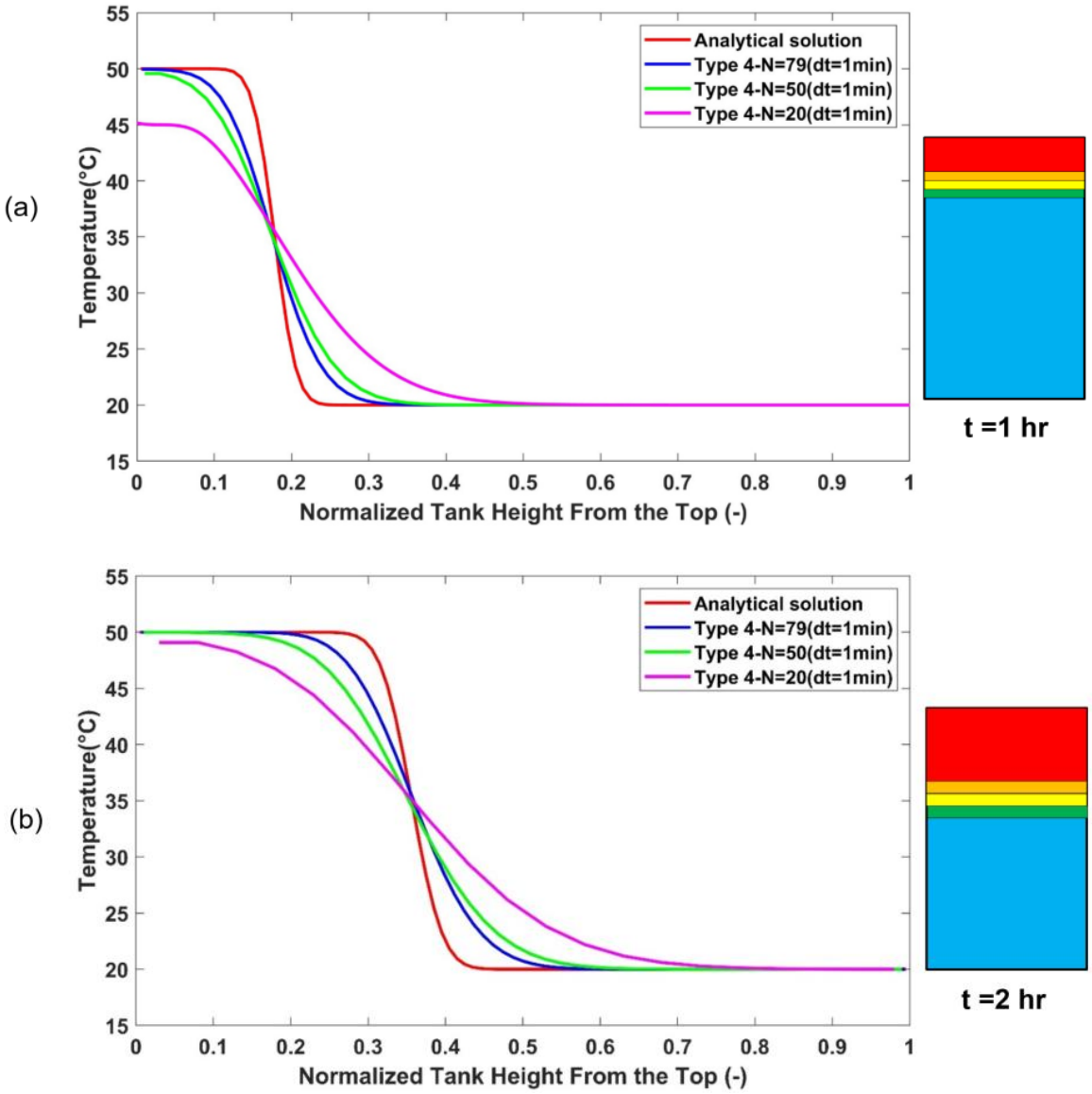

Figure 3.4 Temperature distribution impacted by the grid spacing in Type 4 FI model at (a) t = 1 hr, and (b) t = 2 hr.

(a)

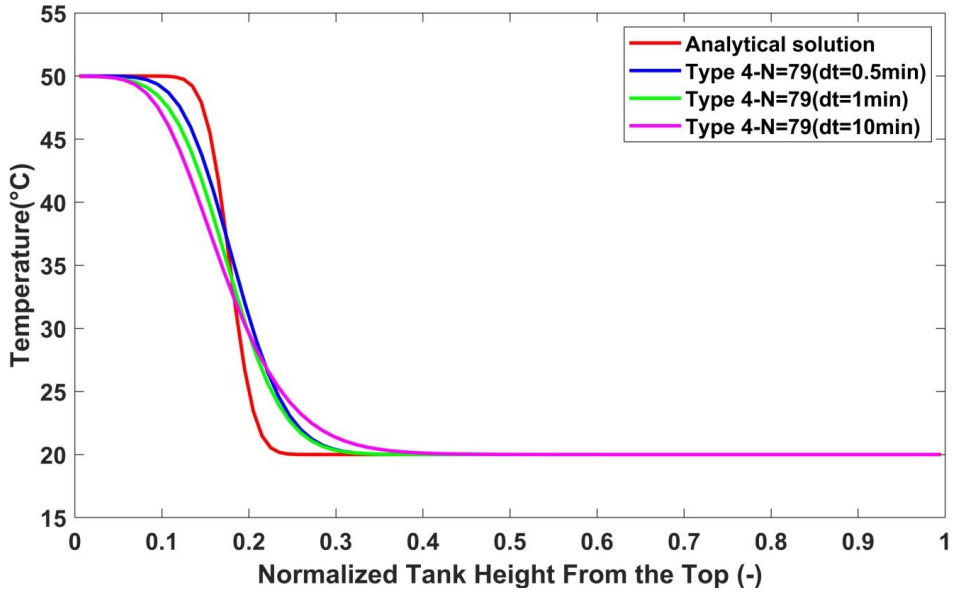

(b)

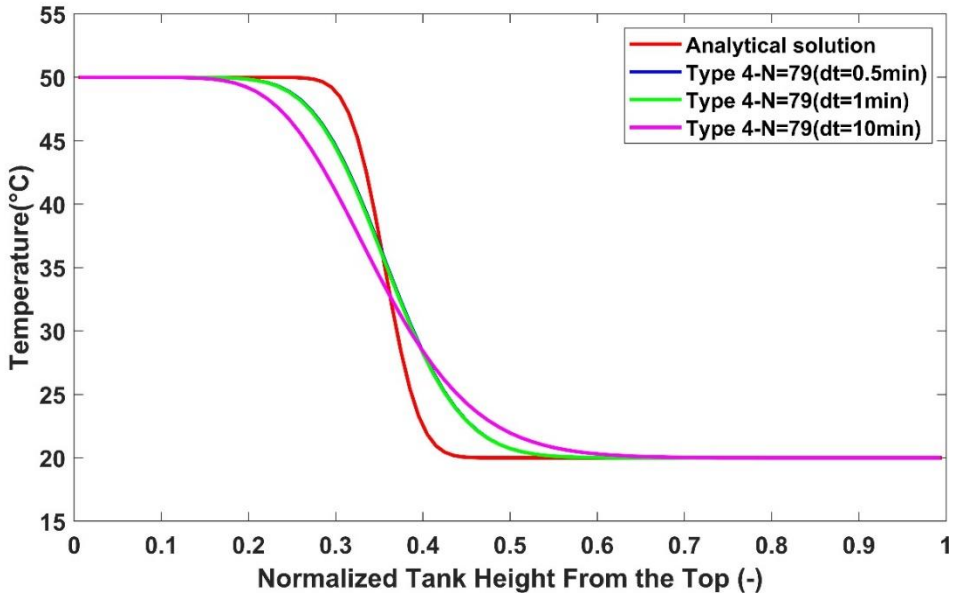

Figure 3.5 Temperature distribution impacted by the size of timestep in Type 4 FI model at (a) t =1 hr, and (b) t = 2 hr.

When neglecting the conduction between the fluid layers within the TES, the entering fluid will reach the bottom of the tank at 5.6 hours, and T_i = 35°C. The TRNSYS predictions of T_i, the temperature of the fluid exiting the bottom of the tank, for various numbers of nodes were plotted against the normalized tank height in Fig 3.6. It revealed that a significant amount of numerical diffusion was generated by the Type 4 model, and such numerical diffusion could be mitigated by refining the grid spacing.

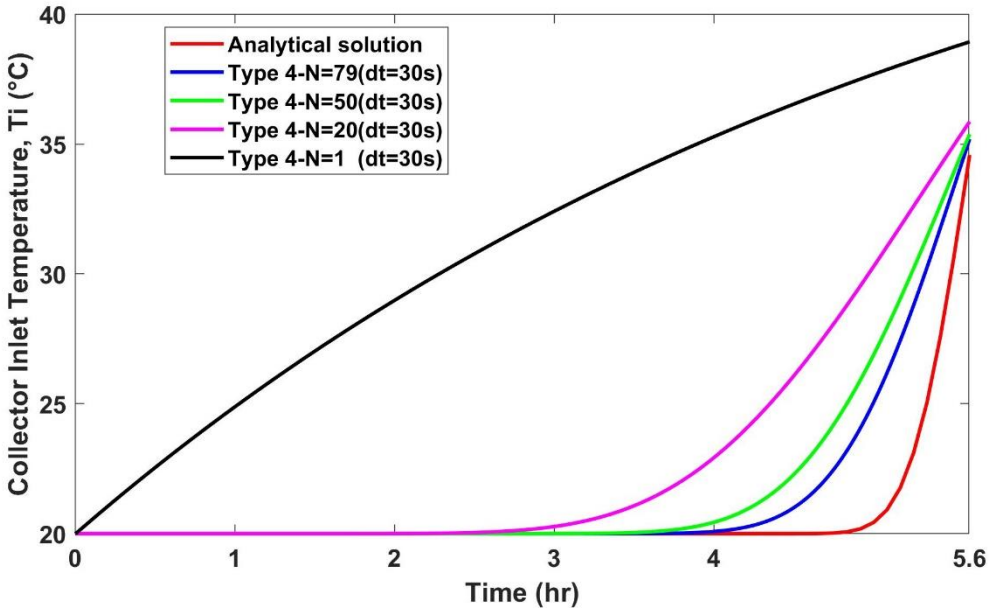

Figure 3.6 Predictions of the collector inlet temperature versus time for Type 4 FI model verification Case 1.

TES Model Verification - Type 4 Model Case 2: Thermal Decay

This case study investigated the capability of Type 4 tank for predicting the temperature decay within the tank and its thermal losses to the surroundings. The case considers a stagnant (no charging/discharging) tank with a uniform initial temperature of 20°C. More simulation parameters can be found in Table 3.4. The TRNSYS nodal temperatures were recorded for 600 hours, and they were compared to the analytical solutions, which are available in Appendix D.

Predicted tank temperature and heat loss as a function of time were shown in Fig 3.7 and 3.8, respectively. Timesteps of 30 and 60 minutes were used in the TRNSYS simulation and were found to produce timestep-independent results. As seen in the figures, good agreement between TRNSYS predictions and analytical solutions were obtained, and respective RMS errors were 0.2°C and 0.8 kJ/hr.

Table 3.4 Simulation parameters for Type 4 TES tank verification Case 2

Description	Value (unit)
Tank Parameters:	
Tank volume	0.303 (m^3)
Tank height	1.514 (m)
Tank initial temperature	20 (°C)
Ambient temperature	6.1 (°C)
Charging flow rate	0 (kg/hr)
Discharging flow rate	0 (kg/hr)
Control signal for auxiliary heaters	0 (-)
Heat loss coefficient	1.081 (W/m^2 °C)
Fluid Properties:	
Density of the fluid	1000 (kg/ m^3)
Heat capacity of the fluid	4190 (J/kg °C)
Fluid diffusivity	1.55E-07 (m^2/s)
Simulation Parameters:	
Timestep	30, 60 (min)
Simulation time	600 (hr)
Number of nodes	1 (-)

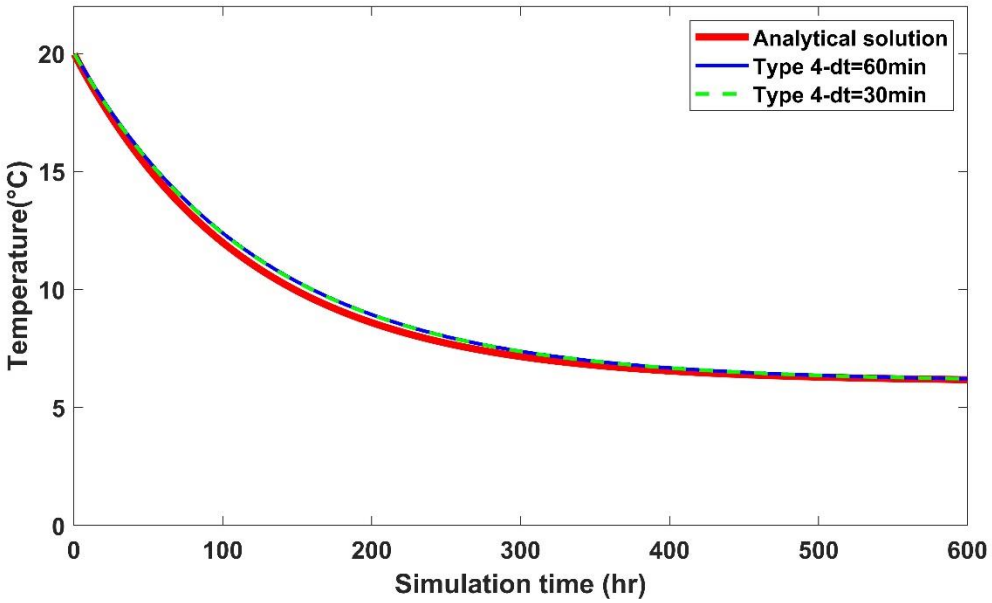

Figure 3.7 Tank temperature distribution versus simulation time for the TES tank verification Case 2 (N=1).

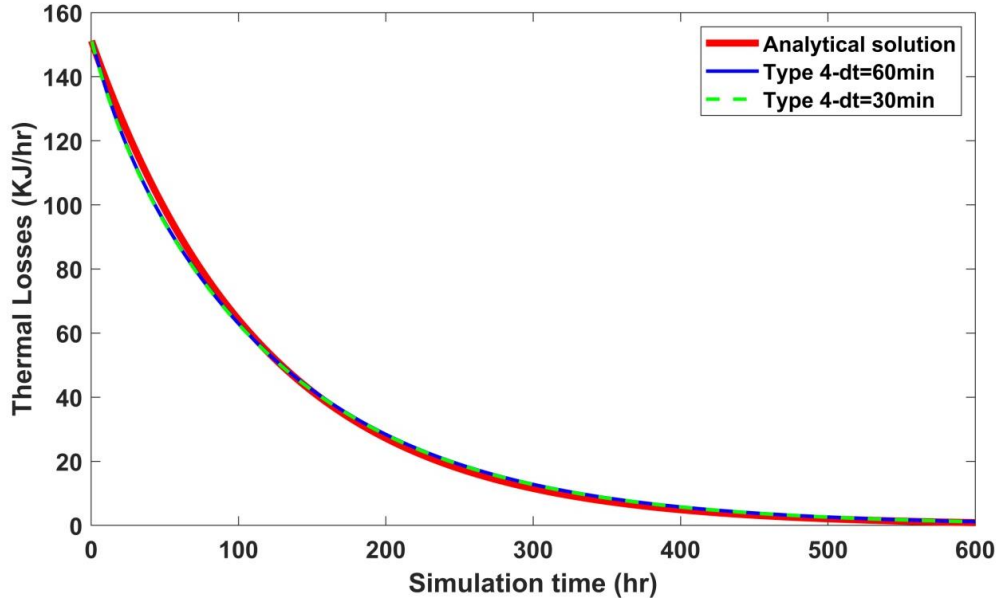

Figure 3.8 Tank thermal losses versus simulation time for the TES tank verification Case 2 (N=1).

TES Model Verification - Type 38 Model Case 1: Thermal Diffusion

In this subsection, the evolution of the thermocline along the axial direction in a Type 38 model was studied. As noted earlier, the Type 38 model is based on an algebraic plug-flow representation such that the interface between the layers of fluid is tracked. Thermal diffusion within the liquid layers is neglected in Case 1. With the Type 38 model, the user is able to access the transient temperature at the top and bottom of the tank, rather than the spatial temperature profile within the tank.

The model was tested by considering an insulated tank that was initially at 20°C and was charged with 50°C fluid at a constant flow rate of 54 kg/hr entering from the top. The tank geometry is given by the data in Table 3.3. The transit time for the fluid to travel from the top to the bottom of the tank is 5.6 hours. The simulation results were compared to the analytical solution and shown in Fig 3.9. It shows that when the thermocline reached the bottom of the tank at 5.6 hours, TRNSYS predicted the evolution of the thermocline as a step function since the diffusivity was neglected. This type of tank model provides an idealization of thermal stratification.

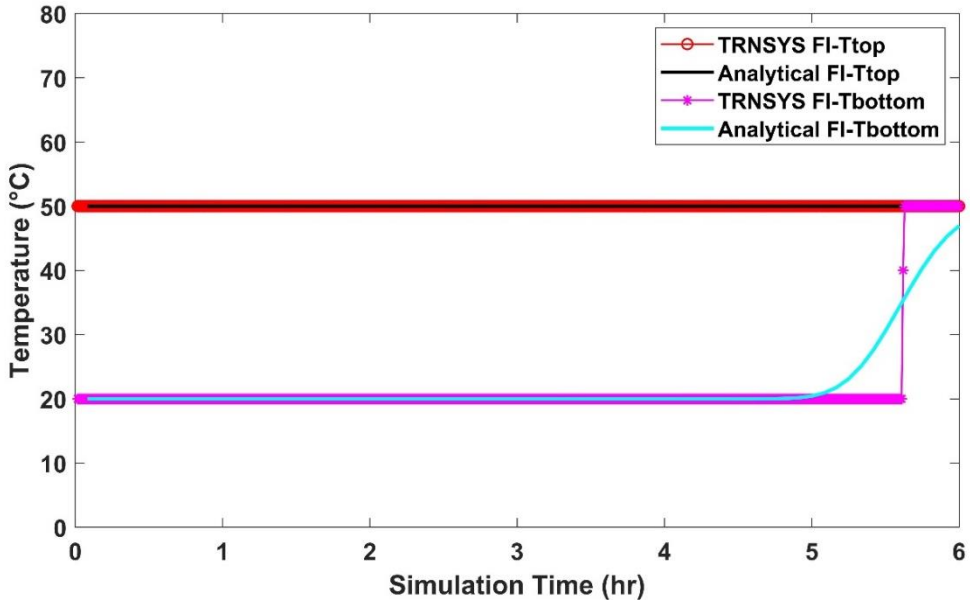

Figure 3.9 Top and bottom temperature evolution within the Type 38 FI model.

TES Model Verification - Type 38 Case 2: Thermal Decay

This case studies the temperature decay within the Type 38 model and its thermal losses to the surroundings. Consider a well-insulated tank, its initial temperature was 20°C, and no fluid entered or exited the tank. TRNSYS results were recorded for 600 hours, and they were compared to the analytical solutions.

TRNSYS predictions for the temperature and thermal losses were demonstrated in Fig 3.10 and Fig 3.11, respectively. Both figures indicated that the deviation between TRNSYS predictions and analytical solutions could be neglected. The respective RMS errors for the temperature and thermal losses were less than 0.04°C and 0.4 kJ/hr.

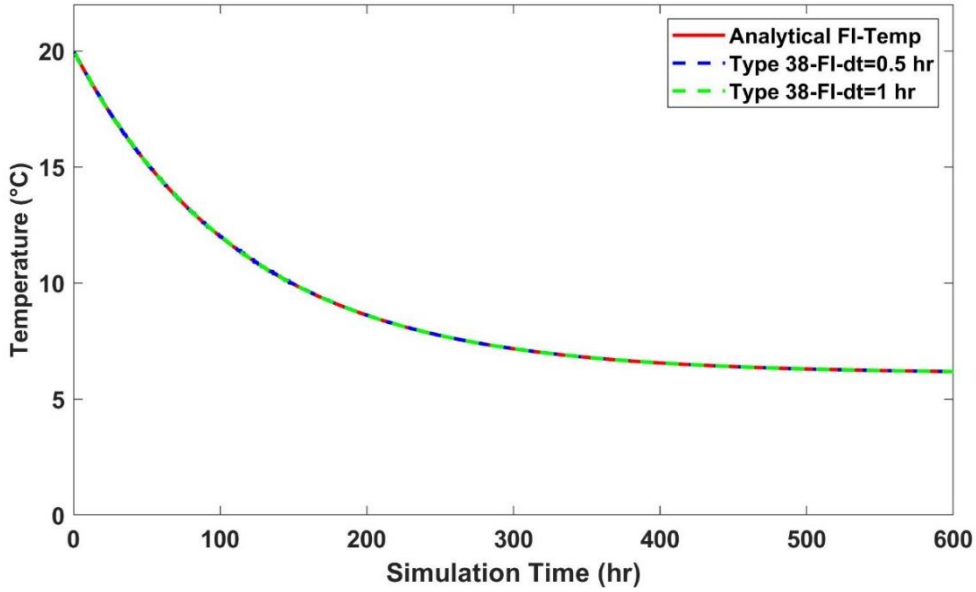

Figure 3.10 Tank temperature distribution versus simulation time for the TES tank verification Case 2.

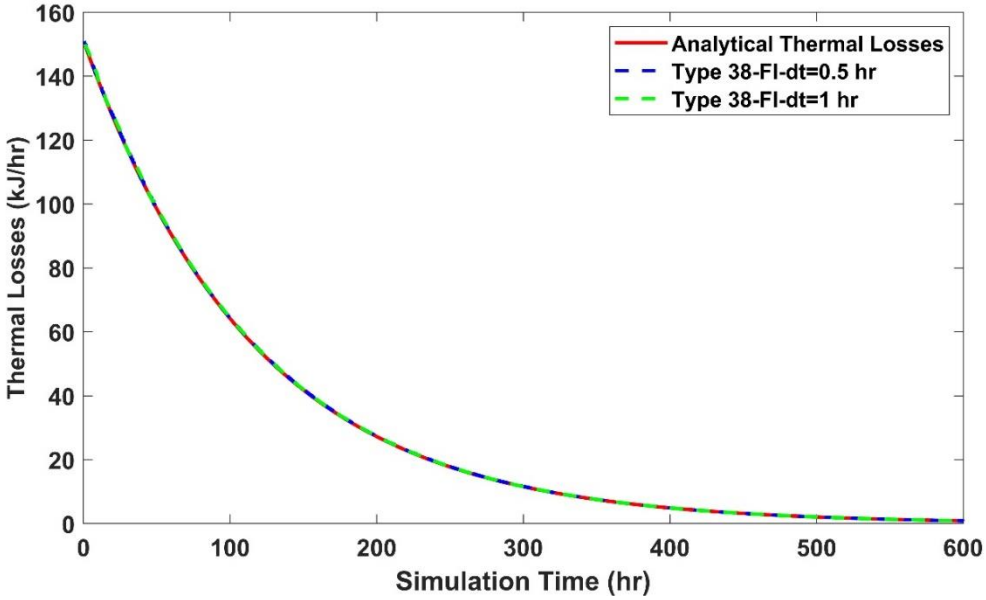

Figure 3.11 Tank thermal losses versus simulation time for the TES tank verification Case 2.

Auxiliary Tank Verification

The auxiliary tank is required to supply additional energy if the fluid leaving the TES tank is below the demand temperature for the household. The auxiliary tank is treated as a fully mixed tank (N=1) with an energy input to maintain the tank at T_{set}. The studies in this subsection investigated the accuracy of predicting both the auxiliary heating requirement and thermal losses to its surroundings.

In a well-insulated tank (Type 60), the signals of the auxiliary heaters were set to zero, and the thermal decay and thermal losses to the surroundings were verified. The TRNSYS result was checked, and excellent agreement with the analytical solution was obtained. Further testing cases for Type 60 model were conducted, and they are:

Case 1: In an insulated tank initially at 20°C without charging and discharging, the tank was set to maintain at the T_{set} of 60°C, and the time required to reach T_{set} was verified.

Case 2: In a well-insulated tank initially at T_{set}, the heating time to compensate for the heat losses to the surroundings was verified.

Case 1: Heating Requirement of the Auxiliary Tank Model (No Heat Losses)

Case 1 explored the capability of Type 60 predicting the heating requirement of the auxiliary heaters. The tank was insulated and initially at 20°C. The preset temperature, T_{set}, was 60°C, and the temperature deadband ($\triangle T_{deadband}$) was 0.5 °C. The two heaters at the bottom of the tank were only activated when the tank temperature was lower than 59.5°C. More tank parameters can be retrieved in Table 3.5. The goal of this verification is to assess the control of the auxiliary heaters.

For this problem, the time for the tank fluid temperature to increase from 20°C to 59.5°C was calculated to be 0.79 hours (Appendix E). The heat output from the auxiliary heaters, as shown in Fig 3.12 and predictions were in agreement with the calculated heating time.

Table 3.5: Simulation parameters for the Aux. tank verification Case 1

Description	Value (unit)
Tank volume	0.151 (m^3)
Tank height	0.5 (m)
Tank heat loss coefficient	0 (W/m^2 °C)
Tank initial Temperature	20 (°C)
Set temperature	60 (°C)
Temperature deadband	0.5 (°C)
Auxiliary heater signals	1 (-)
Auxiliary heater power	4500 (W) X 2
Total number of nodes	1 (-)
Node containing the heaters	1 (-)
Timestep	30 (s)
Simulation time	2 (hr)

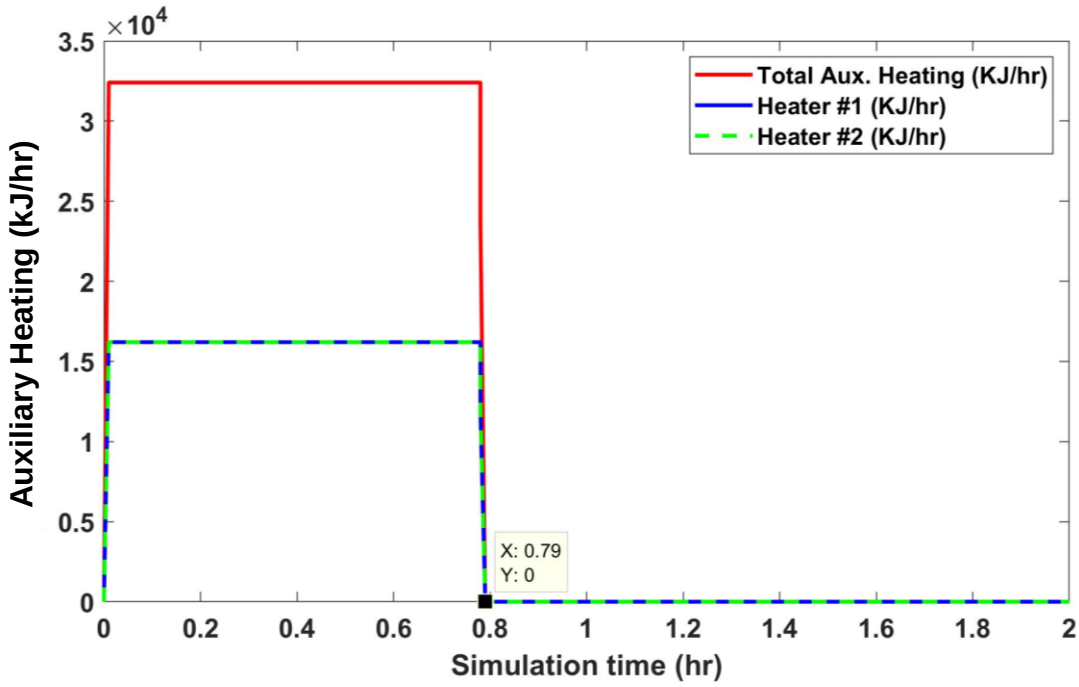

Figure 3.12 The auxiliary heating requirement versus simulation time for the auxiliary tank verification Case 1 (N=1, dt=30 s).

Case 2： Heating Required to Compensate Heat Losses to the Surroundings

Case 2 verified the accuracy of predicting the instant that the tank temperature dropped one deadband ($\Delta T_{deadband}$) and the time required returning to the T_{set}. A well-insulated tank was initially at 60°C and $\Delta T_{deadband}$ = 0.5°C. More simulation parameters are shown in Table 3.6. The analytical solutions in Appendix F indicate the tank will reach 59.5°C at 1.32 hours, and returned to 60°C at 1.34 hours. The TRNSYS predictions were plotted in Fig 3.13, and it is evident that the TRNSYS predictions aligned with the analytical solutions.

Table 3.6: Simulation parameters for auxiliary tank verification Case 2

Description	Value (unit)
Tank volume	0.151 (m^3)
Tank height	0.5 (m)
Tank heat loss coefficient	1.047 (W/m^2 °C)
Tank initial Temperature	60 (°C)
Ambient temperature	19.3 (°C)
Set temperature	60 (°C)
Temperature deadband	0.5 (°C)
Auxiliary heater signals	1 (-)
Auxiliary heater power	4500 (W) X 2
Total number of nodes	1 (-)
Timestep	30 (s)
Simulation time	2 (hr)

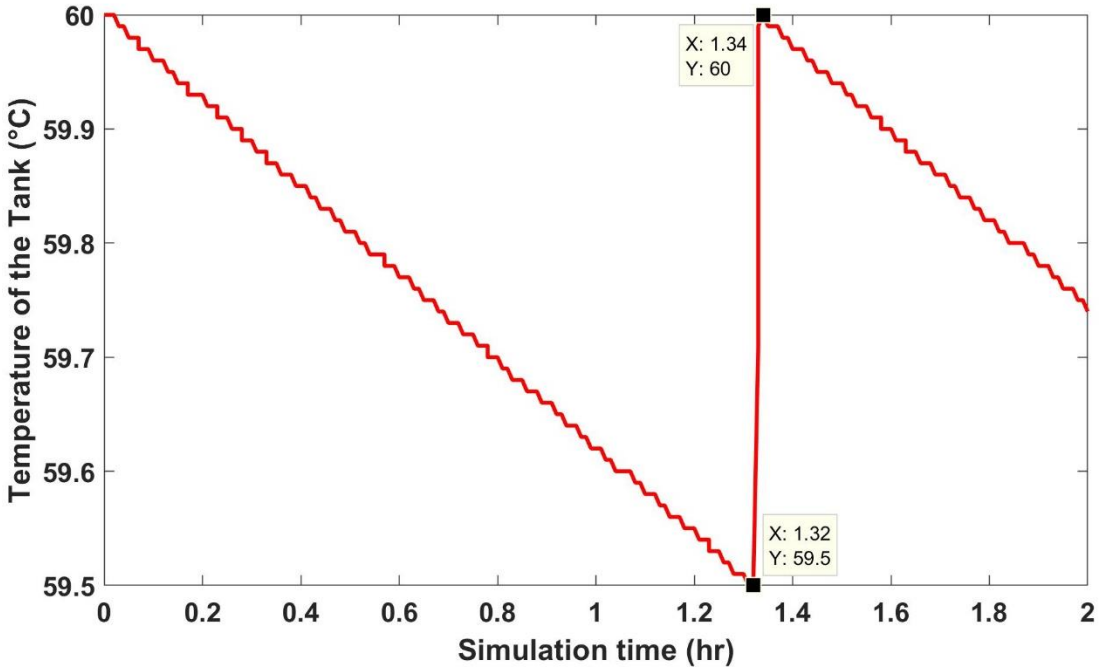

Figure 3.13 The tank temperature versus simulation time for the auxiliary tank verification Case 2 (N=1, dt=30 s).

3.3 System Verification

The SDHW system model presented in Fig 3.1 at the beginning of this chapter was verified with Wuestling et al. [9]. The simulation was conducted for weather data of Madison, Wisconsin, US. The controller on the solar collector side monitored the temperatures of the collector inlet and outlet and actuated the pump when their temperature difference exceeded 8.9°C and ceased the flow when the temperature difference dropped below 1.7°C. The RAND load profile (Fig 2.6) was used to approximate the household demand. Additional simulation parameters were summarized in Table 3.7. The predicted solar fraction, as a function of the collector flow rate per unit collector area, is shown in Fig 3.14 for nodal FI model (Type 4), plug flow FI model (Type 38), and plug flow VI model (Type 38), respectively. As seen in these figures, the current predictions are in excellent agreement with that reported by Wuestling et al.

Fig 3.14 also illustrates that the VI tank model (Fig 3.14(b)) yields better system performance than the FI tank model (Fig 3.14(c)). Since VI model introduces the entering fluid to appropriate elevation based on its temperature, and this allows the coolest fluid being sent to the collector. Thus collector performance will be enhanced and lead to better system performance.

Table 3.7 Simulation parameters for the system validation adapted from Wuestling et al. [9].

Description	Value (unit)
Collector:	
Area	4.2 (m^2)
$(F_R(\tau\alpha))_{test}$	0.805 (-)
$(F_RU_L)_{test}$	4.73 (W/m^2 °C)
$(\dot{m}_{coll})_{test}$	72 l/hr- m^2
Incidence angle modifier coefficient	0.0989
TES tank (Type 4a Fixed Inlet):	
Tank volume	0.303 (m^3)
Tank height	1.514 (m)
Heat loss coefficient	1.081 (W/m^2 °C)
Auxiliary tank (Type 60d):	
Volume	0.151 (m^3)
Heat loss coefficient	1.047 (W/m^2 °C)
Tank height	0.5 (m)
Set temperature	60 (°C)
Temperature deadband	0.5 (°C)
Auxiliary heater power	4500 (W) X 2
Load profile:	
RAND profile	297 (l/day)

Table 3.7 (continued) Simulation parameters for the system validation adapted from Wuestling et al. [9].

Description	Value (unit)
Other simulation parameters:	
Weather data	Weather in May for Madison, WI, US [2880-3624 hr]
Pump control strategy	• γ = 1 when ΔT > 8.9°C • γ = 0 when ΔT <1.7°C. ** **note:** ** γ = pump signal in the solar collector side ** ΔT = the temperature difference between the collector inlet and outlet
Simulation timestep	0.5 (hr)
Simulation time	2880-3624 (hr)

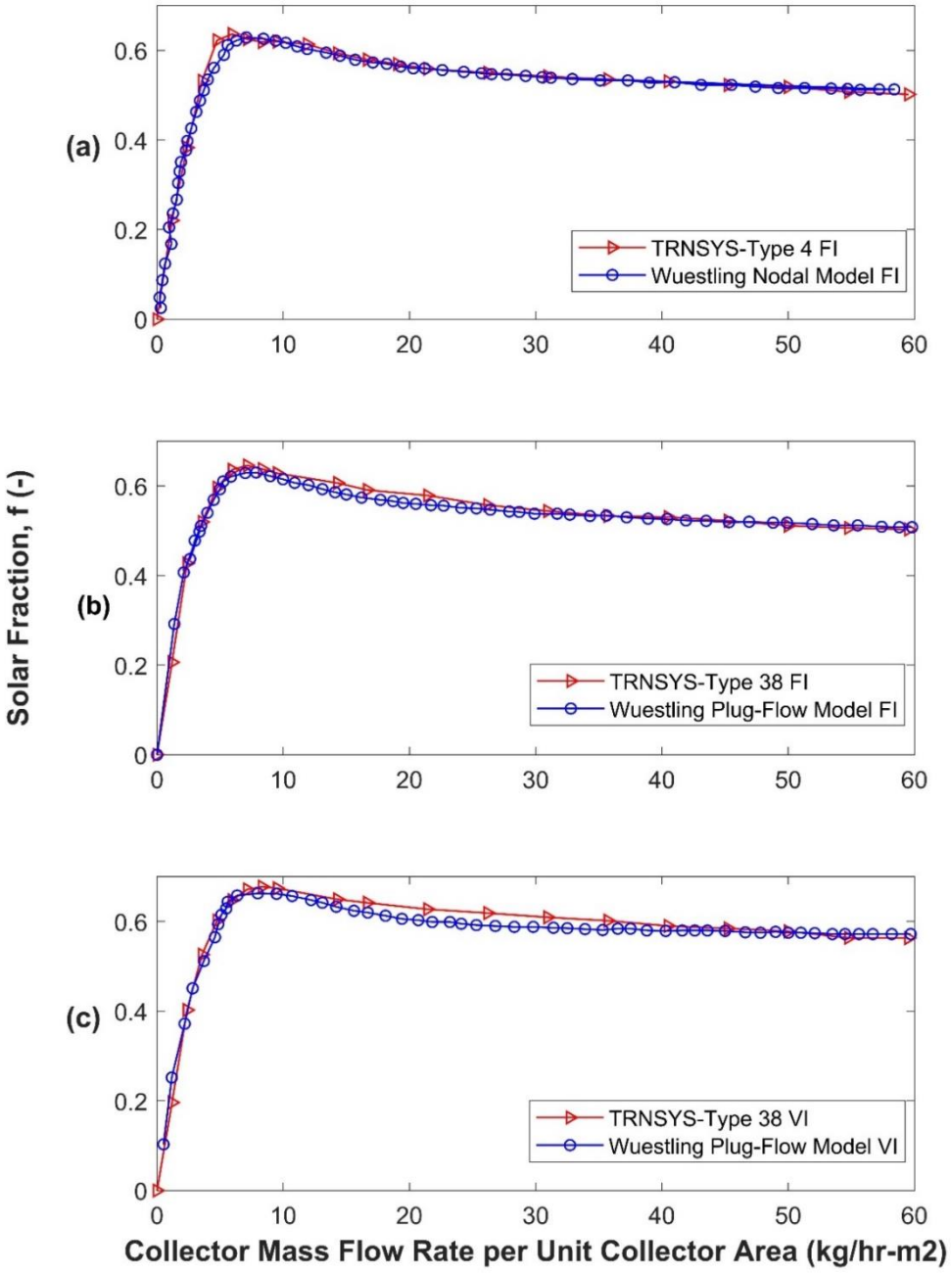

Figure 3.14 TRNSYS SDHW system verification against the results from Wuestling et al. [9]: (a) nodal model (Type 4), (b) Plug Flow Fixed Inlet model (Type 38), and (c) Plug Flow Variable Inlet model (Type 38).

Conclusion

This chapter summarized the verification of the TRNSYS components, including the flat plate solar collector, TES tank, and auxiliary tank; the TRNSYS results were compared to the respective analytical solutions. Also, system verification was completed by comparing the simulation results to Wuestling et al.'s results. The verifications helped to gain an understanding of the use of TRNSYS and the limitations inherent in the tank models.

Section 3.1 investigated the performance of the solar flat plate collector model with an incidence angle modifier (Type 1b). The simulations were completed on a spring day and a winter day, respectively. The predicted collector outlet temperature and the useful energy collected aligned with Hottel-Whillier-Bliss solutions. It was found that the size of timestep has a negligible effect on predicting collector performance.

Section 3.2 is divided twofold into the TES and the auxiliary tank verification subsections.

- TES tank verification:

  Due to the capability of successfully model both the Variable Inlet and Fixed Inlet modes, Type 4 and Type 38 models were selected to model

the TES tank. They were tested under static (no charging/discharging) and dynamic (charging/discharging) conditions. Significant false diffusion, which associated with the grid spacing, was seen in the Type 4 model. Such false diffusion decreases as the number of nodes increase. In contrast, no false diffusion was discovered in the Type 38 model.

- Auxiliary tank verification:

  The Type 60 model was investigated as the auxiliary tank in this subsection. The heating requirements and thermal losses within the tank were verified with their respective analytical solutions, and it observed that the Type 60 model predicted the tank behaviors with good agreement with the analytical solutions.

Section 3.3 verified the TRNSYS SDHW system with Wuestling et al.'s work. The simulation was performed for May in Madison, Wisconsin, and good agreement with the published results was obtained.

Chapter 4

Analysis of the Influence of Key System Parameters on Solar Domestic Hot Water System Performance

Introduction

Solar domestic hot water (SDHW) system performance is measured through the solar fraction, which represents the fraction of the household demand (Q_{load}) provided by the solar system. From the system balance presented in Chapter 2, the solar fraction, f, can be determined from $f = \frac{Q_u - Q_{Loss\ Tanks}}{Q_{load}}$. The quantities Q_u and $Q_{LossTanks}$, and Q_{load} represent the solar energy collected by the collector, the tank heat losses, and the energy required by the household load, respectively.

Collector performance crucially influences the SDHW system performance, and it is determined by the intensity of solar irradiance (G), the magnitude of the collector flow rate ($\dot{m}_{coll}$) and the collector inlet temperature (T_i). It was demonstrated in Appendix A that operating with high $\dot{m}_{coll}$ and low T_i enhances collector performance by reducing collector heat losses. This condition can be attained by enlarging the TES tank volume (V_{TES}) so that the hot fluid enters the top portion of the TES and requires longer traveling time to reach the bottom; thus, the fluid at the bottom stays cool as long as possible. Consequently, collector performance is enhanced. The system performance is thus improved but at a higher cost of $Q_{LossTanks}$ due to the enlarged TES surface area.

TES tank behaviors also affect SDHW performance. Chapter 1 discussed that the research focus should be on reducing the collector inlet temperature rather than maintaining thermal stratification within the top portion of the TES. Thus the significance of the degree of the thermal stratification inside the TES was investigated in this chapter.

The SDHW system can be divided as the solar collector side (solar radiation, the controller, pump and TES tank), and the load side (the TES tank, auxiliary tank, household demand, and mains water) as demonstrated in Fig 4.1. Due to the intermittent characteristic of solar radiation and the stochastic nature of the load demand, the TES tank behaves as a buffer between the collector and the auxiliary tank. It thus belongs to both the solar collector side and the load side.

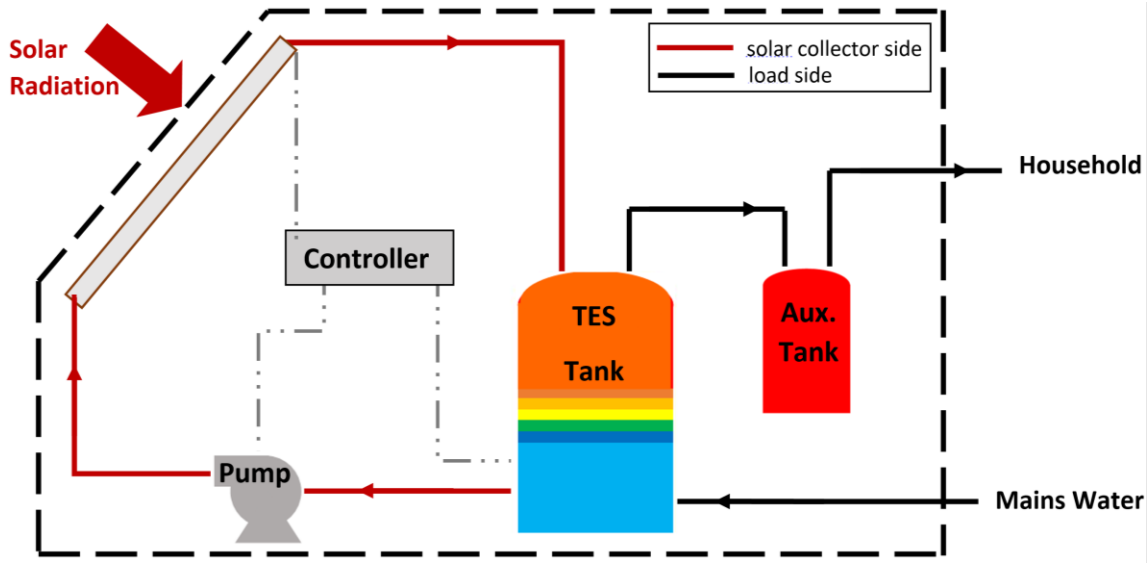

Figure 4.1 Schematic diagram of the SDHW system indicating the solar collector side and the load side.

On the solar collector side, when the collector receives sufficient solar radiation, the fluid at the bottom of the TES is pumped through the collector to transfer and store the thermal energy back into the TES. On the load side, when the household demand starts, the hot water is extracted from the auxiliary tank, and the same amount of cold mains water is introduced to the bottom of the TES concurrently. The magnitudes and duration of the flows on the solar collector and load sides will thus influence the temperature at the bottom of the tank, and hence the collector inlet temperature. An energy balance on the system showed that solar fraction is dependent on the collector losses, which in turn depend on the collector fluid inlet

temperature. The present research explored the following effects on system performance:

- Case 1: Effect of TES volume (V_{TES}) and magnitudes of collector mass flow rate ($\dot{m}_{coll}$)
- Case 2: Effect of the degree of thermal stratification within the TES
- Case 3: Effect of Duration of the collector flow (pump-on time, τ_p)

Predictions of solar fraction for each case study in this chapter were explored as a function of a dimensionless tank volume, which was defined as the ratio of the TES volume to the total daily load volume (V_{TES}/ V_{daily}). Three cases are listed below, and their simulation setups are summarized in Table 4.1. Case 1 and Case 2 repeated typical meteorological year (TMY) weather data of a single sunny spring day for a month to reduce computational cost. Case 3 applied annual weather data since the pump behaviors during spring is significantly different from that during winter. The three cases are:

Case 1 explored system performance affected by $\dot{m}_{coll}$ and V_{TES} (Type 38 model) when:

- Case 1a: Varying V_{TES} and with $\dot{m}_{coll}$ constant
- Case 1b: Varying both V_{TES} and $\dot{m}_{coll}$

Case 2 investigated system performance influenced by the degree of thermal stratification within the TES (Type 4 model) by setting the tank model at various numbers of nodes.

Case 3 studied system performance (Type 38 TES tank model) impacted by the pump-on time (τ_p) by implementing different pump control strategies at different $\dot{m}_{coll}$.

Table 4.1 Simulation parameters adopted from Wuestling et al. [9] for Case 1-3.

Description	Value (unit)
Collector:	
Collector area	4.2 (m^2)
$(F_R(\tau\alpha))_{test}$	0.805 (-)
$(F_R U_L)_{test}$	4.73 (W/m^2 °C)
$(\dot{m}_{coll})_{test}$	72 (l/hr- m^2)
Incidence angle modifier	0.0989 (-)
$(\dot{m}_{coll})_{use}$	• Case 1a: 30 (kg/hr) • Case 1b: 15, 25, 30, 70, 110 (kg/hr) • Case 2: 30 (kg/hr) • Case 3: 30, 60 (kg/hr)
TES tank:	
Tank model	• Case 1: Type 38 • Case 2: Type 4 • Case 3: Type 38
Heat loss coefficient	1.081 (W/m^2 °C)
Auxiliary tank:	
Tank model	Type 60
Volume	0.151 (m^3)
Heat loss coefficient	1.047 (W/m^2 °C)
Set temperature	60 (°C)
Temperature deadband	0.5 (°C)

Table 4.1 (continued) Simulation parameters adopted from Wuestling et al. [9] for Case 1-3.

Description	Value (unit)
Load profile:	
RAND load profile	297 (l/day)
Control Strategy:	
Pump control strategy	Case 1 and Case 2: • γ = 1 when ΔT > 8.9°C • γ = 0 when ΔT <1.7°C. Case 3: • γ = 1 when ΔT > 8.9, or 4.45°C • γ = 0 when ΔT <1.7, or 0.85°C. **** note:** ****** γ = pump signal on the solar collector side ****** ΔT = the temperature difference between the collector inlet and outlet
Weather data:	
Weather input	• Case 1 and Case 2: TMY Weather on May 9 [3096-3120 hour] for Madison, WI, US • Case 3:Annual weather for Madison, WI, US
Mains temperature	• Case 1 and Case 2: 17.7 (°C) • Case 3: 12.1 (°C)
Simulation Parameter:	
Simulation time	• Case 1 and Case 2: 31 (day) • Case 3: 365 (day)
Timestep	30 (s)

Case 1 - System Performance Affected By $\dot{m}_{coll} - V_{TES}$ Effect

Case 1 used the Type 38 (algebraic) model to study the effects of $\dot{m}_{coll}$ and V_{TES} on system performance in two scenarios：

Case 1a: Constant $\dot{m}_{coll}$ and various V_{TES}

The collector flow rate remained constant at 30 kg/hr, and V_{TES} changed at a constant aspect ratio, AR (AR=L/D). It appeared that AR of 3-4 was the most conducive tradeoff between the cost and performance [10], and AR of 3 was selected. System performance (solar fraction) was plotted against the dimensionless tank volume.

Case 1b: Various $\dot{m}_{coll}$ and various V_{TES}

Continued Case 1a, Case 1b analyzed the response of solar fraction to a range of $\dot{m}_{coll}$. The chosen $\dot{m}_{coll}$ were 15, 25, 30, 70, and 110 kg/hr. The solar fractions were also plotted versus the dimensionless tank volume.

Case 1a: Constant $\dot{m}_{coll}$ and Various V_{TES}

In an SDHW system with a 0.3 m^3 TES tank to satisfy the RAND household demand (0.3 m^3/day), the typical pump-on time is approximately 10 hours per day for the weather conditions simulated. The collector flow rate, $\dot{m}_{coll}$, can be determined by matching the total daily amount of fluids going through the collector and household demand. Thus $\dot{m}_{coll}$ = 30 kg/hr and was used in Case 1 study. The solar fraction was plotted against the dimensionless tank volume and was demonstrated in Fig 4.2. It is evident that system performance was initially enhanced by increasing the V_{TES} until a peak value, which occurred in the vicinity of V_{TES}/ V_{daily} = 0.6 (solid green line) for the RAND load profile. In the present research, the regime before the optimal operation point will be denoted as the "beneficial zone" (Fig 4.2), where the system performance benefits from increasing the TES volume, or $\dot{m}_{coll}$. The regime after the optimal point will be noted as the "non-beneficial zone", where system performance drops with increasing the TES volume, or $\dot{m}_{coll}$.

In the simulation environment, the collector inlet temperature (T_i) was recorded at the end of each time step, but the analysis would only require the ones when the pump was activated. An $\dot{m}_{coll} - \text{weighted} - \text{averaged}$ collector inlet temperature, T_{i_avg}, is used. In this chapter, T_{i_avg} will be denoted as T_i for brevity. The method

to calculate T_i is given in Equation (4.1), and the same method can be used to evaluate the $\dot{m}_{coll}$ – averaged collector outlet temperature, T_o.

$$T_{i\_avg} = \frac{\int_0^t \dot{m}_{coll} * T_i \, dt}{\int_0^t \dot{m}_{coll} \, dt} \tag{4.1}$$

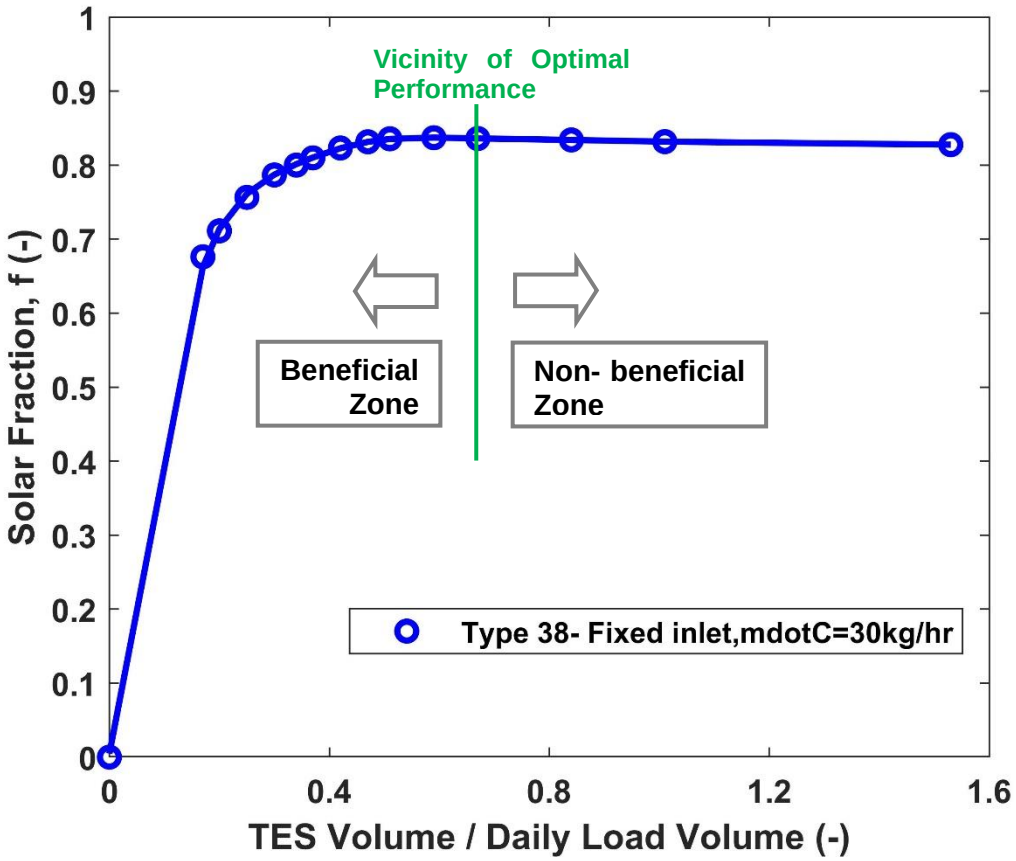

Figure 4.2 Solar fraction versus dimensionless volume for case 1a.

The number of tank turnovers per day on the solar collector side can be defined as the ratio of the total daily mass through the collector ($\dot{m}_{coll} * \tau_p$) to the mass of the TES tank, where τ_p represents the duration of the pump operation. Fig 4.3 shows that the number of tank turnovers decreases when V_{TES} increases. It implies that increasing the volume of the TES acts to increase the transit time for hot collector fluid to reach the tank bottom. This allows for cooler fluid to enter the collector inlet (Fig 4.4). The non-linear nature of the curve in Fig 4.3 is a result of both increases in tank volume as well as the changes in the pump run time (τ_p), which is shown in Fig 4.5. As the tank volume increases, more useful energy (Q_u) would be captured by the collector (Fig 4.6); however, an increase in total thermal losses from the tanks ($Q_{LossTanks}$) was also found due to the enlarged tank surface area (Fig 4.6). This leads to a slight drop in solar fraction with increasing TES volume in the “non-beneficial” zone in Fig 4.2.

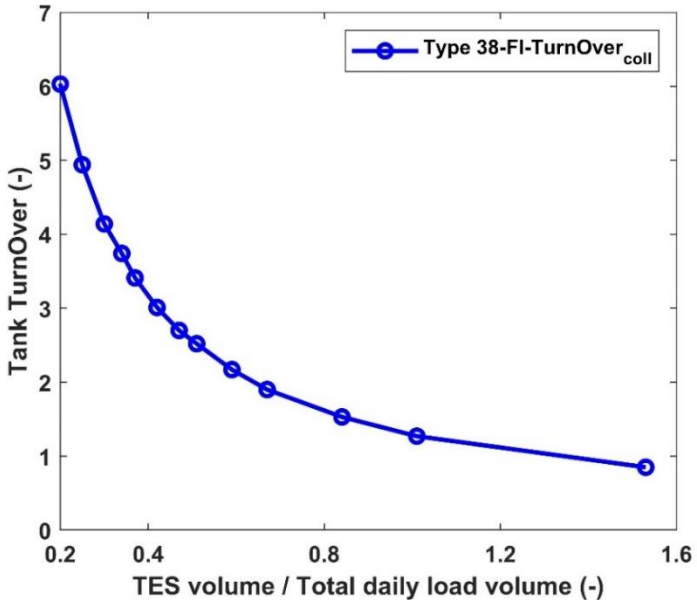

Figure 4.3 Tank turnover on the solar collector side vs. dimensionless tank volume for Case 1a. $\dot{m}_{coll}$ = 30 kg/hr, T_{main} = 17.7 °C.

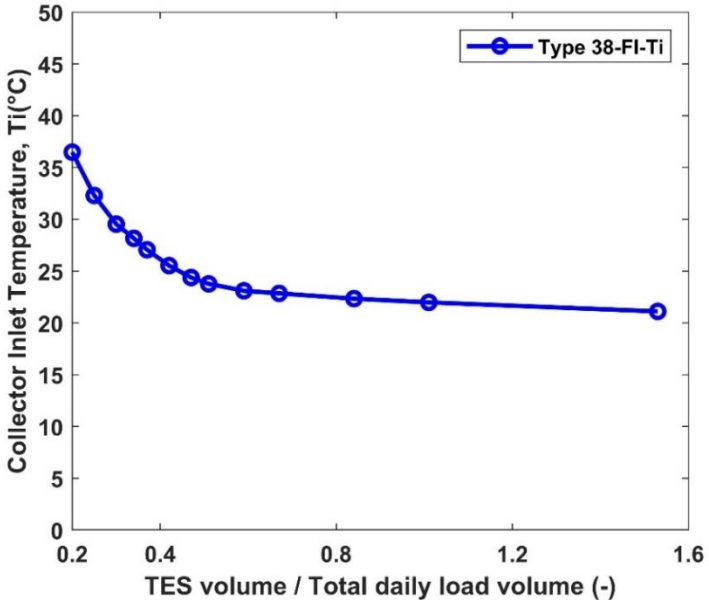

Figure 4.4 T_i vs. dimensionless tank volume for Case 1a. $\dot{m}_{coll}$ = 30 kg/hr, T_{mains} = 17.7°C.

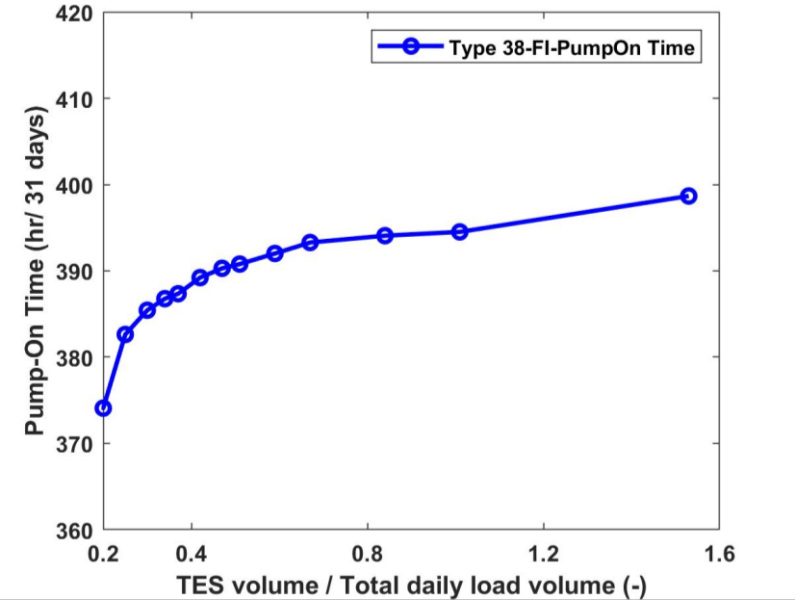

Figure 4.5 Pump-on time vs. dimensionless tank volume for Case 1a. $\dot{m}_{coll}$ = 30 kg/hr,T_{mains} = 17.7°C.

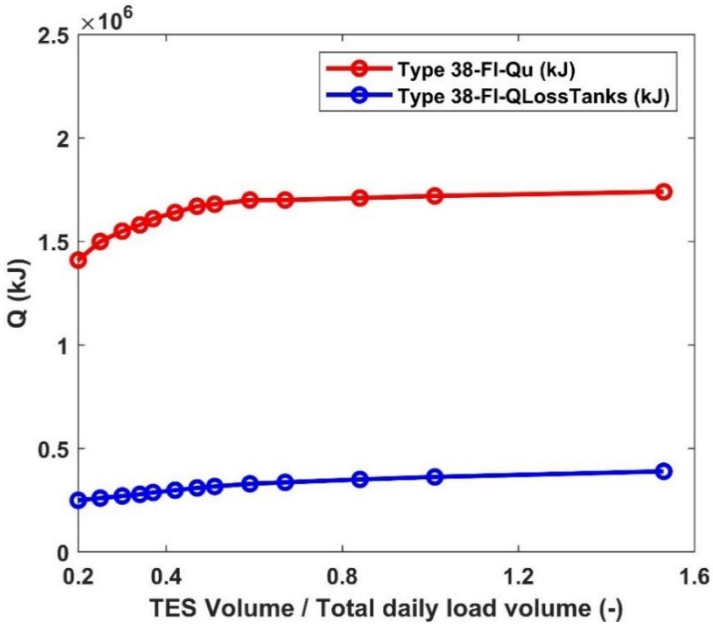

Figure 4.6 Q_u and $Q_{LossTanks}$ vs. dimensionless tank volume for Case 1a. $\dot{m}_{coll}$ = 30 kg/hr, T_{main} = 17.7 °C.

Case 1b: Various $\dot{m}_{coll}$ and various V_{TES}

The chosen $\dot{m}_{coll}$ are 15, 25, 30, 70, and 110 kg/hr in this case study, and the solar fraction was plotted against the dimensionless tank volume. The rate of collecting the useful energy by the flat plate solar collector is determined from the Hottel-Whillier-Bliss relationship presented in Equation (A.1) and repeated below:

$$\dot{Q}_u = A_c[F_R(\tau\alpha) * G - F_R U_L(T_i - T_a)]$$

The collector heat removal factor, F_R, increases when $\dot{m}_{coll}$ increases. $F_R(\tau\alpha)$ represents the gain portion from solar energy, and $F_R U_L$ represents the loss portion. Their respective values at various $\dot{m}_{coll}$ were listed in Table 4.2. It is expected that increasing $\dot{m}_{coll}$ will have a positive impact on system performance only until a certain threshold; subsequently, the effect of rising T_{bottom} (collector inlet temperature) due to the increasing amount of hot fluid mixes with the fluid at the TES bottom starts to play a significant role and compromises the system performance.

This subsection studies the system performance for two $\dot{m}_{coll}$ regions: low flow (within the “beneficial zone”) and higher flow where the system performance degrades (the “non-beneficial zone”).

Table 4.2 The collector heat removal factors for various $\dot{m}_{coll}$.

$\dot{m}_{coll}$ [kg/hr]	$F_R(\tau\alpha)$ [-]	F_RU_L [W/m^2-K]
15	0.468	2.868
25	0.570	3.497
30	0.601	3.685
70	0.703	4.306
110	0.734	4.500

Collector Flow Rate: Beneficial Zone Analysis

Fig 4.7 (a) indicates that collector flow rates of 15 and 25 kg/hr are located in the beneficial zone, and it also shows that solar fractions of 25 and 30 kg/hr are nearly identical. Therefore, it is expected that:

- when increasing $\dot{m}_{coll}$ from 15 to 25 kg/hr, the solar fraction curve as a function of tank volume will be shifted upward. This is seen in Fig 4.7 (b).
- when increasing $\dot{m}_{coll}$ from 25 to 30 kg/hr, the solar fraction curves will nearly coincide with each other and have been proved in Fig 4.7 (b).

The solar fraction for $\dot{m}_{coll}$ = 15 kg/hr in Fig 4.7 (b) remained nearly constant when $\frac{V_{TES}}{V_{daily}}$ > 0.15. Further analysis in the collector inlet temperature (T_i) was plotted in Fig 4.8. In the region of $\frac{V_{TES}}{V_{daily}}$ > 0.15, it shows that the collector inlet temperature when $\dot{m}_{coll}$ = 15 kg/hr (T_i_15) remained constant. Since the total daily fluid that passed through the collector (263 kg) was less than the total daily household demand (297 kg), the temperature of the fluid at the bottom of the tank (T_i_15) would be equal to the mains temperature. The total daily fluid through the collector was evaluated as the product of the daily pump-on time (17.5 hr) and collector flow rate (15 kg/hr). Since the energy collected is dependent on the collector inlet temperature, if that temperature is unaffected by changes in the tank volume, then the useful energy gain Q_u_15 (Fig 4.9) also remained constant. In addition, the growth in $Q_{LossTanks}$_15 had a trivial effect on the solar fraction. The combination of these two effects is the reason that solar fraction remained nearly constant with increases in tank volume beyond the optimal volume.

The solar fraction showed in Fig 4.7 (b) at V_{TES} = 0.303 m^3 is not the same value as that is shown in Fig 4.7 (a). Because Fig 4.7 (a) was completed by Wuestling et al. in the 1980s by using a large timestep (~1 hour). Whereas the system model in this thesis used a finer timestep (30 s) and led to a more accurate system prediction.

(a)

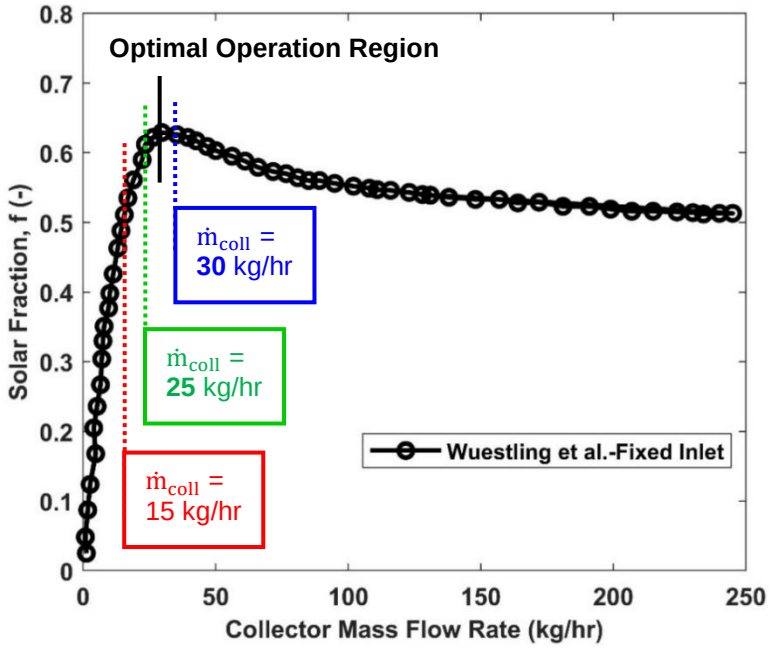

(b)

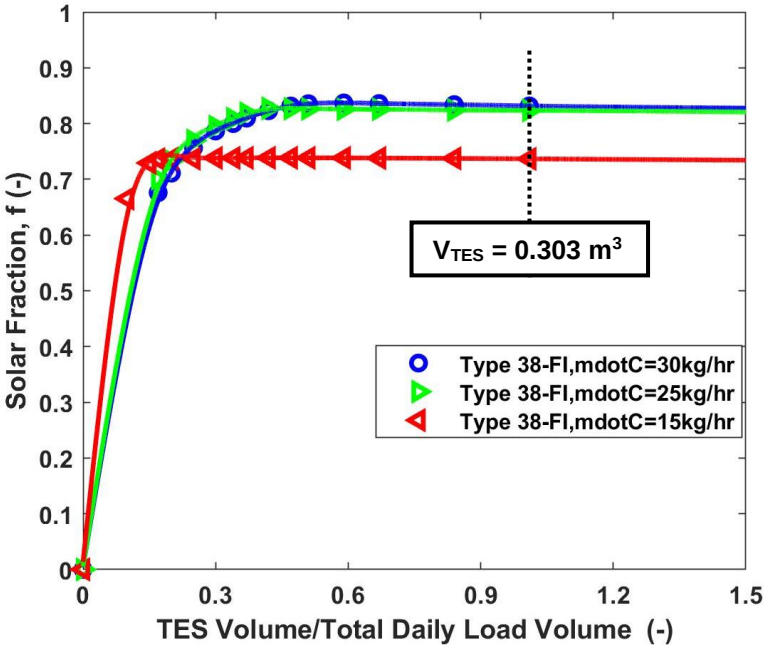

Figure 4.7 solar fraction for study in the beneficial zone. (a) Solar fraction versus collector flow rate. V_{TES} = 0.303 m^3, (b) Solar fraction versus dimensionless tank volume, $\dot{m}_{coll}$=15, 25, 30 kg/hr.

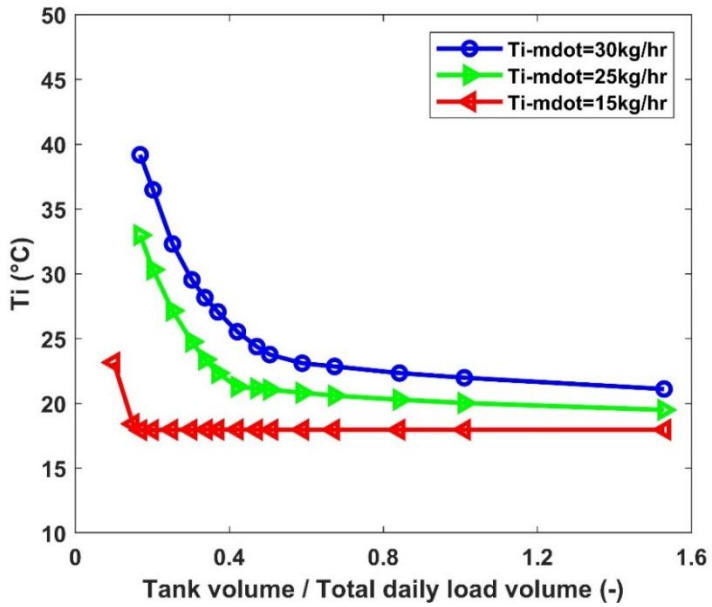

Figure 4.8 T_i vs. dimensionless tank volume for Case 1b (beneficial zone).

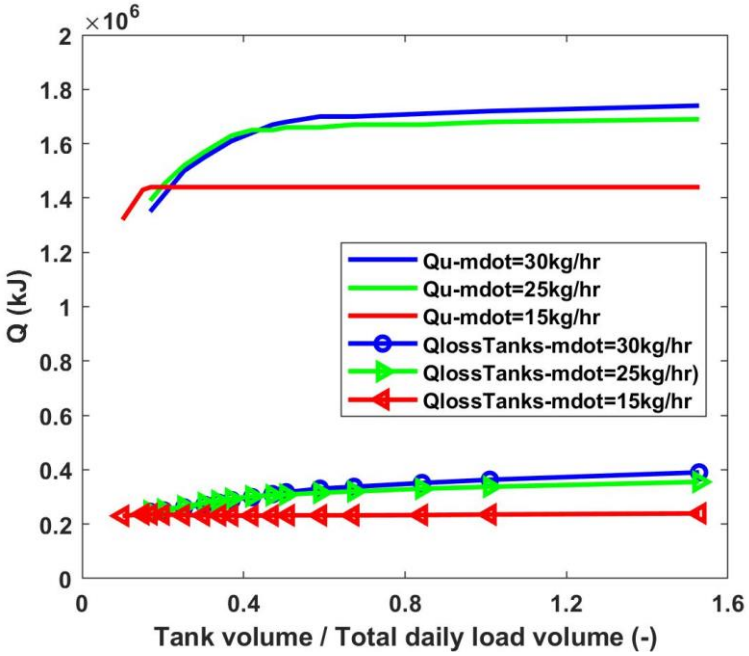

Figure 4.9 Q_u and $Q_{LossTanks}$ vs. dimensionless tank volume for Case 1b (beneficial zone).

As noted earlier, solar collector performance is enhanced by increasing $\dot{m}_{coll}$ and decreasing the collector inlet temperature. The collector inlet temperature is, however, influenced by the combination of $\dot{m}_{coll}$, household load, TES volume, and pump runtime. Fig 4.8 shows the collector inlet temperature as a function of tank volume and $\dot{m}_{coll}$. While the inlet temperature increases with increasing $\dot{m}_{coll}$, the increased magnitude of the collector heat removal factor (F_R – Equation 2.3) results in an overall increase in the energy collected in this regime. This implies that increasing $\dot{m}_{coll}$ is more rewarding than reducing T_i in system performance in the beneficial zone of Fig 4.7 (a). Analogously, enlarging V_{TES} is more crucial in determining system performance in the beneficial zone of Fig 4.7 (b).

Collector Flow Rate: Non-beneficial Zone Analysis

Fig 4.10 (a) demonstrates that the collector flow rate of 30, 70, and 110 kg/hr was located in the non-beneficial zone. Fig 4.10 (b) shows the solar fraction as a function of tank volume and illustrates that by increasing $\dot{m}_{coll}$ resulted in a downward shift in the curve for all tank volumes.

(a)

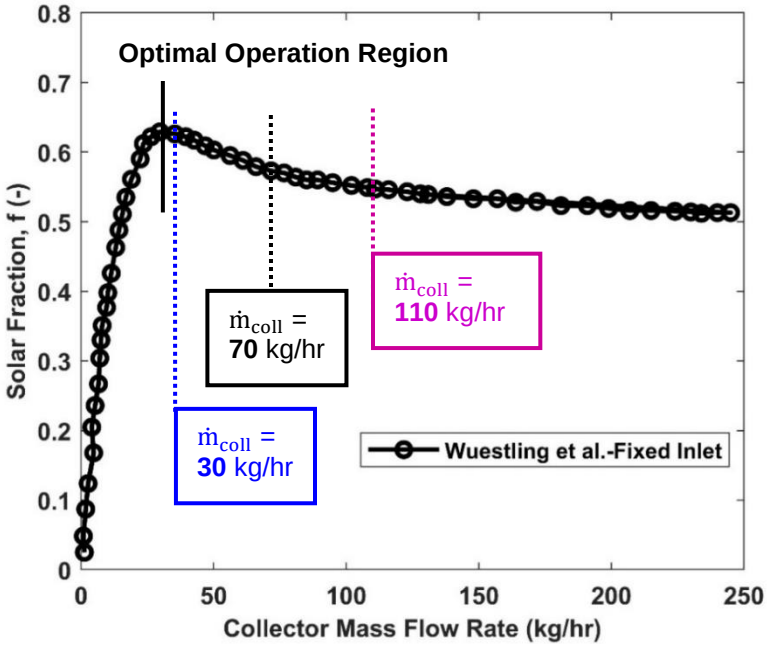

(b)

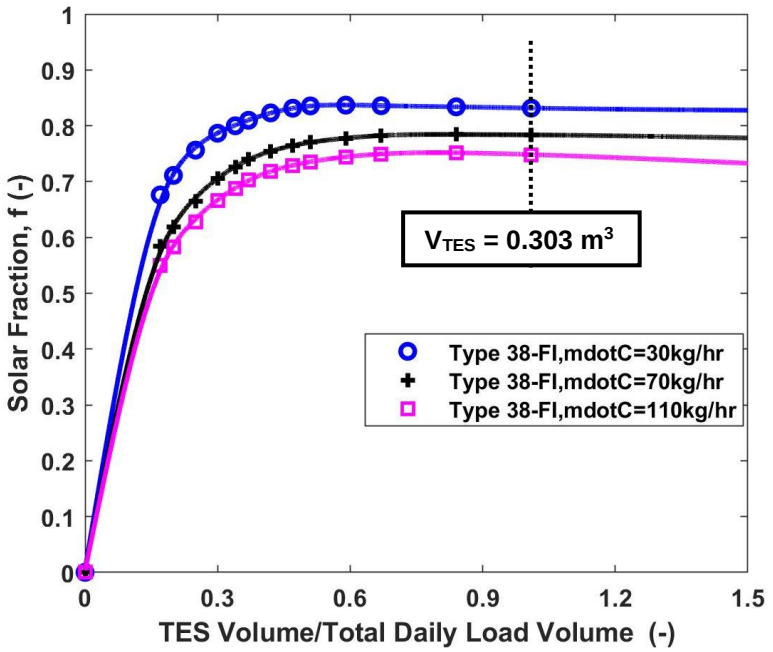

Figure 4.10 solar fraction for study in the non-beneficial zone. (a) Solar fraction versus collector flow rate. V_{TES} = 0.303 m^3. (b) Solar fraction versus dimensionless tank volume, $\dot{m}_{coll}$= 30, 70, 110 kg/hr.

As discussed earlier, the number of tank turnovers on the collector side is a function of $\dot{m}_{coll}$, tank volume, and the pump operating time, which is influenced by the collector inlet temperature. Fig 4.11 illustrates the tank turnover on the collector side as a function of the dimensionless tank volume. It shows that enlarging the TES resulted in lower T_i (Fig 4.12) since the thermocline was postponed to reach the bottom of the tank. It also reveals that at a specified V_{TES}, increasing $\dot{m}_{coll}$ led to a rise in T_i, thus a reduction in the pump-on time (Fig 4.13). Fig 4.14 shows that the collected energy, Q_u, reduced with increasing $\dot{m}_{coll}$ in the non-beneficial zone due to the rise in T_i and the reduction in pump-on time.

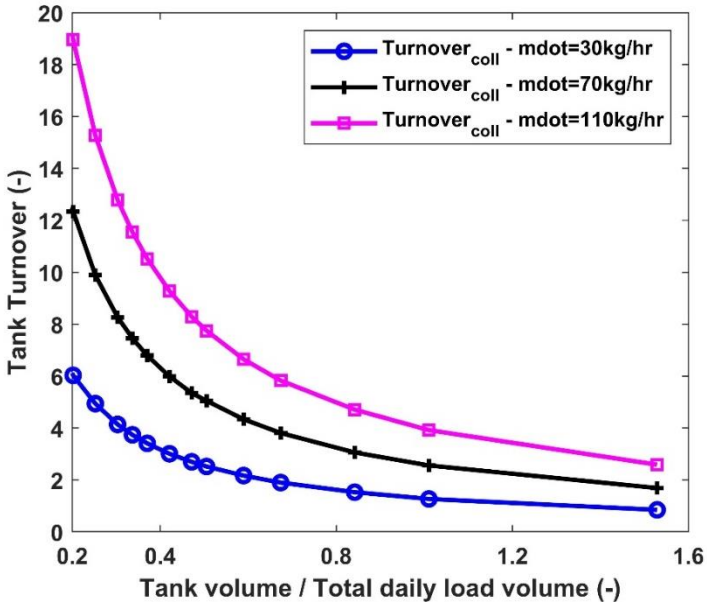

Figure 4.11Tank turnover on the collector side vs. dimensionless tank volume for Case 1b. $\dot{m}_{coll}$ = 30, 70, and 110 kg/hr (non-beneficial zone).

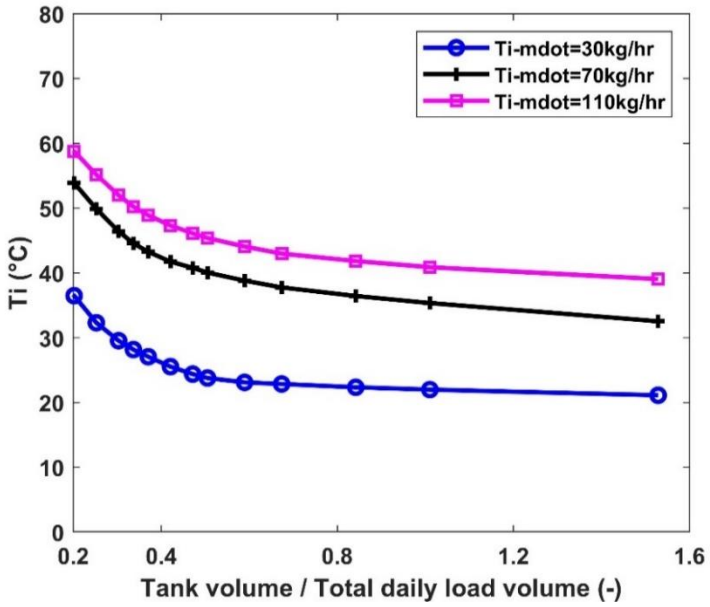

Figure 4.12 T_i vs. dimensionless tank volume for Case 1b. $\dot{m}_{coll}$ = 30, 70, and 110 kg/hr (non-beneficial zone).

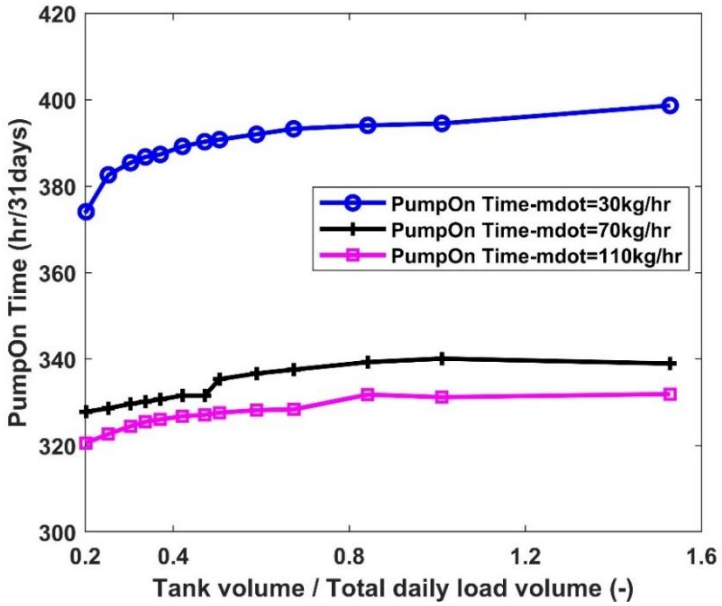

Figure 4.13 Pump-on time vs. dimensionless tank volume for Case 1b. $\dot{m}_{coll}$ = 30, 70, and 110 kg/hr (non-beneficial zone).

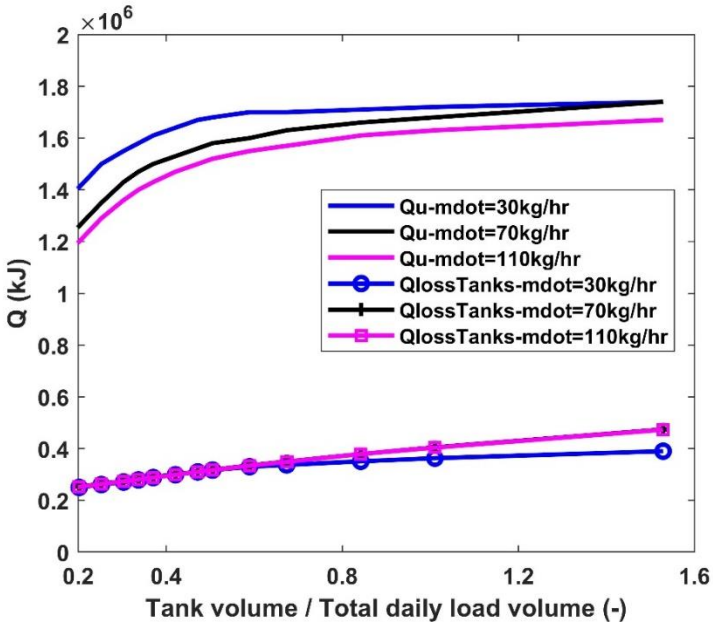

Figure 4.14 Q_u and $Q_{LossTanks}$ vs. dimensionless tank volume for Case 1b. $\dot{m}_{coll}$ = 30, 70, and 110 kg/hr (non-beneficial zone).

As previously discussed, the predicted solar fraction versus tank volume curve is non-linear with an optimal point that is dependent on the system operating conditions and geometry. A correlation is thus required to approximate the optimal dimensionless tank volume, $\left(\frac{V_{TES}}{V_{daily}}\right)_{f_{max}}$, where the peak system performance occurs. Let M_{coll} and M_{load} represent the total daily mass through the collector and household, respectively. The empirical correlation of $\left(\frac{V_{TES}}{V_{daily}}\right)_{f_{max}}$ as a function of $\frac{M_{coll}}{M_{load}}$ is presented in Equation 4.2. Subsequently, the optimal system performance, f_{max}, can be evaluated by the empirical correlation given in Equation 4.3. Since solar irradiance and the household load demands also influence system performance, the f_{max} correlation obtained is solely applicable to the SDHW system subject to this particular weather data and RAND load profile. The accuracy of both correlations is respectively summarized in Table 4.3.

$$\left(\frac{V_{TES}}{V_{daily}}\right)_{f_{max}}$$

$$= \begin{cases} -0.2371\left(\frac{M_{coll}}{M_{load}}\right)^4 + 1.118\left(\frac{M_{coll}}{M_{load}}\right)^3 - 1.753\left(\frac{M_{coll}}{M_{load}}\right)^2 + 1.358\left(\frac{M_{coll}}{M_{load}}\right) - \frac{2.724}{10^4}, & \frac{M_{coll}}{M_{load}} < 1.9 \\ 0.84, & \frac{M_{coll}}{M_{load}} \geq 1.9 \end{cases} \quad (\mathbf{4.2})$$

$$f_{max} = -\frac{3.905}{10^4} - 0.1437\left(\frac{M_{coll}}{M_{load}}\right) + 2.71\left(\frac{V_{TES}}{V_{daily}}\right)_{f_{max}} + \frac{8.947}{10^3}\left(\frac{M_{coll}}{M_{load}}\right)^2 + \frac{7.412}{10^2}\left(\frac{M_{coll}}{M_{load}}\right)\left(\frac{V_{TES}}{V_{daily}}\right)_{f_{max}} - 1.9\left[\left(\frac{V_{TES}}{V_{daily}}\right)_{f_{max}}\right]^2 \quad (\mathbf{4.3})$$

Table 4.3 The accuracies of empirical correlations presented in Equation (4.2) and (4.3).

Description	Equation (4.2) $\left(\frac{V_{TES}}{V_{daily}}\right)_{f_{max}} = f\left(\frac{M_{coll}}{M_{load}}\right)$	Equation (4.3) $f_{max} = f\left(\frac{M_{coll}}{M_{load}}, \left(\frac{V_{TES}}{V_{daily}}\right)_{f_{max}}\right)$
SSE	0.001694	0.0002581
R-square	0.9966	0.9995
RMSE	0.04116	0.007185

The empirical correlation between $\left(\frac{V_{TES}}{V_{daily}}\right)_{f_{max}}$ and $\frac{M_{coll}}{M_{load}}$ was presented in Fig 4.15. In the region of $\frac{M_{coll}}{M_{load}} < 1.9$, the correlation was obtained by polynomially curve fitting the six simulation data to the 4th power. Since 67% of data points located in the region of $1 < \frac{M_{coll}}{M_{load}} < 1.9$, it would provide a better prediction when compared to that in the region of $0 < \frac{M_{coll}}{M_{load}} < 1$. Furthermore, It is found that as $\dot{m}_{coll}$ increased, larger tanks were required to obtain the optimal f_{max} value. For systems with high $\dot{m}_{coll}$, the hot fluid on the top portion of the TES requires less transit time to reach the bottom, thus increasing the V_{TES} will increase the time required for the thermocline to reach the bottom of the tank. In the region of $\frac{M_{coll}}{M_{load}} \geq 1.9$, it is found

that $\left(\frac{V_{TES}}{V_{daily}}\right)_{f_{max}}$ was insensitive to the changes in $\dot{m}_{coll}$ and remained at 0.84. The predicted $\left(\frac{V_{TES}}{V_{daily}}\right)_{f_{max}}$ was also preliminarily verified with the numerical result of the SDHW system to satisfy a RAND household demand in an annual TMY weather, and no evidence showed against the correlation.

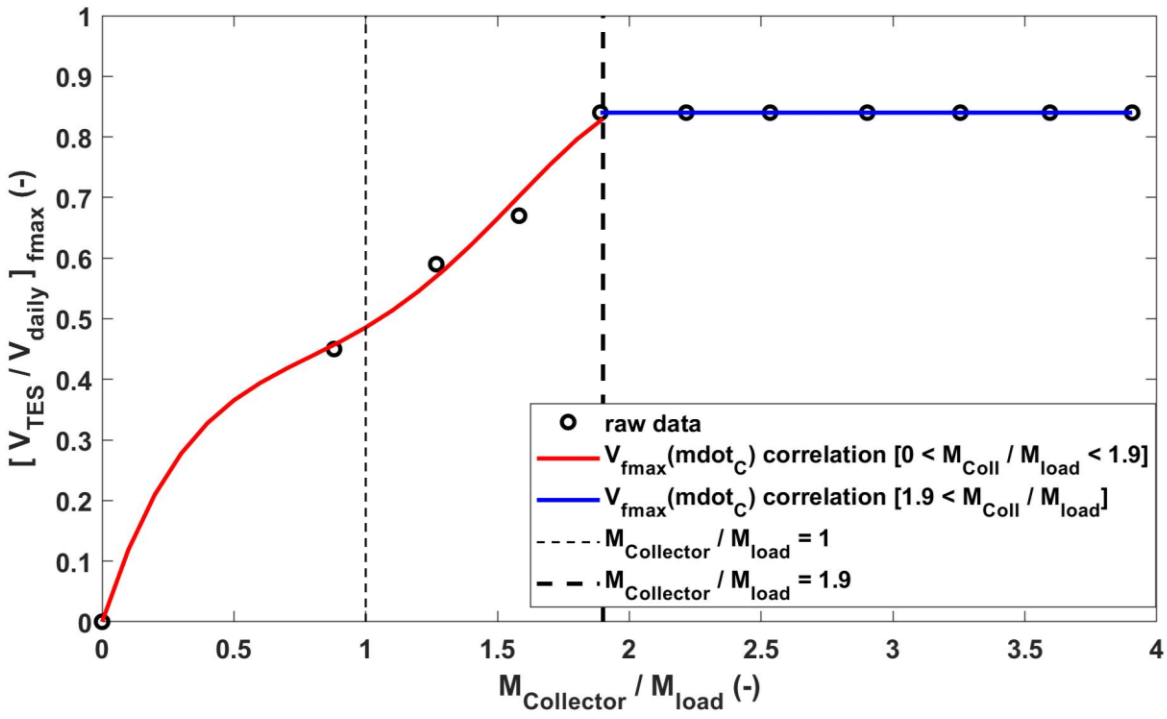

Figure 4.15 $\left(\frac{V_{TES}}{V_{daily}}\right)_{f_{max}}$ versus $\frac{M_{coll}}{M_{load}}$. $M_{Collector}$ and M_{load} represent the total daily mass through the collector and daily household demand, respectively. $M_{Collector}$ = (averaged τ_p) * $\dot{m}_{coll}$.

The contour map in Fig 4.16 represents Equation 4.3, which describes the optimal solar fraction as a function of $\left(\frac{V_{TES}}{V_{daily}}\right)_{f_{max}}$ and $\frac{M_{coll}}{M_{load}}$. The correlation was 2nd order polynomial curve fitting based on 11 data, which were illustrated as red dots in Fig 4.16. Since the solar irradiation and the household demands were not dimensionalized, this correlation was solely applicable to this particular weather input and RAND household demand.

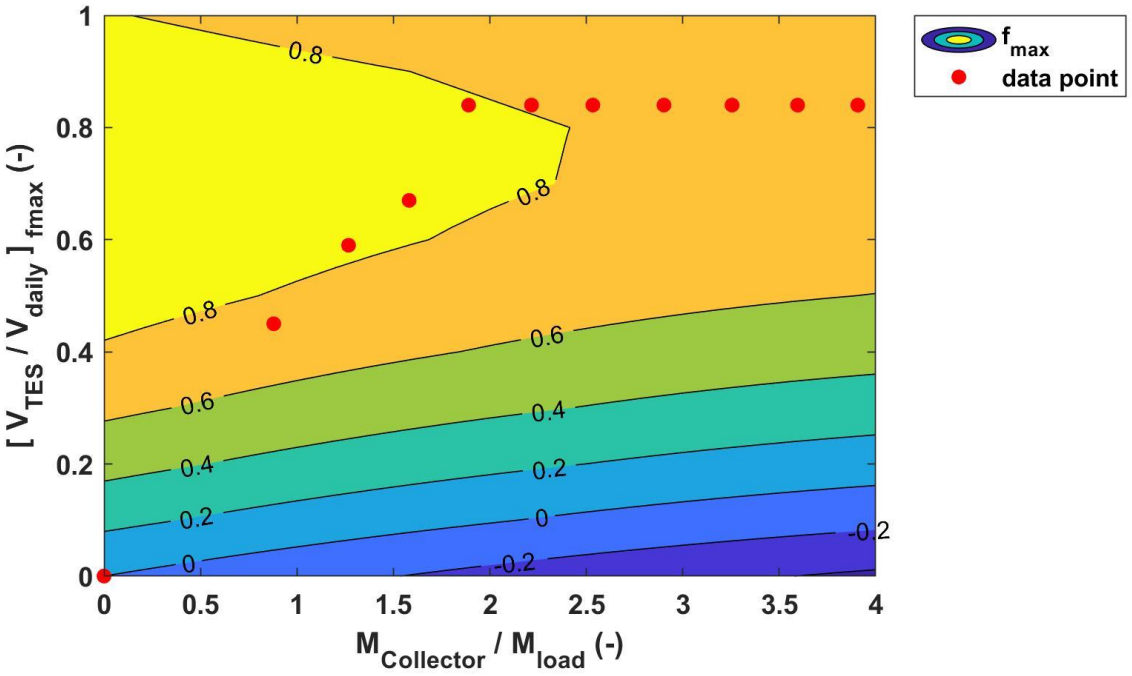

Figure 4.16 The contour map of the optimal system performance (f_{max}) as a function of the optimal dimensionless tank volume $\left(\left(\frac{V_{TES}}{V_{daily}}\right)_{f_{max}}\right)$ and the mass ratio $\left(\frac{M_{coll}}{M_{load}}\right)$.

Case 1 Summary

Q_u and $Q_{LossTanks}$ primarily determine the SDHW system performance. Fig 4.17 lists the parameters affecting solar fraction in a hierarchy order. System performance can be enhanced by increasing Q_u and reducing $Q_{LossTanks}$.

f vs. $\dot{m}_{coll}$:

Collector performance (Q_u) can be improved by increasing $\dot{m}_{coll}$ and reducing T_i. Studies had shown that solar fraction was initially enhanced by increasing $\dot{m}_{coll}$, and this benefit progressively diminished. Continuously increasing $\dot{m}_{coll}$ lead to a reduction in the transition time for the warm fluid on the top of the TES traveling towards the bottom. This caused a temperature rise in T_i and outweighed the benefit of increasing $\dot{m}_{coll}$. Consequently, the collector would incur more energy losses, and system performance would degrade. Therefore, increasing $\dot{m}_{coll}$ in the beneficial zone, and reducing T_i in the non-beneficial zone is paramount in enhancing system performance.

f vs. V_{TES}:

A low T_i can be achieved by enlarging the TES but at a higher cost of $Q_{LossTanks}$. The solar fraction was initially improved by enlarging V_{TES}, but the growth in $Q_{LossTanks}$ became more pronounced in determining system performance

progressively. Thus, enlarging V_{TES} improves system performance in the beneficial zone, and this benefit progressively diminished if continuously increasing V_{TES}.

A correlation between $\left(\frac{V_{TES}}{V_{daily}}\right)_{f_{max}}$ and $\frac{M_{coll}}{M_{load}}$ was also obtained. It appeared that the optimal operating collector flow rate occurred when $\frac{M_{coll}}{M_{load}} \approx 1$. Moreover, $\left(\frac{V_{TES}}{V_{daily}}\right)_{f_{max}}$ increased when $\dot{m}_{coll}$ increased until $\frac{M_{coll}}{M_{load}} \approx 1.9$ and remained constant at 0.84 subsequently.

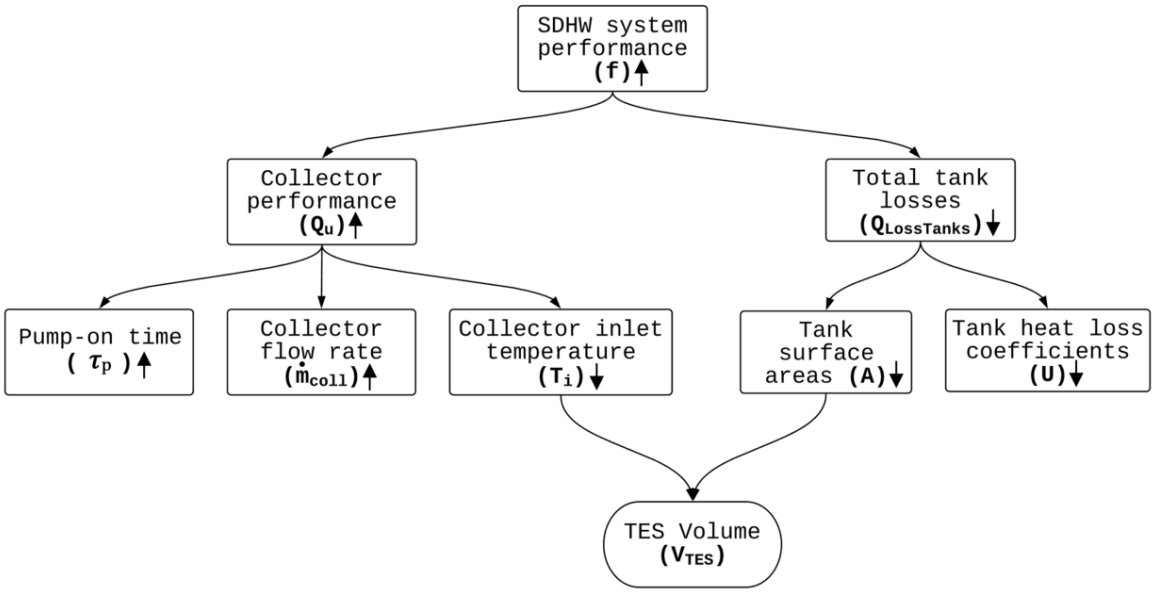

Figure 4.17 Hierarchy diagram of the parameters that affect the SDHW system performance.

Reducing T_i enhances collector performance and, thus, system performance. Moreover, the literature suggests that maintaining a high degree of thermal stratification within the TES would send cold fluid to the collector. Thus ensuring a high degree of thermal stratification was crucial in improving system performance. This will be explored in the following section of Case 2.

Case 2 - Effect of the Thermal Stratification on System Performance

The energy balance on the solar thermal systems indicates that the role of the TES was essentially to send cold fluid to the collector (low T_i) and that thermal stratification in the top portion was not as crucial in influencing the solar fraction. This hypothesis was explored in this section by using the nodal tank model (Type 4 model).

Case 2 was conducted at various degrees of stratification by varying the number of nodes (N) in the TES. One of the simulations was completed in a Variable Inlet (VI) TES model, which allowed the maximum degree of thermal stratification and provided the upper limit of system performance. Since Type 4 involves noticeable numerical diffusion, the TRNSYS result of the Type 38 VI model was also plotted in Fig 4.18 for the benchmark of the accuracy. The other extreme studying case was conducted in a fully mixed Fixed Inlet TES tank (N=1), and the lower limit of the system performance was observed. The simulations were also completed in Fixed Inlet (FI) model when N= 79, 40, and 20. The solar fractions were plotted in Fig 4.18. $T_{i,}$ Q_u, and $Q_{LossTanks}$ were plotted in Fig 4.19-21, respectively.

It observed in Fig 4.18 (a) that the VI system yielded the highest solar fraction. This was primarily due to the achievement of sending the lowest T_i (Fig 4.19), which led to the most Q_u (Fig 4.20), and $Q_{LossTanks}$ were similar (Fig 4.21) for all the simulations. In contrast, the fully mixed TES sent the hottest fluid to the collector, the system performance thus incurred with the most collector losses. Furthermore, when N was decreased (N = 79, 40, 20), the solar fraction dropped approximately 1% as the magnified view in Fig 4.18(b). The respective variations in T_i, Q_u, and $Q_{LossTanks}$ were also trivial. This implies that the effort of enhancing the degree of thermal stratification within the TES had a negligible effect (~1%) on system performance. This also agrees with the hypothesis posed earlier that the role of the TES is to deliver cold fluid to the collector, as distinct from enhancing the thermal stratification.

(a)

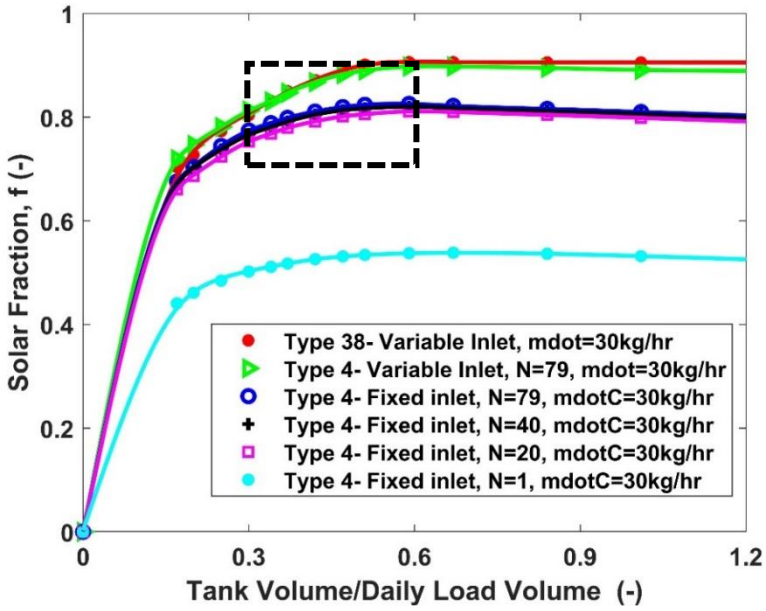

(b)

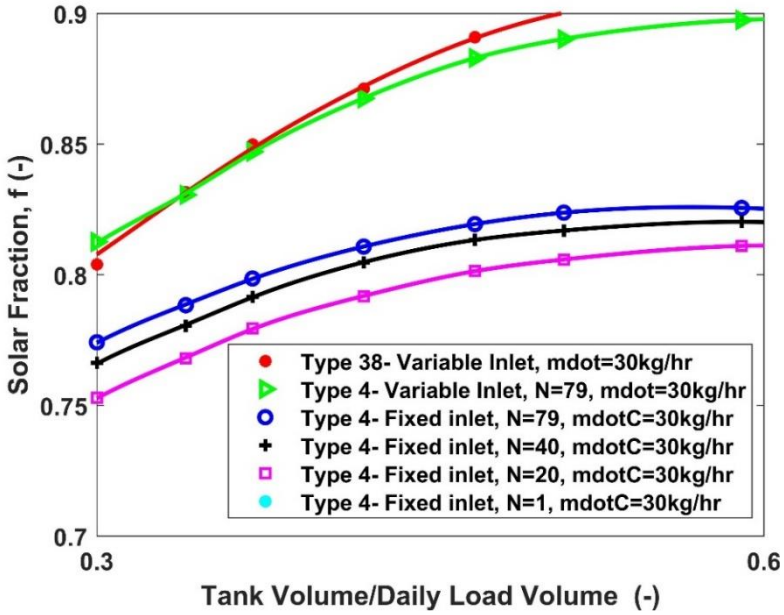

Figure 4.18 Solar fraction versus dimensionless tank volume for case 2. (a) Solar fraction versus dimensionless tank volume at various degrees of thermal stratification; (b) Detail view for the dotted area in (a), when $0.3 < x < 0.6$.

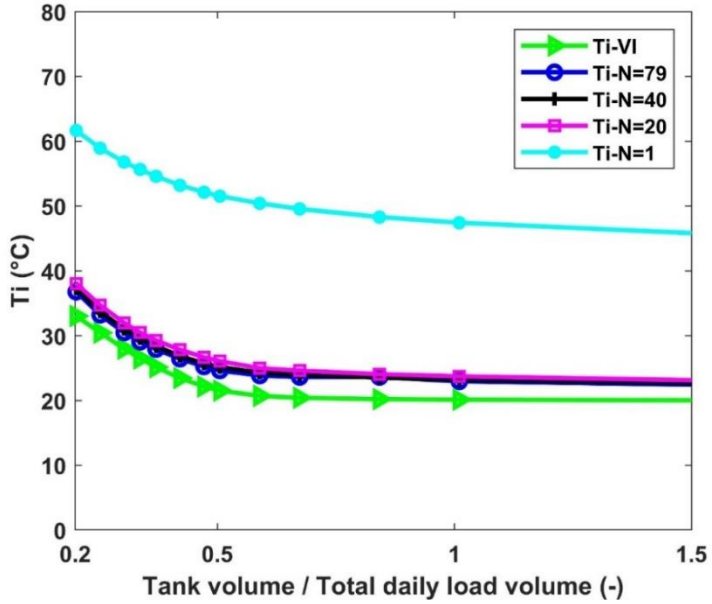

Figure 4.19 T_i vs. dimensionless tank volume for Case 2. N=79, 40, 20, and 1, $\dot{m}_{coll}$ = 30 kg/hr.

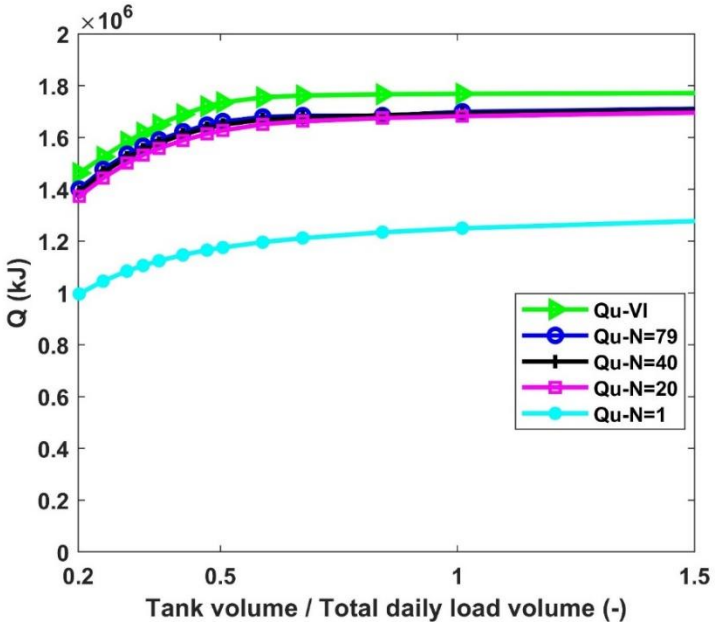

Figure 4.20 Qu vs. dimensionless tank volume for Case 2. N=79, 40, 20, and 1, $\dot{m}_{coll}$ = 30 kg/hr.

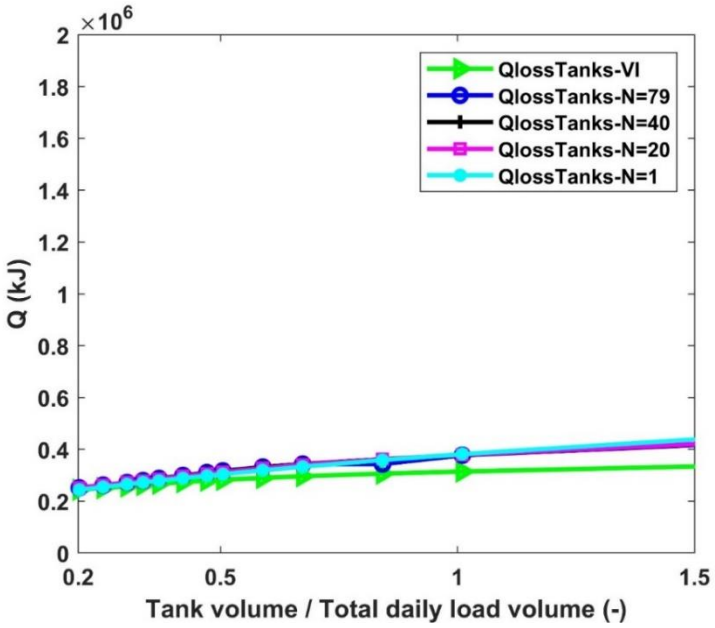

Figure 4.21 $Q_{lossTanks}$ vs. dimensionless tank volume for Case 2. N=79, 40, 20, and 1, $\dot{m}_{coll}$ = 30 kg/hr.

Case 3 - Effect of the Pump-on Time on System Performance

In annual simulations, it is found that the useful energy gain collected by the collector, Q_u, is more significant than the total thermal losses in the tanks, $Q_{LossTanks}$. Therefore Q_u is crucial in determining the solar fraction of the SDHW system. Q_u can be calculated by the Hottel-Whillier-Bliss equation in Appendix B, but also by equation (4.4), where τ_p, T_o, and T_i represent the pump-on time, collector outlet and inlet temperature, respectively.

$$Q_u = \int \dot{m}_{coll} * C_p * (T_o - T_i)\ dt \qquad (4.4)$$

The pump was controlled by monitoring the temperature difference between the collector inlet and outlet ($\triangle T$): the pump was turned on when $\triangle T$ exceeded a predetermined temperature deadband ($\triangle T_{on}$) and off when $\triangle T$ fell below a lower temperature deadband ($\triangle T_{off}$). The pump-on time was adjusted by controlling these temperature deadbands. Three study cases used the algebraic tank model (Type 38) and subjected to the annual Typical Meteorological Year weather data for Madison, WI, US, were performed in this subsection, and their pump control strategies were summarized in Table 4.4.

It is noted that as $\dot{m}_{coll}$ increases, the energy collected increases proportionally. Moreover, since the solar fraction is determined by the net energy collected from the solar collector, rather than just the temperature difference between inlet and outlet, an exploration of the influence of the pump control strategy was justified. As such, a relaxing of the control parameter at high flow rates (i.e. Comparing Case 3c to 3a) was considered in this section.

Table 4.4 Summaries of pump control strategies for Case 3 a-c.

Case #	$\dot{m}_{coll}$	ΔT_{on}	ΔT_{off}
Case 3a	$\dot{m}_{coll} = 30$ kg/hr	$\Delta T_{on} = 8.7°C$	$\Delta T_{off} = 1.7°C$
Case 3b	$\dot{m}_{coll} = 30$ kg/hr	$\frac{1}{2}\Delta T_{on} = 4.35°C$	$\frac{1}{2}\Delta T_{off} = 0.85°C$
Case 3c	$2\dot{m}_{coll} = 60$ kg/hr	$\frac{1}{2}\Delta T_{on} = 4.35°C$	$\frac{1}{2}\Delta T_{off} = 0.85°C$

Studying Parameter: ΔT

The temperature difference between the collector outlet and inlet, ΔT, is determined by T_i and T_o. Case 1 earlier indicated that increasing $\dot{m}_{coll}$ in the non-beneficial zone will cause a temperature rise in T_i. Consequently, increasing $\dot{m}_{coll}$ from 30 to 60 kg/hr will lead to an increase in T_i, as shown in Fig 4.22 ($T_{i\_a} \approx T_{i\_b} < T_{i\_c}$). Fig 4.23 indicates that $\Delta T_a > \Delta T_b > \Delta T_c$, which implies that the system with a higher requirement to turn on the pump and lower $\dot{m}_{coll}$ yields a higher ΔT, and the system with a lower requirement and higher $\dot{m}_{coll}$ yields a lower ΔT.

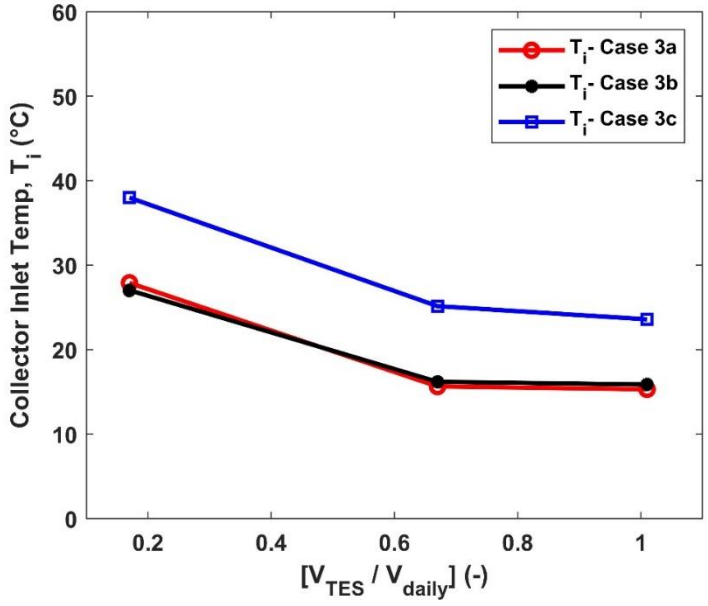

Figure 4.22 T_i vs. dimensionless tank volume for Case 3.

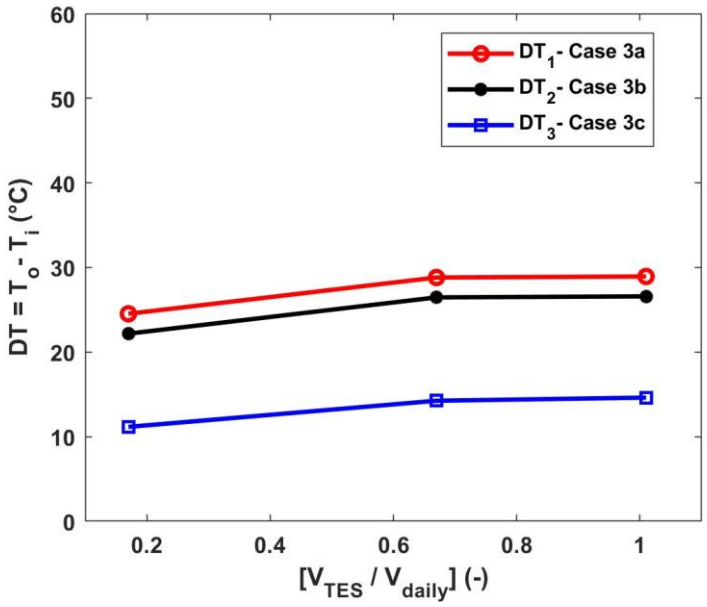

Figure 4.23 ΔT vs. dimensionless tank volume for Case 3. $\Delta T = T_{i,avg} - T_{o,avg}$.

Analysis of the Pump Run Time

The pump-on time was presented in Fig 4.24, which showed that $\tau_{p\_b} > \tau_{p\_a} > \tau_{p\_c}$. Case 3b yield the longest pump-on time due to its minimum requirement (lowest ΔT_{on}) to operate the pump and low T_i, whereas Case 3a had the highest requirement to activate the pump. Although Case 3c had the minimum requirement to activate the pump, the pump-on time was incurred by high T_i.

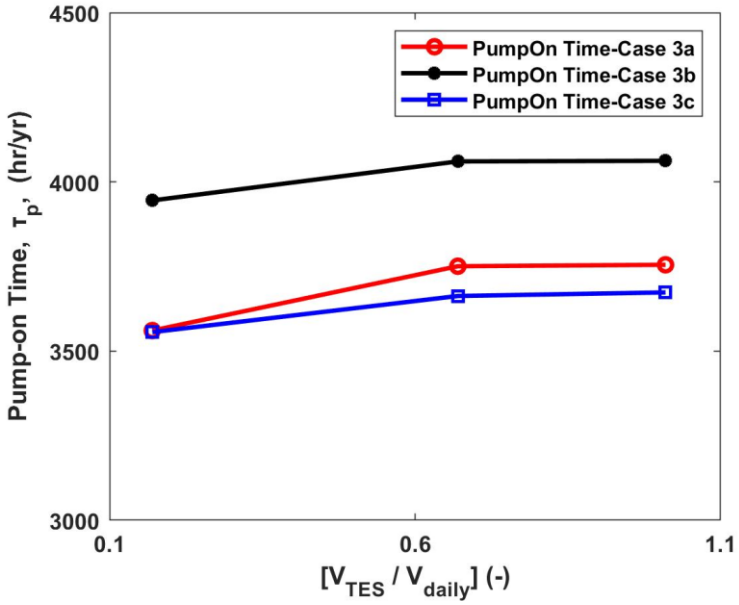

Figure 4.24 Pump-On time vs. dimensionless tank volume for Case 3.

Previously Equation 4.4 showed that Q_u is influenced by both ΔT and τ_p. Case 3a and Case 3b shared the same $\dot{m}_{coll}$, however, due to different pump control strategy, Case 3a yielded a higher ΔT but a lower τ_p, whereas Case 3b yielded a lower ΔT but a higher τ_p. Fig 4.25 indicates that the difference between Q_{u_a} and Q_{u_b} was negligible. The same finding was shown in $Q_{LossTanks}$. Despite employing different pump control strategy, the effect of ΔT counterbalanced the effect of τ_p. Thus changing the pump control strategy has a negligible effect on system performance and was pro in Fig 4.26.

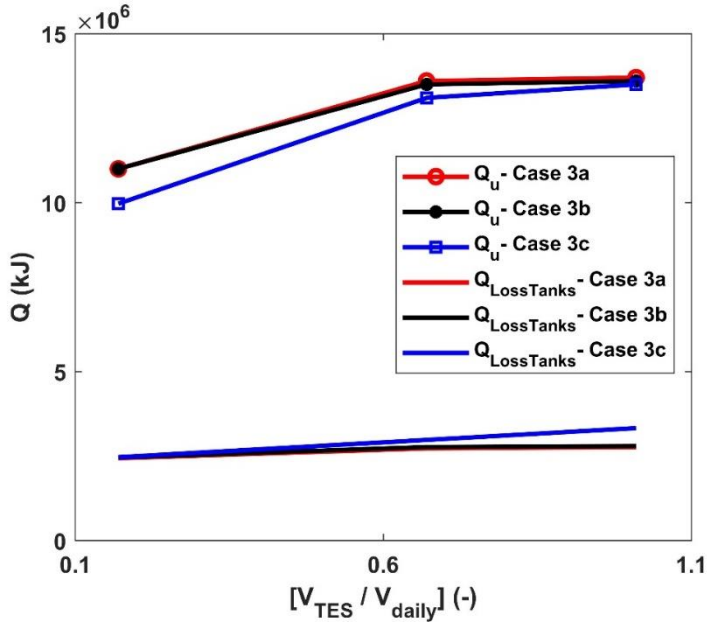

Figure 4.25 Qu, or $Q_{LossTanks}$ vs. dimensionless tank volume for Case 3.

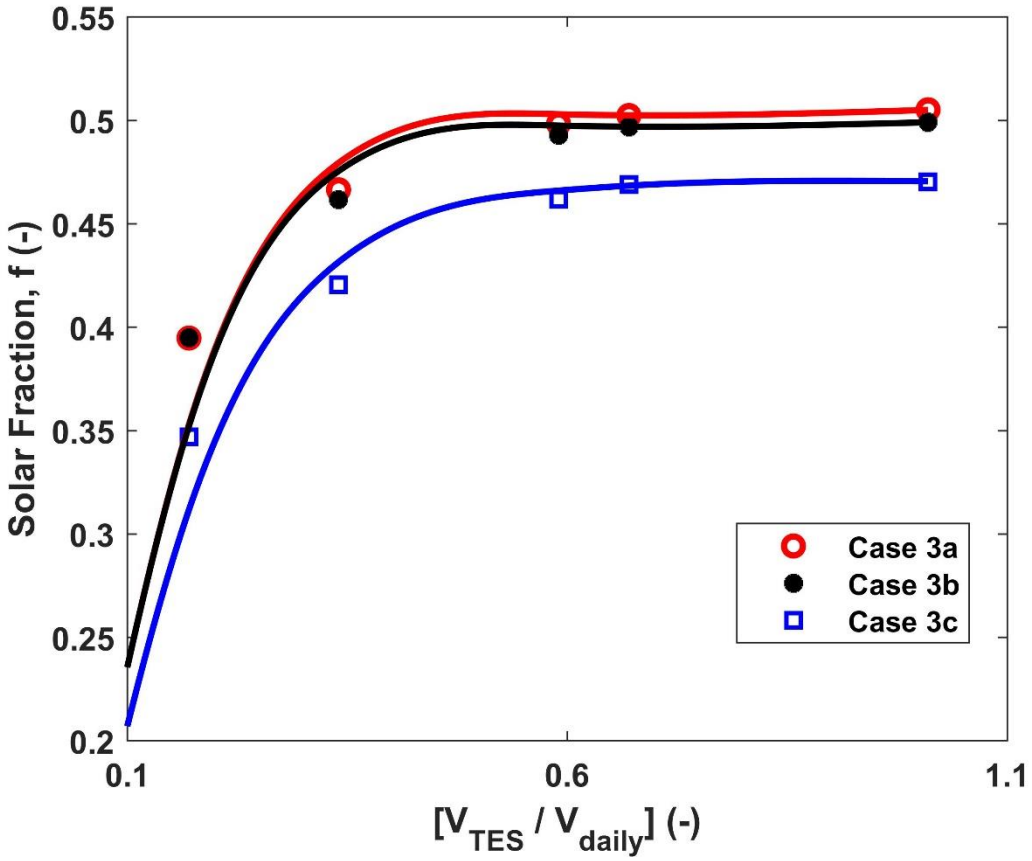

Figure 4.26 Solar fraction versus dimensionless tank volume for TMY annual weather in Madison, Wisconsin, US. RAND household demand was employed.

Conclusion

The case studies presented in this chapter investigated SDHW system performance influenced by $\dot{m}_{coll}$, degree of thermal stratification within the TES, and pump-on time in multiple TES tank sizes. An empirical correlation was obtained to determine the optimal dimensionless TES volume at a given collector flow rate during Case 1 study. Case 2 illustrated that the role of the TES is to send cold water to the collector, and systems with various degrees of thermal stratification yielded similar solar fraction. Finally, Case 3 revealed that changing the pump control strategy had an insignificant effect on system performance at a given collector flow rate.

Case 1 studied the effect $\dot{m}_{coll}$ on the solar fraction in multiple TES tank sizes, and it discovered that varying $\dot{m}_{coll}$ shifted the solar fraction curve vertically. By increasing $\dot{m}_{coll}$ the system performance increased until the optimum. Further increases in $\dot{m}_{coll}$ impeded system performance due to increases in collector inlet temperatures. Furthermore, the V_{TES} had an analogous effect on system performance. It was observed that by enlarging the V_{TES}, system performance was enhanced in the beneficial zone, yet this benefit diminished if continuously enlarging the TES after the peak performance. This was because the growth in

$Q_{LossTanks}$ progressively became more pronounced in determining system performance. Furthermore, the optimal V_{TES} could be determined by the empirical correlation presented in Equation (4.2). The correlation also revealed that the optimal collector flow rate occured at $\frac{M_{coll}}{M_{load}} \approx 1$ and $\left(\frac{V_{TES}}{V_{daily}}\right)_{f_{max}}$ remained constant at 0.84 when $\frac{M_{coll}}{M_{load}} > 1.9$.

Case 2 investigated system performance affected by the degree of thermal stratification within the TES. It showed that enhancing thermal stratification (N = 20, 40, 79) in the TES model, T_i, Q_u, $Q_{LossTanks}$, and solar fraction changed within 1%. Thus the degree of thermal stratification within the TES had a negligible effect on system performance. The role of the TES is to deliver cold fluid to the collector rather than enhancing thermal stratification.

Case 3 explored the effect of the pump-on time on system performance. It found that at a given collector flow rate, changing pump control strategy had a negligible effect on system performance.

Chapter 5
Conclusions and Future Recommendation

5.1 Summary and Conclusion

Solar domestic hot water (SDHW) systems show great potential to offset the dependence on energy from fossil fuels. System performance (solar fraction) primarily can be enhanced by increasing the useful energy gained by the collector (Q_u) and reducing the total thermal losses by tanks ($Q_{LossTanks}$). A verified TRNSYS model was used to study the system performance affected by the key parameters including the magnitude of the collector mass flow rate ($\dot{m}_{coll}$), the volume of the thermal energy storage (TES) tank, the degree of thermal stratification within the TES tank, and the duration of fluid passing through the collector (pump-on time).

SDHW system performance was investigated at various $\dot{m}_{coll}$ in various TES tank sizes to fulfill a RAND household demand for a month of repetitive daily weather (May 9 in Madison, WI, US). The results indicated that solar fraction was improved by increasing $\dot{m}_{coll}$ or V_{TES} in the beneficial zone and this benefit diminished if continuously increasing $\dot{m}_{coll}$ or V_{TES}. The beneficial zone was defined by the regime before the optimal performance, which could be estimated by the correlation obtained in Chapter 4 Case 1 Equation (4.2). It described the optimal dimensionless tank size $\left(\left(\frac{V_{TES}}{V_{daily}}\right)_{f_{max}}\right)$ as a function of the mass ratio $\left(\frac{M_{coll}}{M_{load}}\right)$. It

also discovered that the optimal operating $\dot{m}_{coll}$ occurred when $\frac{M_{coll}}{M_{load}} \approx 1$. Moreover, $\left(\frac{V_{TES}}{V_{daily}}\right)_{f_{max}}$ was positively related to $\dot{m}_{coll}$ until $\frac{M_{coll}}{M_{load}}$ reached 1.9 and remained constant at 0.84 subsequently. The correlation was primarily verified by the annual system simulations to fulfill RAND household demand and subjected to TMY weather data of Madison, WI, US, and no evidence showed against the correlation.

The effect of thermal stratification within the TES on SDHW system performance was explored. Simulations were conducted by repeating daily spring weather for a month to satisfy RAND household demand in multiple sizes of the TES tank. It was observed that the perfectly stratified TES model (Variable Inlet model) yielded the lowest collector inlet temperature (T_i) and the highest solar fraction (f); whereas the fully mixed TES model delivered the hottest T_i and the poorest system performance. When the thermal stratification was controlled by changing the number of nodes in the model (N = 79,40,20), the change in T_i was within 0.5°C, and a minor variation (~1%) in the solar fraction was discovered. Therefore, the role of the TES tank is to deliver cold fluid to the collector rather than enhancing thermal stratification.

Annual system performance influenced by the pump-on time (τ_p) was analyzed at different $\dot{m}_{coll}$ in various TES sizes. Different pump control strategies ($\Delta T_{on/off}$) were employed by monitoring the temperature difference between the collector inlet and outlet ($\Delta T = T_o - T_i$) to adjust the pump-on time. By maintaining constant $\dot{m}_{coll}$ and narrowing $\Delta T_{on/off}$, the benefit of attaining a longer pump-on time was counterbalanced by the reduction in ΔT. The system performance was negligibly affected (~0.5%) by employing different pump control strategies. During the operation of the same pump control strategy but increasing $\dot{m}_{coll}$ (high flow rates in the non-beneficial zone), the results revealed that system performance incurred by a reduction in both pump-on time and $\triangle T$.

5.2 Suggestions for Future Work

An empirical correlation between $\left(\frac{V_{TES}}{V_{daily}}\right)_{f_{max}}$ and $\frac{M_{coll}}{M_{load}}$ was established and preliminarily verified with different solar irradiance inputs, further verification can be implemented for various weather data and household demands to augment more confidences towards the correlation.

The influence of the degree of thermal stratification within the TES was studied in the nodal tank model (Type 4), which involves a considerable amount of numerical diffusion. An updated tank model with less numerical diffusion can replace the current TES model to predict more accurate results.

The effect of pump control strategy on system performance was explored for different collector flow rates, which were considered as high flow rates (located in the non-beneficial zone). Further studies can be conducted to explore the effect of the pump control strategy for low-collector-flow-rate systems.

Bibliography

[1] N. R. Canada, “Energy and Greenhouse Gas Emissions (GHGs),” Oct. 06, 2017. https://www.nrcan.gc.ca/energy/facts/energy-ghgs/20063 (accessed Apr. 24, 2020).

[2] H. Chen, “G7 Fossil Fuel Subsidy Scorecard,” *NRDC*, 06032018. https://www.nrdc.org/resources/g7-fossil-fuel-subsidy-scorecard (accessed Apr. 24, 2020).

[3] N. R. Canada, “Energy Efficiency Trends in Canada 1990 to 2013,” Sep. 20, 2016. https://www.nrcan.gc.ca/energy/publications/19030#a3 (accessed Apr. 24, 2020).

[4] “Drake Landing Solar Community.” https://www.dlsc.ca/ (accessed Apr. 24, 2020).

[5] “Go Solar- Your guide to harnessing the power of the sun,” the City of Vaughan, Vaughan, Ontario, 2009. [Online]. Available: http://www.vaughan.ca/cityhall/environmental_sustainability/General%20Documents/GoSolar_Book-2009.pdf.

[6] “Solar Energy Maps Canada (Every Province),” *energyhub.org*, May 12, 2018. https://energyhub.org/solar-energy-maps-canada/ (accessed Apr. 24, 2020).

[7] “TRNSYS - Official Website.” http://sel.me.wisc.edu/trnsys/ (accessed Apr. 24, 2020).

[8] K. G. T. Hollands and M. F. Lightstone, “A review of low-flow, stratified-tank solar water heating systems,” *Sol. Energy*, vol. 43, no. 2, pp. 97–105, Jan. 1989, doi: 10.1016/0038-092X(89)90151-5.

[9] M. D. Wuestling, S. A. Klein, and J. A. Duffie, “Promising Control Alternatives for Solar Water Heating Systems,” *J. Sol. Energy Eng.*, vol. 107, no. 3, pp. 215–221, Aug. 1985, doi: 10.1115/1.3267681.

[10] Z. Lavan and J. Thompson, “Experimental study of thermally stratified hot water storage tanks,” *Sol. Energy*, vol. 19, no. 5, pp. 519–524, Jan. 1977, doi: 10.1016/0038-092X(77)90108-6.

[11] L. J. Shah and S. Furbo, “Entrance effects in solar storage tanks,” *Sol. Energy*, vol. 75, no. 4, pp. 337–348, Oct. 2003, doi: 10.1016/j.solener.2003.04.002.

[12] A. A. Hegazy, “Effect of inlet design on the performance of storage-type domestic electrical water heaters,” *Appl. Energy*, vol. 84, no. 12, pp. 1338–1355, Dec. 2007, doi: 10.1016/j.apenergy.2006.09.014.

[13] N. Altuntop, M. Arslan, V. Ozceyhan, and M. Kanoglu, “Effect of obstacles on thermal stratification in hot water storage tanks,” *Appl. Therm. Eng.*, vol. 25, no. 14, pp. 2285–2298, Oct. 2005, doi: 10.1016/j.applthermaleng.2004.12.013.

[14] D. E. Adams and J. H. Davidson, “Tank Stratification with a Flexible Manifold,” presented at the Proceedings of Solar ’93, Washiongton, DC, 1993.

[15] J. H. Davidson and D. A. Adams, “Fabric Stratification Manifolds for Solar Water Heating,” *J. Sol. Energy Eng.*, vol. 116, no. 3, pp. 130–136, Aug. 1994, doi: 10.1115/1.2930071.

[16] S. Seddegh, X. Wang, A. D. Henderson, and Z. Xing, “Solar domestic hot water systems using latent heat energy storage medium: A review,” *Renew. Sustain. Energy Rev.*, vol. 49, pp. 517–533, Sep. 2015, doi: 10.1016/j.rser.2015.04.147.

[17] Y. Tian and C. Y. Zhao, “A review of solar collectors and thermal energy storage in solar thermal applications,” *Appl. Energy*, vol. 104, pp. 538–553, Apr. 2013, doi: 10.1016/j.apenergy.2012.11.051.

[18] S. A. Kalogirou, “Solar thermal collectors and applications,” *Prog. Energy Combust. Sci.*, vol. 30, no. 3, pp. 231–295, Jan. 2004, doi: 10.1016/j.pecs.2004.02.001.

[19] R. Liang, J. Zhang, L. Ma, and L. Zhao, “Dynamic simulation on thermal performance of gas–liquid separated solar collector system with R245fa,” *Appl. Therm. Eng.*, vol. 68, no. 1, pp. 69–75, Jul. 2014, doi: 10.1016/j.applthermaleng.2014.04.017.

[20] Y. Jaluria and S. K. Gupta, “Decay of thermal stratification in a water body for solar energy storage,” *Sol. Energy*, vol. 28, no. 2, pp. 137–143, Jan. 1982, doi: 10.1016/0038-092X(82)90292-4.

[21] M. Shaarawy, “Numerical Analysis of Thermal Strati cation in Large Horizontal Thermal Energy Storage Tanks,” Thesis, McMaster University, Hamilton, On.

[22] D. J. Nizami, M. F. Lightstone, S. J. Harrison, and C. A. Cruickshank, “Negative buoyant plume model for solar domestic hot water tank systems incorporating a vertical inlet,” *Sol. Energy*, vol. 87, pp. 53–63, Jan. 2013, doi: 10.1016/j.solener.2012.10.001.

[23] M. F. Lightstone, “A Numerical Study of Thermal Stratification in Solar Energy Storage Tanks,” University of Waterloo, Waterloo, Ontario, 1987.

[24] M. A. Abdoly and D. Rapp, “Theoretical and experimental studies of stratified thermocline storage of hot water,” *Energy Convers. Manag.*, vol. 22, no. 3, pp. 275–285, Jan. 1982, doi: 10.1016/0196-8904(82)90053-X.

[25] P. C. Eames and B. Norton, “The effect of tank geometry on thermally stratified sensible heat storage subject to low Reynolds number flows,” *Int. J. Heat Mass Transf.*, vol. 41, no. 14, pp. 2131–2142, Jul. 1998, doi: 10.1016/S0017-9310(97)00349-9.

[26] Y. H. Zurigat, P. R. Liche, and A. J. Ghajar, “Influence of inlet geometry on mixing in thermocline thermal energy storage,” *Int. J. Heat Mass Transf.*, vol. 34, no. 1, pp. 115–125, Jan. 1991, doi: 10.1016/0017-9310(91)90179-I.

[27] T. Bouhal, S. Fertahi, Y. Agrouaz, T. El Rhafiki, T. Kousksou, and A. Jamil, “Numerical modeling and optimization of thermal stratification in solar hot water storage tanks for domestic applications: CFD study,” *Sol. Energy*, vol. 157, pp. 441–455, Nov. 2017, doi: 10.1016/j.solener.2017.08.061.

[28] A. M. Shariah and G. O. G. Löf, “The optimization of tank-volume-to-collector-area ratio for a thermosyphon solar water heater,” *Renew. Energy*, vol. 7, no. 3, pp. 289–300, Mar. 1996, doi: 10.1016/0960-1481(95)00132-8.

[29] M. N. A. Hawlader, S. K. Chou, and M. Z. Ullah, “The performance of a solar assisted heat pump water heating system,” *Appl. Therm. Eng.*, vol. 21, no. 10, pp. 1049–1065, Jul. 2001, doi: 10.1016/S1359-4311(00)00105-8.

[30] K. Çomaklı, U. Çakır, M. Kaya, and K. Bakirci, “The relation of collector and storage tank size in solar heating systems,” *Energy Convers. Manag.*, vol. 63, pp. 112–117, Nov. 2012, doi: 10.1016/j.enconman.2012.01.031.

[31] C. Unrau, “Numerical Investigation of One-Dimensional Storage Tank Models and the Development of Analytical Modelling Techniques,” McMaster University, Hamilton, 2017.

[32] R. Dickinson, “Analysis and Development of Draw Strategies for a Multi-Tank Thermal Storage System for Solar Heating Applications,” Carleton University, Ottawa, Ontario, 2012.

[33] W. E. Buckles and S. A. Klein, “Analysis of solar domestic hot water heaters,” *Sol. Energy*, vol. 25, no. 5, pp. 417–424, Jan. 1980, doi: 10.1016/0038-092X(80)90448-X.

[34] “Influence of the DHW load profile on the fractional energy savings: a case study of a solar Combi-system with TRNSYS simulations,” *Fuel Energy Abstr.*, vol. 43, no. 3, p. 200, May 2002, doi: 10.1016/S0140-6701(02)85844-1.

[35] U. Jordan, K. Vajen, F. Physik, and F. Solar, “Realistic Domestic Hot-Water Profiles in Different Time Scales,” p. 18.

[36] R. Hendron and J. Burch, “Development of Standardized Domestic Hot Water Event Schedules for Residential Buildings,” 2007, pp. 531–539, doi: 10.1115/ES2007-36104.

[37] S. Edwards, I. Beausoleil-Morrison, and A. Laperrière, “Representative hot water draw profiles at high temporal resolution for simulating the performance of solar thermal systems,” *Sol. Energy*, vol. 111, pp. 43–52, Jan. 2015, doi: 10.1016/j.solener.2014.10.026.

[38] G. F. Csordas, A. P. Brunger, K. G. T. Hollands, and M. F. Lightstone, “Plume entrainment effects in solar domestic hot water systems employing variable-flow-rate control strategies,” *Sol. Energy*, vol. 49, no. 6, pp. 497–505, Dec. 1992, doi: 10.1016/0038-092X(92)90158-7.

[39] J. DUFFIE and W. BECKMAN, “Solar Engineering of Thermal Processes, 4th Edition,” *Wiley.com*. https://www.wiley.com/en-ca/Solar+Engineering+of+Thermal+Processes%2C+4th+Edition-p-9780470873663 (accessed Apr. 30, 2018).

[40] H. M. Teamah, M. F. Lightstone, and J. S. Cotton, “An alternative approach for assessing the benefit of phase change materials in solar domestic hot water systems,” *Sol. Energy*, vol. 158, pp. 875–888, Dec. 2017, doi: 10.1016/j.solener.2017.10.033.

[41] Y. Allard, M. Kummert, M. Bernier, and A. Moreau, “1 École Polytechnique de Montréal, Département de génie mécanique, P.O. Box 6079, succursale centre-ville, Montréal (Québec) H3C 3A7, Canada 2 Laboratoire des Technologies de l’Énergie (LTE), Hydro-Québec, P.O. Box 990, Shawinigan (Québec) G9N 7N5, Canada,” p. 8.

Appendix A Analysis of the Flat-Plate Collector Performance

Collector performance can be measured by the rate of collecting useful energy, $\dot{Q}_u$, which is demonstrated in the Hottel-Whillier-Bliss relationship shown in Equation A1. Parameters that influence collector performance are $F_R(\tau\alpha)$, $F_R U_L$, A_c, and T_i, and will be discussed in this appendix.

$$\dot{Q}_u = A_c[F_R(\tau\alpha) * G - F_R U_L(T_i - T_a)]$$

$$= \dot{m}_{coll} * C_p * (T_o - T_i) \quad \text{(A1)}$$

Where A_c = collector area

$F_R(\tau\alpha)$ = intercept of the collector efficiency versus $(T_i\text{-}T_a)/G$ curve

G = solar irradiance

$F_R U_L$ = negative slope of the collector efficiency versus $(T_i\text{-}T_a)/G$ curve

T_i = collector inlet temperature

T_a = ambient temperature

$\dot{m}_{coll}$ = collector mass flow rate

C_p = heat capacity of the fluid

T_o = collector outlet temperature

The collector heat removal factor, F_R, is influenced by $\dot{m}_{coll}$, recall Equation 2.3 and repeated as:

$$F_R = \frac{\dot{m}_{coll} * C_p}{A_c U_L}\left[1 - exp\left(-\frac{A_c U_L F'}{\dot{m}_{coll} * C_p}\right)\right]$$

Studies on the effect of $\dot{m}_{coll}$ on $F_R(\tau\alpha)$ and F_RU_L were performed and shown in Fig A1. It appears that an increase in $\dot{m}_{coll}$ leads to growths in both $F_R(\tau\alpha)$ and F_RU_L, and these effects progressively diminish if continuously increasing $\dot{m}_{coll}$ after ~60 kg/hr.

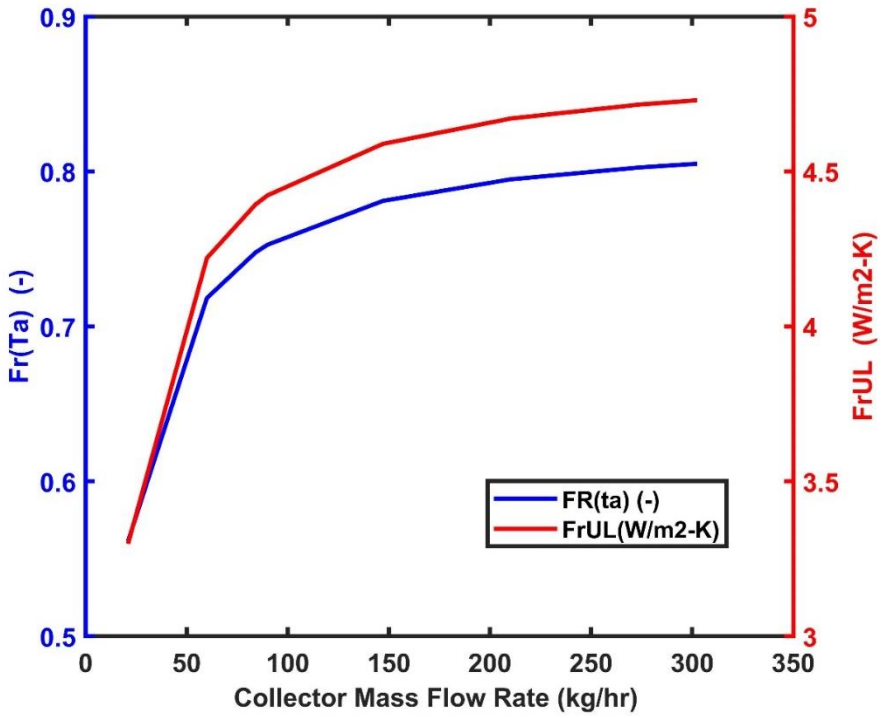

Figure A.1 The effects of collector flow rates on $F_R(\tau\alpha)$ and F_RU_L. A_c = 4.2 m^2, $F_R(\tau\alpha)_{test}$ = 0.805, $F_RU_{L\,test}$ = 4.73 W/m^2-K, $\dot{m}_{coll\_test}$ = 72 kg/hr-m^2.

Collector performance can be enhanced by increasing $\dot{m}_{coll}$, yet at the cost of raising T_i. A higher $\dot{m}_{coll}$ leads to intensive mixing for the fluid in the vicinity of the entrance and plume entrainment as the fluid penetrates further. Consequently, the bottom temperature raises, and warmer fluid is sent to the collector. Thus, collector performance is sacrificed. Increasing $\dot{m}_{coll}$ causes contrary effects on collector performance, when the condition of high $\dot{m}_{coll}$ and low T_i can be satisfied, the collector performance will approach the peak operation. A low T_i could be achieved by enlarging the TES, so the hot fluid on the top requires longer transit time to reach the bottom. Thus the fluid at the bottom stays cool as long as possible.

The collector area (Ac) is another parameter that impacts collector performance, thus influences system performance. The TRNSYS prediction of the system performance (solar fraction) to various Ac is shown in Fig A2. It reveals that solar fraction has a nearly linear growth when increasing Ac. The solar fraction reached unity when Ac = 6 m^2 and indicates that the load demands are 100% satisfied by the solar domestic hot water system.

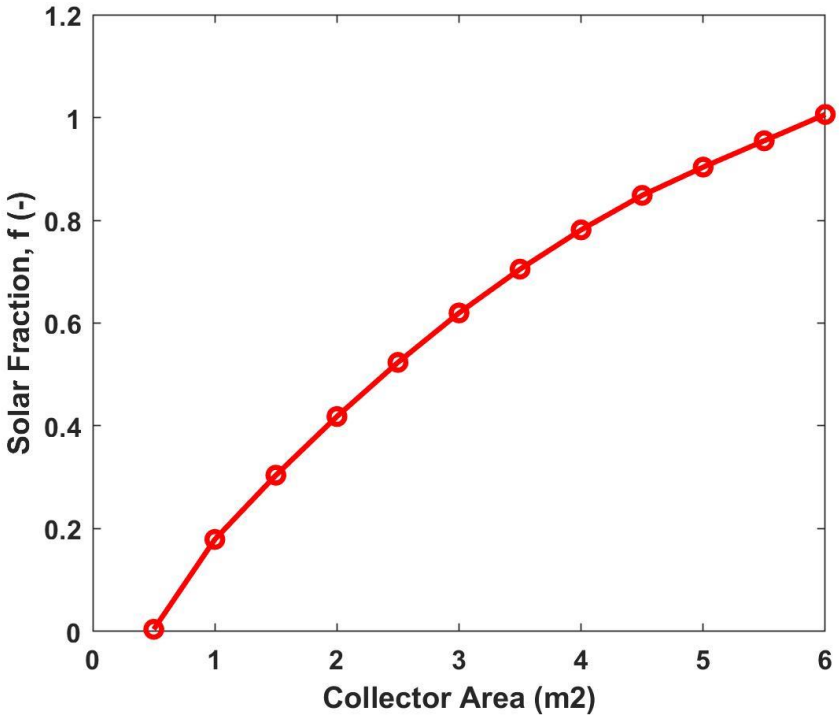

Figure A.2 Solar fraction versus collector area. Simulation parameters were adapted from Wuestling et al. [9]. $F_R(\tau\alpha)_{test}$ = 0.805, $F_RU_{L\ test}$ = 4.73 W/m^2°C, $\dot{\mathbf{m}}_{\mathbf{coll\_test}}$ = 72 kg/hr-m^2. $\dot{\mathbf{m}}_{\mathbf{coll}}$ = 30 kg/hr. RAND load profile was employed.

Appendix B Analytical Solutions of TRNSYS Type 1b Flat-Plate Solar Collector Model

When the incidence angle (θ) measures less than 60°, both methods to evaluate the useful energy gain collected by the collector, Q_u, are presented in Equation B1. Therefore, the collector outlet temperature, T_o, could be calculated as Equation B2.

$$Q_u = \tau_p * A_c[F_R(\tau\alpha) * G * \kappa_{\tau\alpha} - F_R U_L(T_i - T_a)]$$

$$= \tau_p * \dot{m}_{coll} * C_p * (T_o - T_i) \quad (B1)$$

Where τ_p = pump-on time

A_c = collector area

$F_R(\tau\alpha)$ = intercept of the collector efficiency versus $(T_i - T_a)/G$

$F_R U_L$ = negative slope of the collector efficiency versus $(T_i - T_a)/G$

G = solar irradiance

$K_{\tau\alpha}$ = incidence angle modifier $= 1 - b_o\left(\frac{1}{\cos\theta} - 1\right)$

b_o = incidence angle modifier first-order coefficient

θ = incidence angle

T_i = collector inlet temperature

T_o = collector outlet temperature

T_a = ambient temperature

$$T_o = \frac{A_c[F_R(\tau\alpha) * G * \kappa_{\tau\alpha} - F_R U_L(T_i - T_a)]}{\dot{m}_{coll} * C_p} + T_i \quad (B2)$$

$F_R(\tau\alpha)$ and F_RU_L Adjustment upon Change in the Collector Flow Rate:

The collector heat removal factor, F_R, is dependent upon the collector flow rate, thus the corrections for $F_R(\tau\alpha)$ and F_RU_L are required when the collector flow rate changes. Ideally, $(F_R(\tau\alpha))_{test}$ and $(F_RU_L)_{test}$ were collected at a measured flow rate, so-called $(\dot{m}_{coll})_{test}$. If the collector is used at a flow rate other than $(\dot{m}_{coll})_{test}$, the proper adjustments in $F_R(\tau\alpha)$ and F_RU_L are required. Duffie and Beckman [39] suggested a ratio, r, which is defined in Equation B3 to calculate the proper values of $F_R(\tau\alpha)$ and F_RU_L.

$$r = \frac{F_R(\tau\alpha)|_{use}}{F_R(\tau\alpha)|_{test}} = \frac{F_R U_L|_{use}}{F_R U_L|_{test}} = \frac{\left\{\frac{\dot{m}_{coll} * C_p}{A_c * F'U_L} * \left[1 - exp\left(-\frac{A_c * F'U_L}{\dot{m}_{coll} * C_p}\right)\right]\right\}_{use}}{\left\{\frac{\dot{m}_{coll} * C_p}{A_c * F'U_L} * \left[1 - exp\left(-\frac{A_c * F'U_L}{\dot{m}_{coll} * C_p}\right)\right]\right\}_{test}} \quad (B3)$$

Where $F'U_L$ is assumed to be independent of the collector flow rate and can be evaluated at the testing condition as Equation B4:

$$F'U_L = -\frac{\dot{m}_{coll} * C_p}{A_c * F'^{U_L}} * \ln\left(1 - \frac{F_R U_L * A_c}{\dot{m}_{coll} * C_p}\right) = 4.87 \frac{W}{m^2 K} \quad (B4)$$

Appendix C Analytical Solution for TES Tank Verification Case 1

This appendix explains the method to calculate the evolution of the thermocline at the instantaneous time of interest. The analytical solutions will be discussed for generic cases.

The distance between the top of the tank to the center of the thermocline, C, can be determined by Equation C1:

$$C = \int \frac{\dot{m}_{charge}}{\rho * A_{cross-section}} \, dt \tag{C1}$$

The temperature for fluid locates above the thermocline (x < C) can be evaluated as Equation C2:

$$T(x,t)_{top} = \left[\left(T_{initial} + T_{charge} \right) - \left(T_{avg} + \left(T_{inital} - T_{avg} \right) * erf\left(\frac{C - x}{\sqrt{4\alpha t}} \right) \right) \right] \tag{C2}$$

Where T_{inital} = initial temperature of the tank

T_{charge} = temperature of the charging fluid

T_{avg} = average temperature of $T_{initial}$ and T_{charge}

α = thermal diffusivity of the fluid

x = distance from the top of the tank

t = instantaneous time of interest

The temperature for fluid locates below the thermocline (x>C) can be evaluated by Equation C3:

$$T(x,t)_{bottom} = T_{avg} + \left(T_{inital} - T_{avg}\right) * erf\left(\frac{x - C}{\sqrt{4\alpha t}}\right) \quad \text{C3)}$$

Appendix D Analytical Solutions for TES Tank Verification Case 2

A well-insulated tank was initially at a temperature of $T_{initial}$, which was lower than the surrounding temperature, T_a. The schematic diagram of the energy balance is demonstrated in Fig D1 and can be expressed as Equation (D1).

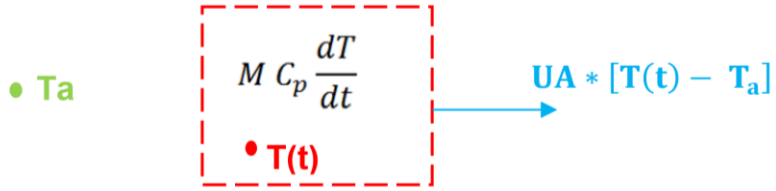

Figure D.1 Schematic diagram of energy balance of a well-insulated TES tank. T_a is the ambient temperature, U represents the tank heat loss coefficient, A indicates the surface area of the tank.

$$MC_p \frac{dT}{dt} = -UA * [T(t) - T_a] \quad (D1)$$

Solving the equation D1 to get the analytical solution for the nodal temperature as Equation (D2):

$$T(t) = T_a + (T_{initial} - T_a) * e^{-\frac{t}{\tau}} \quad (D2)$$

$$\text{Where } \tau = \text{time constant} = \frac{MC_p}{UA}$$

$$T_a = \text{ambient temperature}$$

$$T_{initial} = \text{initial temperature}$$

$$t = \text{simulation time}$$

Appendix E Analytical Solutions for Auxiliary Tank Verification, Case 1

The amount of energy, Q, required to compensate for the temperature difference with the preset temperature (T_{set}) can be calculated as Equation (E1).

$$Q = M * C_p * (T_{tank} - T_{initial}) = \tau' * \dot{Q}_{aux} \quad \text{(E1)}$$

Where M = mass of the fluid within the tank

C_p = thermal capacity of the fluid

T_{tank} = average temperature of the tank

τ' = time required to reach T_{set}

$\dot{Q}_{aux}$ = power of the heating elements

Thus:

$$\tau' = \frac{M\, C_p * (T_{in} - T_{initial})}{\dot{Q}_{aux}} = \frac{0.151\ m^3 * 1000 \frac{kg}{m^3} * 4190 \frac{J}{kg\,℃} * (60 - 20)℃}{4500\ W * 2}$$

$$= 2812\ s = 0.78\ hr$$

Appendix F Analytical Solutions for Auxiliary Tank Verification, Case 2

A well-insulated auxiliary tank was initially at 60 °C, and the heaters were not present during the entire simulation. The temperature deadband was set at 0.5 °C.

The tank temperature can be calculated as Equation (F1).

$$T(t) = T_a + (T_{initial} - T_a) * e^{-\frac{t}{\tau}} \quad \text{(F1)}$$

where, $\tau = \text{time constant} = \frac{\text{MC}_\text{p}}{\text{UA}}$

Ta = ambient temperature

$T_{initial}$ = initial temperature

T = time

Thus, the time required for the tank temperature to drop one temperature deadband can be calculated according to the Equation (F1). It takes 1.32 hours for the tank temperature to reach 59.5 °C. It takes 35.1s (0.1 hours) for the tank to be recharged to T_{set} according to Equation (F2).

Since $Q = M * C_p * \Delta T_{deadband} = \tau' * \dot{Q}_{aux}$

$$\tau' = \frac{M * C_p * \Delta T_{deadband}}{\dot{Q}_{aux}} \quad (F2)$$

Where M = mass of the fluid within the tank

C_p = thermal capacity of the fluid

$\Delta T_{deadband}$ = deadband temperature

τ' = time required to reach T_{set}

$\dot{Q}_{aux}$ = power of the heating element